Reconfiguring mine water reticulation systems for cost savings

W. Conradie

orcid.org 0000-0001-6555-1231

Dissertation submitted in partial fulfilment of the requirements
for the degree *Master of Engineering in Mechanical Engineering*
at the North-West University

Supervisor: Prof. M. Kleingeld

Graduation May 2018

Student number: 23556676

Abstract

Title: Reconfiguring mine water reticulation systems for cost savings

Author: Mr W. Conradie

Promoter: Prof. M. Kleingeld

Degree: Master of Engineering in Mechanical Engineering

Keywords: Water reticulation system, dewatering, pumps, reconfiguring, energy-efficiency, load shifting, cost savings.

Rising electricity costs in South Africa force companies, including gold mines, to minimise their energy consumption (EC). More than 30% of the total energy demand for deep-level mines is consumed by the water reticulation system (WRS). Energy intensive centrifugal pumps are housed in the dewatering system of the WRS. Significant energy and cost savings can be realised by decreasing the amount of water transferred through the dewatering system. To achieve this, cold-water *supply* or *demand* needs to be decreased.

Water supply optimisation is a typical demand-side management (DSM) initiative that reduces EC of the dewatering system, by minimising cold-water supply to underground services. However, it only reduces water supply within the blasting shift, which is typically 6–8 hours per day. Load shifting (LS) is a DSM initiative that optimises the time-of-use operating schedule on dewatering pumps. Note that a decrease in water supply to underground tertiary air-cooling systems increases the LS performance of dewatering pumps.

For a decrease in water demand for the entire day, the WRS can be reconfigured. This entails removing chilled water cars and replacing them with strategically placed centralised bulk air-coolers. This results in increased energy and cost savings over the entire duration of a day.

A methodology was developed to accurately evaluate energy and cost savings of the dewatering system for a reconfigured WRS. Actual data obtained from the mine was verified through calculations and simulations. This data was then used as inputs to evaluate EC of the dewatering system for the original and reconfigured WRS.

The methodology was applied on a reconfigured WRS of a gold mine in South Africa. The predicted energy-efficiency and cost saving was **49.1 GWh** and **R31.8 million** per annum, respectively.

Acknowledgements

The content within this dissertation is my own work and research. I would like to express my gratitude to those who gave me guidance when I needed it. I hope that I have mentioned everyone which played a vital role in the compiling of this dissertation and who encouraged through challenging times. Please contact me if you think you should be included in the acknowledgement.

I would firstly like to give all glory to God for giving me the opportunity to be His follower. I thank Him for giving me strength to accomplish my goals in life.

I thank my parents, Deon and Marieta Conradie, for their love and guidance through the years, and the opportunity they gave me to study.

Thank you to Drieke van der Merwe for encouraging me throughout the writeup of this dissertation. I appreciate all the support and motivation from her.

I would like to thank Abrie Schutte for his advice, encouragement, support and commitment as mentor throughout the development of this dissertation.

Thank you to my friends and colleagues at ETA Operations. Your encouraging talks and recommendations helped.

Lastly, I would like to thank Enermanage (Pty) Ltd and its sister companies for financial support to complete this study. I express my gratitude to Prof. E. H. Matthews for giving me the opportunity to further my studies.

Table of Contents

List of Figures

List of Tables

List of Equations

Abbreviations

EIUG	Energy Intensive User Group
NERSA	National Energy Regulator of South Africa
ESCO	Energy Service Company
3CPFS	Three-chamber pipe feeder system
DSM	Demand-side management
PRV	Pressure reducing valve
VSD	Variable speed drive
BAC	Bulk air-cooler
CBAC	Centralised bulk air-cooler
FP	Refrigeration plant
PCT	Pre-cooling tower
PCD	Pre-cool dam
HX	Heat exchanger
DC	Direct-contact
CC	Closed-circuit
CWC	Chilled water car
EMS	Energy Management System
REMS-P	Real-time Energy Management System for
WSO	Water supply optimisation
SCADA	Supervisory control and data acquisition
TOU	Time-of-use
Eskom	Electricity supply commission of South Africa
SA	South Africa
WRS	Water reticulation system
VRT	Virgin rock temperature
EC	Energy consumption
REC	Reference energy consumption
RWC	Reference water consumption
EE	Energy-efficiency
LS	Load shift
HP	High pressure
WB	Wet-bulb
CSV	Comma separated value

List of Symbols

Symbol	Description	Units
W	Measure of power	*Watt*
J	Measure of energy	*Joule*
Wh	Measure of energy	*Watt.hour*
Pa	Measure of pressure	*Pascal*
K	Measure of temperature	*Kelvin*
C_p	Specific heat capacity of water	$\frac{J}{K}$
m	Measure of mass	kg
$\dot{m}$	Mass flow rate	$\frac{kg}{m^3}$
P	Power	*W*
p	Pressure	*Bar* | *Pa*
Δp	Difference in pressure between two points	*Bar* | *Pa*
ΔT	Temperature difference	$°C$ | *K*
Q	Measure of fluid volume flow rate	$\frac{m^3}{s}$
L	Length	*m*
v	Fluid flow velocity	$\frac{m}{s}$
f	Fluid friction factor	-
D	Hydraulic diameter	*m*
g	Gravitational constant	$\frac{m}{s^2}$

Symbol	Description	Units
$\boldsymbol{H}$	Head	m
A	Area	m^2
$\boldsymbol{\rho}$	Measure of fluid density	$\frac{kg}{m^3}$
η	Efficiency	-
Re	Reynolds number	-
$\boldsymbol{\pi}$	Pie	≈ 3.142
k	Denotes 1×10^3	*kilo*
M	Denotes 1×10^6	*Mega*
G	Denotes 1×10^9	*Giga*

CHAPTER 1 INTRODUCTION AND BACKGROUND

[1]

"If you want to live a happy life, tie it to a goal. Not to people or things."

– Albert Einstein

[1] Moab Khotsong mine, courtesy of 911metallurgist.com.

1.1 Largest energy providers and consumers in South Africa

Over 90% of the electricity supply in South Africa (SA) is generated from coal. Eskom is the main electricity provider, supplying 95% of the total electricity demand in SA [1]. After the energy crisis in 2008, the SA government increased funding to focus more on renewable energy. The government also increased its promotion of energy-efficiency (EE) measures to energy intensive industries and to the public [2]. In January 2008, Eskom included a "load shedding" plan to decrease electricity usage during certain periods of a day when demand on the national grid would often exceed the available electricity supply [3].

Rising energy costs in SA present an increasing struggle for industries, especially to members of the Energy Intensive User Group (EIUG). The EIUG of SA consists of 31 members accounting for more than 40% of the total electricity consumed in SA [4]. Figure 1 identifies the largest EIUG in SA, where iron/steel processing, precious and non-ferrous metal refineries, and gold mining are the three largest energy consumers in SA. The mining sector consumes more than 24% of the total electricity supplied to the EIUG of SA [5].

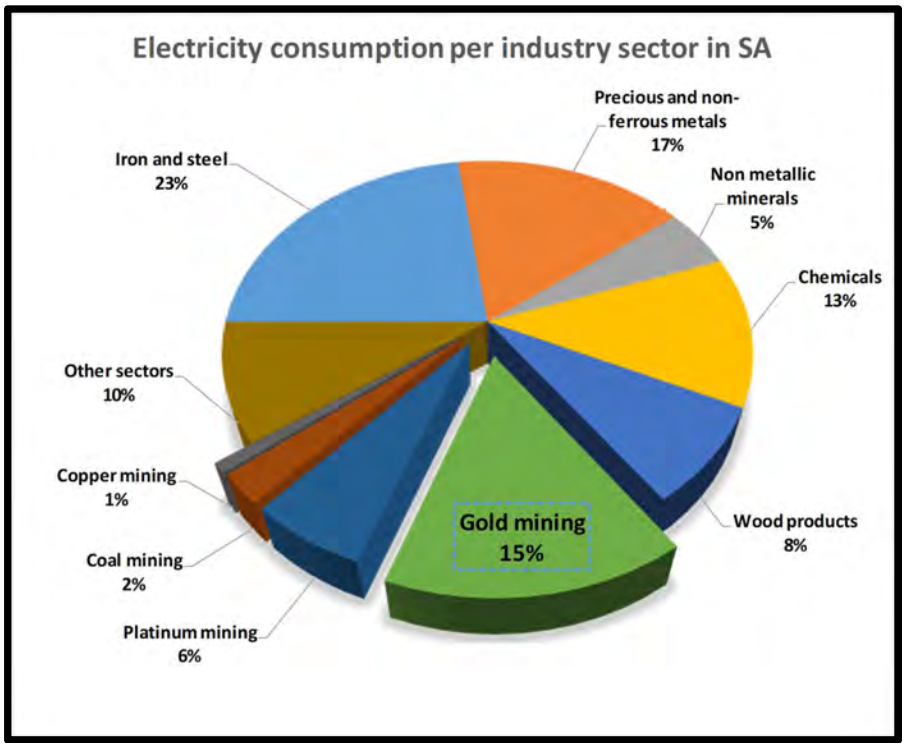

Figure 1: Industrial sector electricity consumption [5]

The EIUG has a specific time-of-use (TOU) electricity pricing structure, which falls under the Eskom Megaflex pricing category. Eskom peak periods and electricity tariffs differ seasonally, where summer peak periods are 07:00–10:00 and 18:00–20:00, and winter peaks are 06:00–09:00 and 17:00–19:00. The 2017/2018 Megaflex TOU schedule and tariffs can be found in Table 56 – Table 59 in Appendix A and Appendix B, respectively [6].

1.2 Energy consumption of South African gold mines

Deep-level gold mines in SA reach depths of 3.5–4.0 km. Energy intensive mining equipment is needed for ore extraction processes. Figure 2 shows the electricity distribution for the mining systems, which include man- and rock winders, compressors, ventilation fans, refrigeration plants (FPs), bulk air-coolers (BACs) and centrifugal pumps. A water reticulation system (WRS) on a gold mine houses the pumping system and FPs. A WRS consumes approximately 30–35% of the total electricity demand on a SA gold mine.

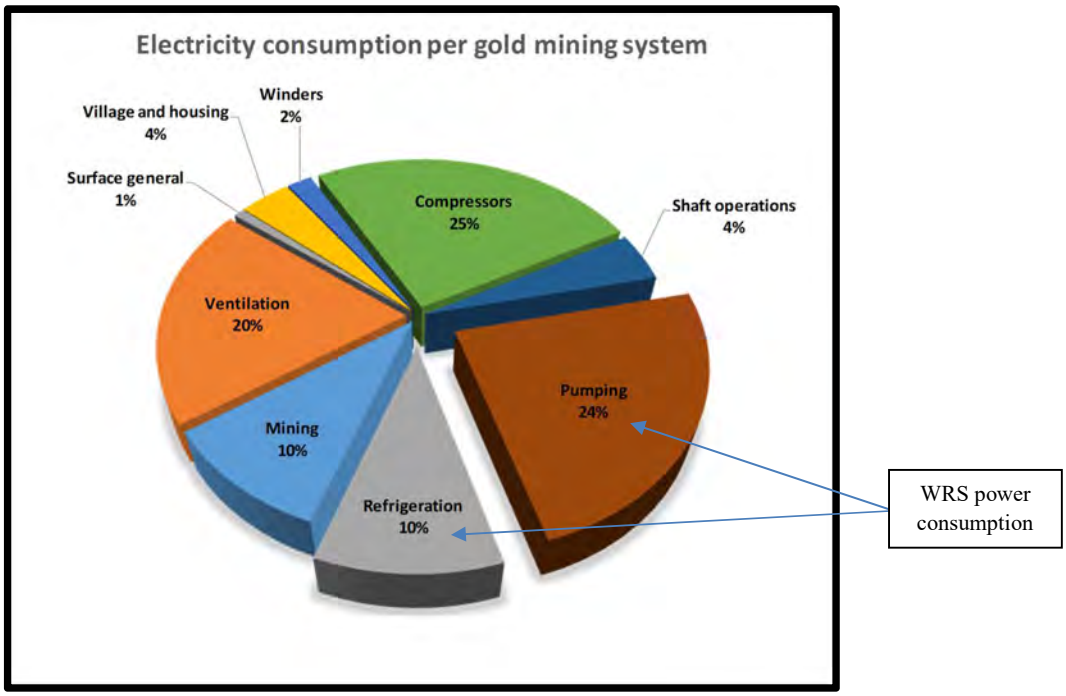

Figure 2: Electricity consumption per mining system [5]

Within expensive Eskom peak periods, energy intensive mining systems should be switch off or throttled to reduce energy consumption (EC) and save on operational costs [7]. The main concern of mine employees is to increase production and not to save energy, which creates opportunities for third-party contractors to investigate and evaluate EE and cost saving initiatives. EE can be defined as the process of improving systems and equipment to obtain an equal or increased amount of service delivery, while decreasing energy input [8].

Energy service companies (ESCOs) investigate, implement and evaluate energy and cost saving techniques to enable energy intensive industries to minimise their EC and operational costs. The energy and cost saving initiatives ESCOs implement and/or evaluate on a mine WRS are:

- Installation of more efficient pump rotors.
- Installation of VSDs on large centrifugal pumps.
- Optimisation of FPs and ventilation systems.
- Optimisation of water supply through pressure and flow control.
- Investigating load shifting opportunities.

Figure 3 shows statistics for gold production and the number of employees on gold mines in SA. It can be observed that the amount of gold produced decreased from approximately 250 tonnes in 2007 to 150 tonnes in 2016. This decrease could be due to several economic and technical factors, which include lower ore grades, increased EC and a general increase in input costs [9].

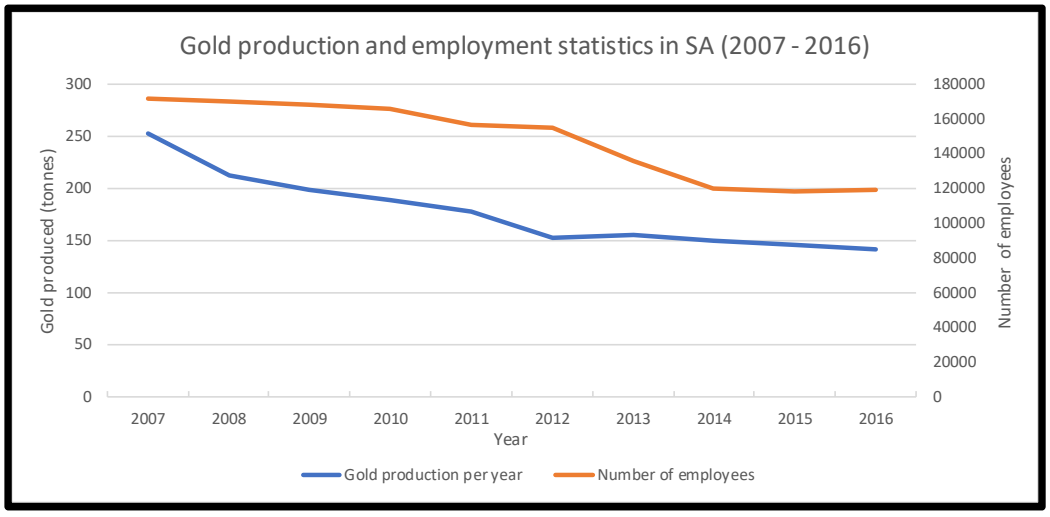

Figure 3: Gold production and employment statistics in SA (2007 – 2016) [10]

Gold production is limited by technical constraints such as the stoping width on a typical SA gold mine, which is approximately 1m. Most mining equipment is too large to fit in these small spaces. This causes the SA gold mining industry to be highly dependent on labour to complete mining activities at the stopes. Figure 3 shows a correlation between the amount of gold produced and the number of employees. More than 90% of employees on gold mines are miners. The number of people employed by SA gold mines decreased by more than 50 000 from 2007 to 2016.

Figure 4 shows the average Megaflex electricity costs for 2007–2017. It indicates that the price of electricity increased with an average of 17.8% from 2007 to 2016.

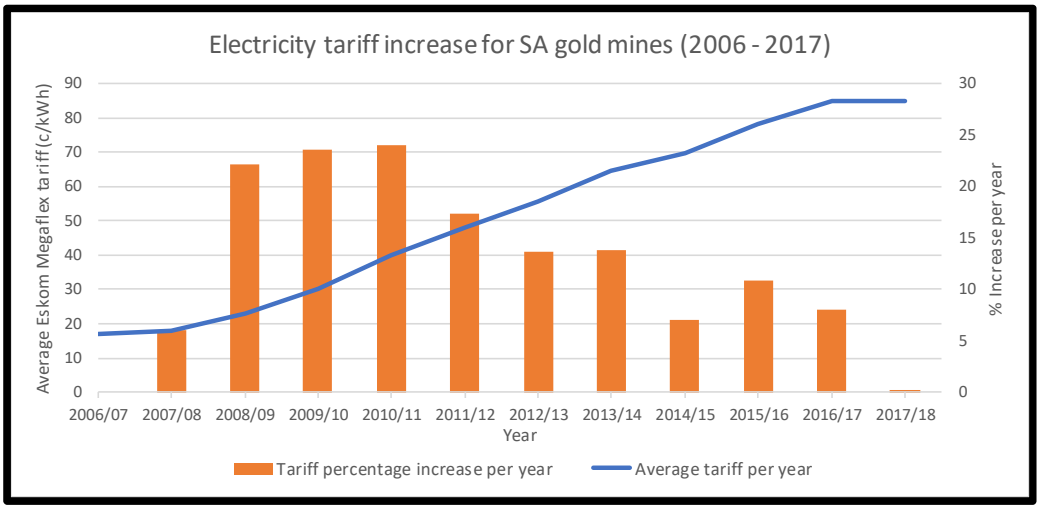

Figure 4: Historical Eskom Megaflex tariff increase (2007-2017) [11]

From 2016 to 2017, the average electricity tariff only increased by 2%. This is due to Eskom supplying excess electricity capacity to the national grid, with a surplus of 5600 MW at peak periods [1]. Figure 5 shows the average year-on-year selling price of gold per kilogram and the percentage change of the gold selling price for 2007–2016.

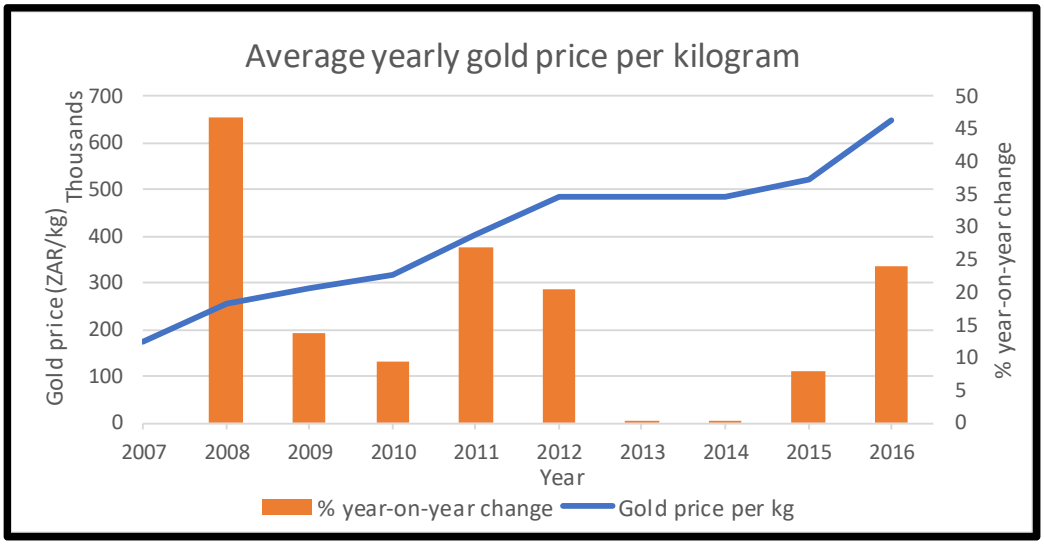

Figure 5: Sales price per kilogram of gold (ZAR/kg) statistics for 2007–2016 [12]

When combining Figure 3 and Figure 5, the year-on-year gold sales in SA for 2007–2016 can be obtained and are shown in Figure 6. It is clear that although gold production has declined, sales per year have increased.

Sales profits are highly dependent on the price of gold. This means that if the gold price decreases, production needs to increase to compensate for the loss of revenue. An increase in production requires an increase in labour, which in turn results in an increase in salary expenses. All these factors affect a mine's profitability.

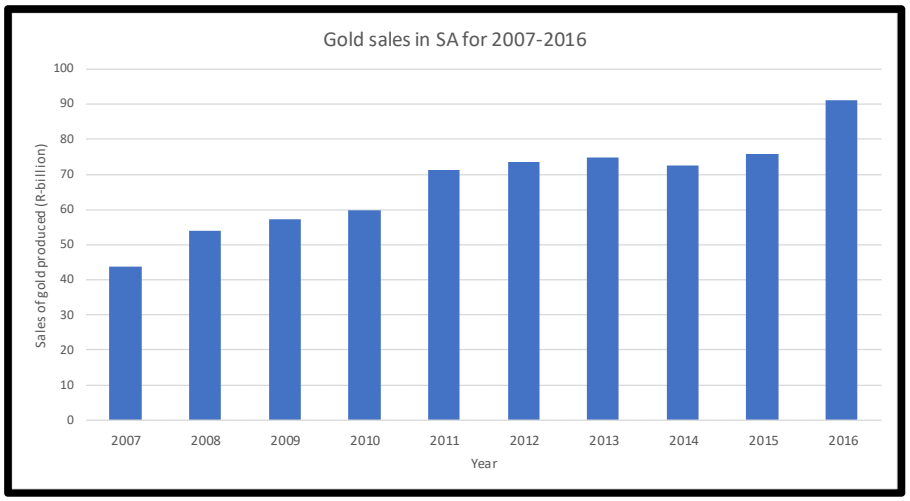

Figure 6: Year-on-year sales for gold produced in SA [10] [12]

The amount of gold produced is directly related to the productivity of miners, which in turn is affected by air temperatures at working areas. Figure 7 displays the results of a study conducted on the performance of gold production compared to underground wet-bulb (WB) air temperatures. The optimal underground WB air temperature for most gold mines is approximately 27–28°C [13] [14].

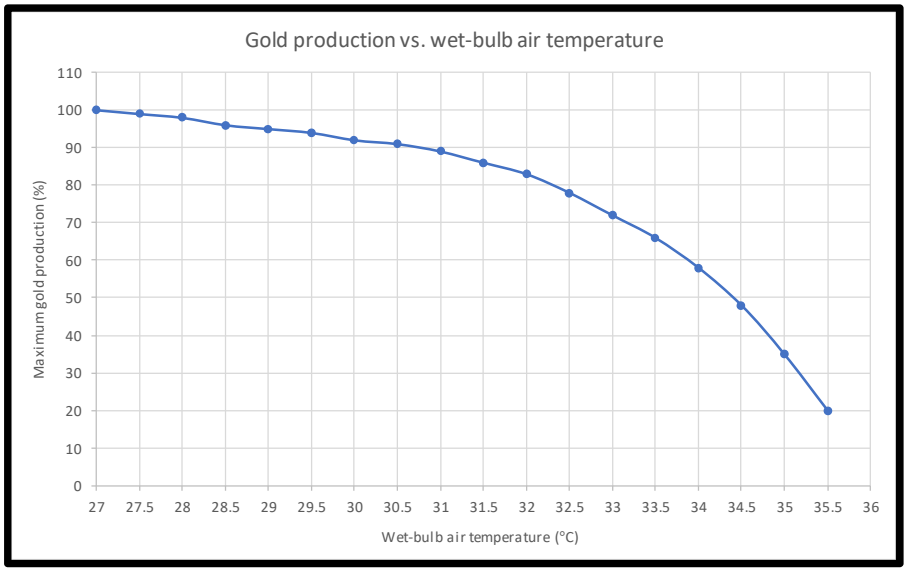

Figure 7: Gold production performance versus underground WB air temperatures

It can be observed that miner productivity decreases with an increase in WB temperature. For a WB temperature of over $32°C$, miner productivity for the extraction of gold drastically decreases. The maximum allowable WB air temperature at underground working areas should not exceed $32°C$. The health and safety of employees will be compromised if temperatures rise above this value [13] [14].

The virgin rock temperature (VRT) in SA gold mines increases by 10–$12°C$ per vertical kilometre in the Johannesburg region. At depths of 1–3 km, the VRT varies in the range of 35–$80°C$ [14] [15]. More than 30% of the energy demand from SA gold mines is consumed by FPs and ventilation fans [5].

Note that when the VRT is excessively high, a significant amount of cooling power is required to effectively cool air for safe and productive working areas. This will increase the performance of miners; however, both aspects should be considered. It is thus important to increase production and keep refrigeration costs minimal. This means an optimal balance between underground WB temperature and miner efficiency should be kept in mind.

Improving the efficiency of the WRS will aid in reducing underground WB temperatures and/or minimise power consumption of FPs.

1.3 Background on mine water reticulation systems

Figure 8 shows an overview of a typical mine WRS. A mine's WRS cycle consists of three elements: the chilled water distribution network (**A**), additional cross-cut cooling and mining activities (**B**), and the dewatering process (**C**). These processes will be described in further detail below.

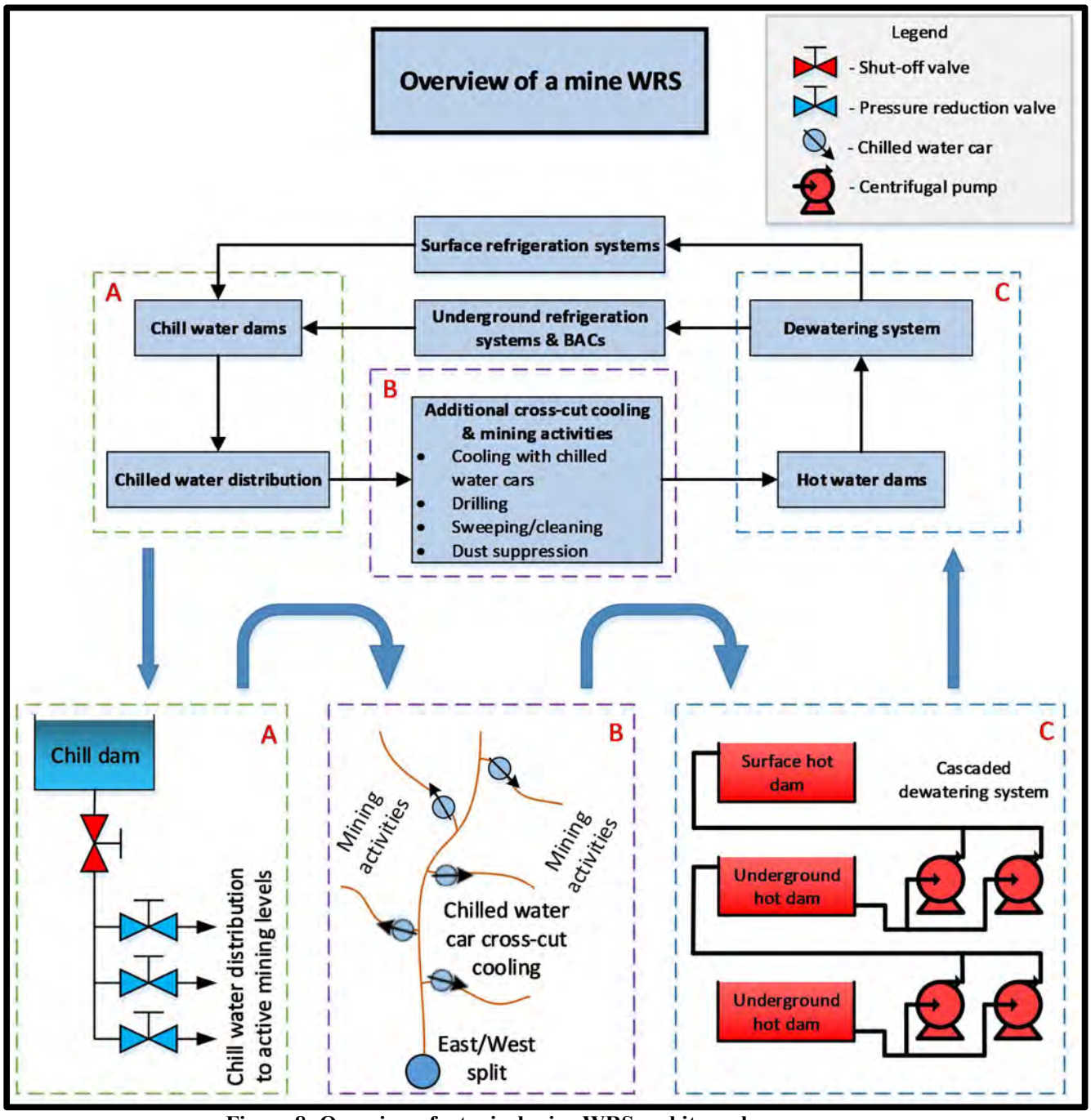

Figure 8: Overview of a typical mine WRS and its cycle processes

The primary purpose of a mine WRS is to distribute cold water to air-cooling systems and mining activities. Ventilation through fans alone provide adequate cooling for mines less than 800 m deep, depending on design criteria. Mines that are 800 m–1.4 km deep only require primary cooling for underground activities. This can be achieved by cooling ventilation air at surface BACs. When mines reach depths greater than 1.4 km, acceptable underground working conditions can usually no longer be achieved through primary cooling methods alone.

Cold water is used for the following mining activities [16]:

- Rock drilling, where it is used as working fluid for drilling equipment.
- Cleaning of work places.
- Dust suppression after blasting.
- Cooling of newly blasted ore while it is moved to loading stations.

These mining activities cause the cold water to heat slightly. This heated water is discarded on the ground of the haulage. The water heats up further as it flows in delved channels on the ground and into hot storage dams. Hot water in these dams typically reaches temperatures of 25–30$°C$.

Water that accumulates in the hot storage dams is pumped through the dewatering system and cooled at surface and underground FPs. The water is cooled within the evaporator unit of an FP to approximately 3–5$°C$ [17]. The cascaded dewatering process completes the WRS cycle.

Cascading pump stations house centrifugal pumps, which are connected in parallel configurations. These pumps typically have power consumptions of 1000–4000 kW, depending on the required head and flow rate.

Secondary and tertiary air-cooling may be required for mines deeper than 1.4 km [18]. This is because auto-compression causes air to heat up as it moves to deeper mining levels. Secondary cooling entails air from the surface being cooled at underground BACs. This is done to achieve safe and productive working conditions for the lower mining levels.

An underground BAC may either be a direct-contact (DC) spray heat exchanger (HX) or closed-circuit (CC) cooling-coil HX bank. DC BACs are thermally more efficient than CC BACs. However, DC BACs require additional energy for pumping, whereas CC BACs do not [18].

Figure 9 shows an underground layout of mining sections, with the reach of each cooling stage indicated.

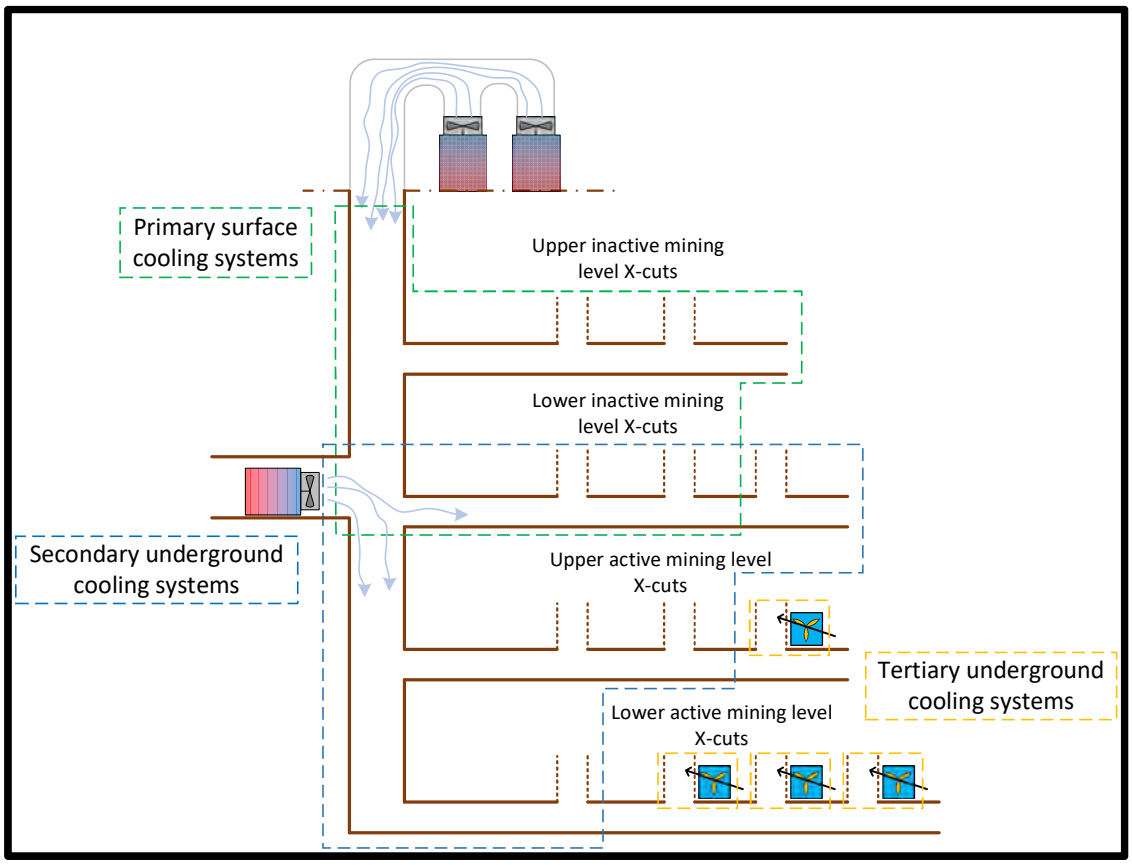

Figure 9: Reach of primary, secondary and tertiary cooling solutions

Cold air from primary cooling methods only reach most of the sections on the upper levels of a gold mine. Secondary cooling solutions reach most of the middle levels in very deep mines. For the deepest mining levels, tertiary cooling solutions might need to be applied. These solutions include chilled water cars (CWCs), which can be installed at cross-cuts where inadequate working conditions exist [16].

The principle of heat exchange for CWCs is the same as for CC cooling-coil BACs. Cold water flows into the tubes of an HX bank and hot air flows over the tubes. Heat is removed from the air and transferred to the water. When water exits a cooling-car, it is discarded onto the ground of the haulage, where it flows in delved channels and into hot water storage dams.

A mine WRS is not a closed-loop system. Water sometimes needs to be added or removed. If the supply cannot keep up with demand, water is purchased from the local water board and added to the WRS.

Fissure water enters a WRS through cracks in the mine walls and from nearby abandoned mines. Water is removed from dams when their levels become excessive. This is done by treating the water for pollutants in surface slime dams and then discarding it into the surrounding environment.

1.4 Energy and cost saving initiatives on mine water reticulation systems

As mentioned, ESCOs investigate and evaluate energy and cost saving strategies for energy intensive industries. Their aim is to identify possible energy related problems, especially where EC and mining systems are not optimally managed.

Eskom frequently struggles to meet national electricity demand, especially during peak times. There are two solutions to this problem. The first is for the supplier, in this case Eskom, to invest in new generating capacity. The second is for the consumer, in this case the mine, to decrease its EC [19].

It is more profitable for the consumer if they reduce their EC than it is for the supplier to invest in additional generating capacity. This concept is known as demand-side management (DSM), and it is dependent on the amount of machinery in use, as well as the user's efficiencies and operating procedures [19].

ESCOs achieve energy and cost savings on mining systems by [19]:

- Investigating feasibility of different DSM strategies.
- Identifying the most viable solution.
- Creating a detailed control philosophy.
- Implementing and evaluating the DSM measures.

The benefits of implementing DSM techniques on a WRS include a reduction in [19]:

- Energy consumption, due to a decrease in water consumption.
- Operational costs, due to load shifting of dewatering pumps.
- Pump maintenance costs.

The flow rate of the cold water that is sent down the mineshaft has a direct effect on the efficiency of the dewatering system. This is because all components of the WRS are connected and form a cycle. The cold-water supply flow rate is effectively decreased when cold-water demand for underground mining activities decreases.

Water supply optimisation (WSO) is a DSM initiative that aims to minimise cold-water supply, thereby improving EE.

The effective implementation of WSO increases the EE of a WRS, even if water supply is optimised for only a couple of hours per day. WSO projects are typically implemented during blasting shift because no mining activities are in progress. The process for implementing EE measures on a mine WRS is discussed below.

Energy-efficiency

Electricity suppliers continuously face challenges in promoting economically sound EE measures to industries in SA. Eskom aims to provide industries with energy reduction incentives, including tax deductions and subsidies to replace old technology with more efficient alternatives [8].

Figure 10 shows a non-optimised baseline of a dewatering system, where the orange blocks represent initial energy load.

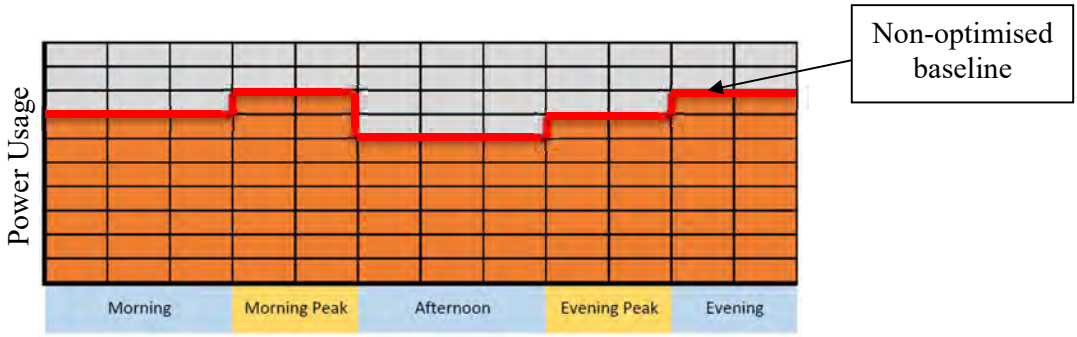

Figure 10: EE – Non-optimised power baseline

Figure 11 shows the EE-optimised power profile versus the non-optimised baseline.

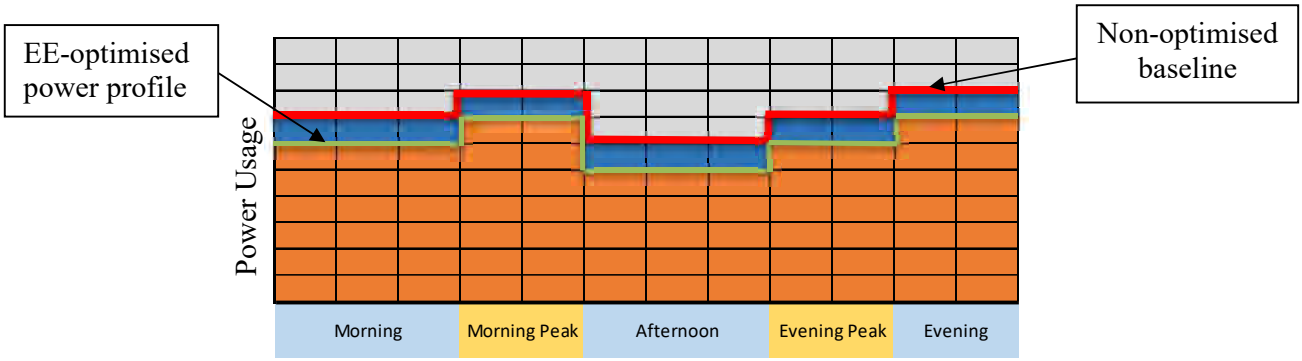

Figure 11: EE – Optimised power profile vs. initial baseline

The EE-optimised power profile is obtained by subtracting the blue blocks from the initial energy load. In this example, it can be observed that the total EC is decreased throughout the entire day. If a system experiences a continuous reduction in power consumption of 400 kW, an EE saving of 9 600 kWh can be achieved per day.

Table 1 summarises the results for the EE-optimised system in Figure 11.

Table 1: EE results for Figure 11

Description	Number of blocks
Non-optimised energy load – orange blocks in Figure 10.	85
EE-optimised energy load – orange blocks Figure 11.	73
Decreased energy load – blue blocks in Figure 11.	12

It is clear that EE DSM initiatives decrease EC, because the number of orange blocks decreased [20].

The successful implementation of EE initiatives may also lead to operational improvements, which includes [8]:

- Decreased product waste.
- Decreased environmental costs.
- Increased equipment reliability.
- Decreased operation and maintenance costs.

EE initiatives implemented on a WRS can affect the load shift (LS) performance of dewatering pumps. LS is a DSM initiative that aims to decrease operational costs during expensive TOU periods. LS performance increases when there is a decrease in cold-water demand for underground air-cooling equipment and/or mining activities. This results in slower accumulation of water volume in hot dams, which means that pumps can be switched off for longer periods. The process for implementing LS techniques on a mine WRS is discussed below.

Load shifting

Cost savings can be realised if LS techniques are applied effectively on a mine WRS, especially in winter peak periods [20]. Appendix A and Appendix B show the Eskom Megaflex schedules and tariffs for low and high demand periods respectively. It is evident from Appendix B that the electricity peak period tariffs for winter months are approximately three times that of summer months.

Figure 12 shows a non-optimised baseline of a dewatering system, where the orange blocks represent its initial energy load.

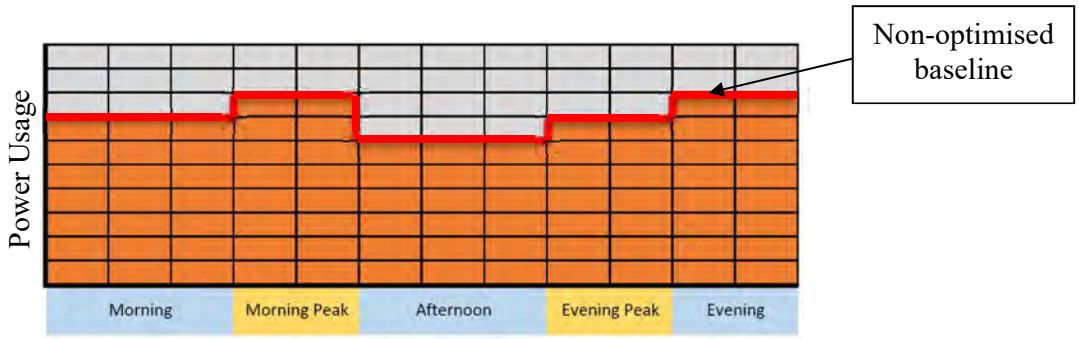

Figure 12: LS – Non-optimised power baseline

Figure 13 shows the process for applying LS techniques on a mine dewatering system.

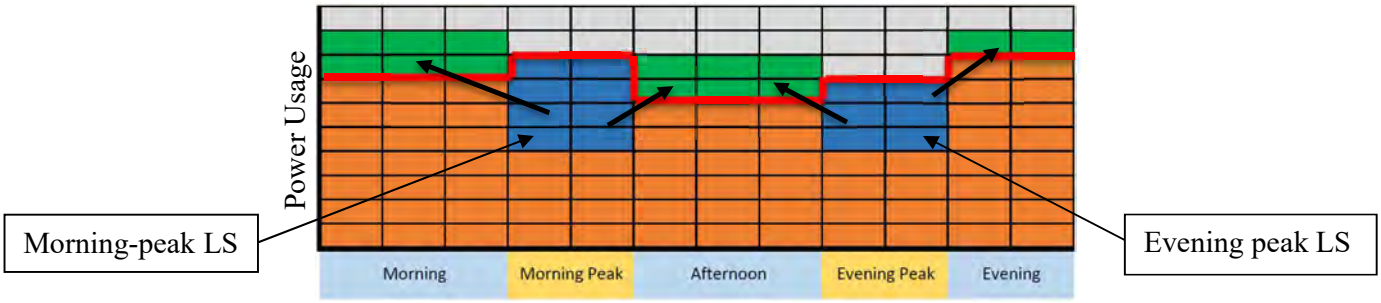

Figure 13: LS – Process for application on dewatering system

LS entails moving electrical load from peak periods where electricity is expensive, to low-demand periods where electricity is cheaper [21]. The blue blocks represent the electrical load that is shifted out of the peak periods to standard and off-peak periods. The green blocks indicate the locations where the energy represented by the blue blocks was shifted to.

If hot dams can store incoming water volumes for these periods, most or all the dewatering pumps may be switched off for the duration of these periods. This will result in cost savings; however, no energy saving will be realised. Figure 14 shows the LS-optimised power profile versus the non-optimised baseline.

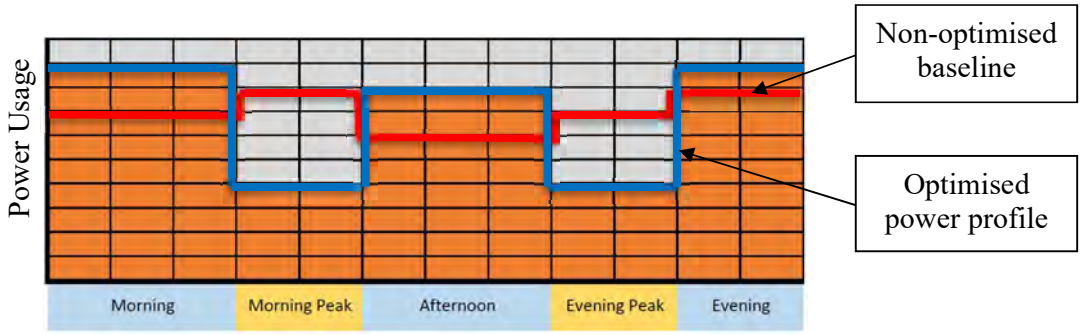

Figure 14: LS – Optimised power profile vs. initial baseline

Table 2 summarises the results for the LS implemented in Figure 13.

Table 2: LS results for Figure 13

Description	Number of blocks
Non-optimised energy load – orange blocks in Figure 12.	85
LS-optimised energy load – orange & green blocks in Figure 13.	85
Energy load that is shifted from morning peak – blue blocks in Figure 13.	8
Energy load that is shifted from evening peak – blue blocks in Figure 13.	6

It can be observed that the number of orange blocks remained the same before and after the LS was applied. This confirms that LS does not affect power consumption and only cost savings are realised [20].

1.5 Problem statement and study objective

Air-cooling systems on SA gold mines consume significant quantities of cold water. Mining activities such as drilling, cleaning, sweeping and dust suppression also utilise water. For mines deeper than 1.4 km, primary and secondary air-cooling solutions may not provide sufficient cooling for lower mining levels. Tertiary air-cooling equipment, which includes CWCs, is installed at working areas to improve this deficiency.

There may be many CWCs installed underground which consume a significant portion of cold water sent underground. Mining employees tend to be negligent in moving CWCs from inactive cross-cuts to active ones. They would rather install additional CWCs when mining activities expand to new cross-cuts. Miners also do not close the cold-water supply to CWCs on inactive cross-cuts. This results in unnecessary cooling of inactive cross-cuts, which in turn means water is used ineffectively.

Water is discarded on the ground of the haulage after it was utilised at CWCs and mining activities. This water ends up in hot storage dams, where the dewatering pumps transfer water to FPs. The amount of cold water consumed has a direct effect on the EC of the dewatering system, where an increase in water demand results in an increase in EC. This problem is addressed by WRS reconfiguration.

A WRS reconfiguration entails the removal of CWCs and replacing them with centralised bulk air-coolers (CBACs). This reduces cold-water consumption to cool air for ventilating most of the lower level cross-cuts. EE is achieved for the reconfigured WRS and the effects thereof result in a decrease in EC for the dewatering system, due to the reduction in water to be pumped.

Traditional WSO techniques decrease cold-water supply within the blasting shift, which is 5–8 hours per day. The reconfiguration decreases water demand for tertiary air-cooling equipment throughout the entire day. This results in a substantial increase in energy and cost savings for the dewatering system, over using traditional WSO techniques.

The objective of this study is to accurately evaluate energy and cost savings for the dewatering system of a reconfigured WRS implemented on a gold mine in SA. A methodology, which includes data analysis, calculations and simulations, will be created and applied to achieve this objective. Verification of power consumption and flow rate data obtained from logging equipment will be discussed throughout this dissertation. The verified data will be used to accurately quantify energy and cost savings.

1.6 Overview of chapters

Chapter 1 provides the introduction to this dissertation. Background to energy suppliers and consumers in SA and gold mines are discussed. A summary of a mine WRS and energy/cost savings initiatives are included. The problem statement, study objective and overview of the chapters included in this dissertation follows.

Chapter 2 includes the literature study on mine WRS. This section provides more insight to the findings of researchers investigating similar problems. An overview of a typical mine WRS is included. Water- and air-cooling systems, as well as other cold-water consumers, are described. An overview of a mine dewatering system is included. Techniques to reduce water consumption are also discussed in this chapter.

Chapter 3 focuses on the evaluation of a reconfigured mine WRS. A methodology for evaluating the EC of a dewatering system for a reconfigured WRS is developed and discussed. The process of acquiring data and information for each of the components of a dewatering system is discussed. Specifications of the original and reconfigured WRS are provided. Evaluation steps to achieve the objective of this study are also discussed.

Chapter 4 includes the results of the methodology applied on the specified reconfigured WRS in Chapter 3. An overview of the reconfigured WRS is provided. The results for energy and cost savings quantification are included in Section 4.7. A summary for the validation of the methodology is included in Section 4.8.

Chapter 5 serves as the conclusion for the dissertation. The potential for reconfiguring a mine WRS is discussed in Section 5.1. Lastly, recommendations for future research are discussed in Section 5.2.

CHAPTER 2 LITERATURE STUDY

[2]

"I destroy my enemy when I make him my friend."

- Abraham Lincoln

[2] Courtesy of Mining Review Africa, April 2016.

2.1 Preamble

Chapter 1 provides an overview of the main electricity suppliers in SA. The mining industry consumes more than 24% of the total electricity supply for energy intensive industries in the country. Rising electricity costs force gold mines to decrease their energy demand or shift their electrical load from expensive to cheaper periods. ESCOs investigate, implement and evaluate energy and cost saving techniques to enable mines to minimise their EC and operational costs.

A mine's WRS houses the pumping system and FPs. The total EC of a WRS is 30–35% of the total energy demand for a gold mine in SA. The primary purpose of a WRS is to distribute cold water to air-cooling systems in the mine and for use in general mining activities. Cooling by surface refrigerated air does not provide sufficient cooling for lower mining levels of mines deeper than 1.4 km. Secondary cooling methods must be used, which include underground FPs, BACs, and CWCs.

As discussed in Section 1.4, WSO increases the efficiency of a WRS. LS can achieve cost savings but does not result in EE gains. Traditional WSO techniques reduce cold-water supply within the blasting shift, which is approximately 5–8 hours per day. Reconfiguring a WRS reduces water demand continuously and sustainably throughout the day. This results in significant energy and cost savings for the dewatering system of the WRS.

This chapter includes literature and background to explain the terms and equations used in the methodology developed in Chapter 3. A detailed overview of a WRS is included in this chapter. Descriptions of WRS components are included to provide more information about the working principle of a WRS. Various constraints to water supply are discussed as well as previous studies conducted on DSM initiatives on mine WRSs.

2.2 Water supply and demand on South African gold mines

Deep-level gold mines in SA consume significant amounts of cold water through air-cooling systems and mining activities. Figure 15 shows the three processes (or sub-systems) of a mine WRS. These processes include the water distribution network, water-/air-cooling systems, and dewatering system.

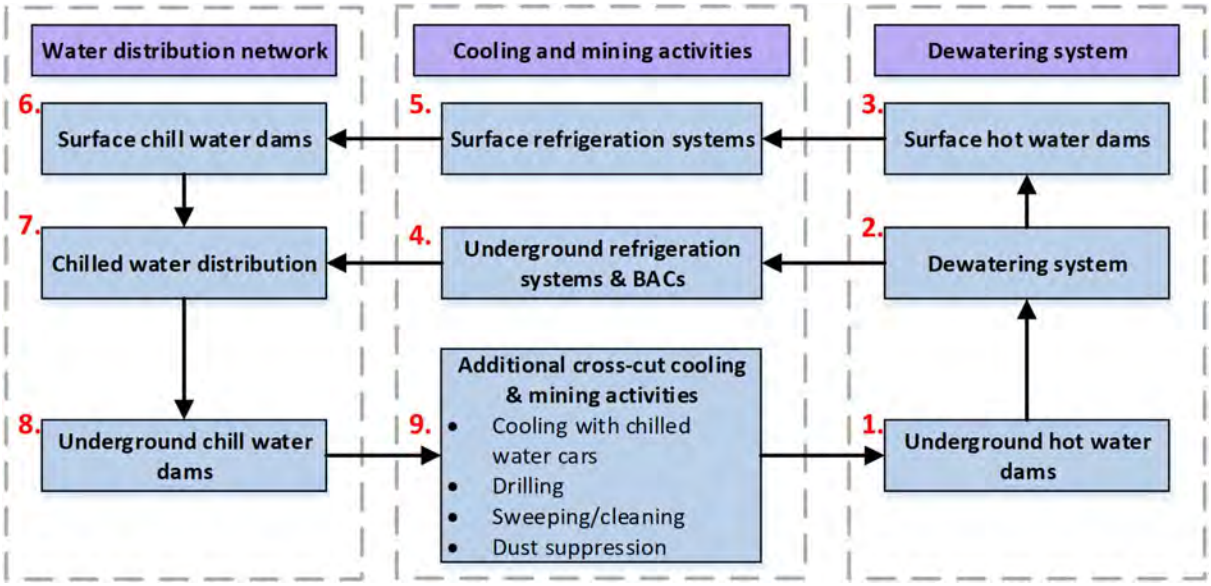

Figure 15: Processes in a mine WRS

Mine WRSs are mainly used for cooling water to cool down the air that is used for ventilation. Refer to Figure 15 for the following steps in the circulatory processes of a WRS:

1. Used mining and fissure water accumulates and is stored in underground hot dams.
2. Water is pumped through dewatering pumps to surface hot storage dams and underground FPs.
3. After pumping through the dewatering system, water is deposited into surface hot storage dams.
4. For very deep mines, there may exist underground FPs for additional deep-level cooling.
5. Surface FPs draw hot water from surface storage dams and cool water to 3–5°C.
6. Cold water is stored in surface chill storage dams and can be fed to underground services.
7. The chilled water distribution network consists of high-pressure piping and energy recovery devices, which distributes the water to underground mining activities.
8. Underground chill water dams store water to be used for underground mining activities.
9. Cold water is used for additional cooling of ventilation air in cross-cuts and for mining activities such as drilling, sweeping, cleaning, and dust suppression.

2.2.1 Overview of a mine WRS

Figure 16 shows an overview of the components of a mine WRS. It is important to note the WRS of each mine is different and that their layout is normally designed to ensure sufficient water supply to meet the demand. The WRS design for mines shallower than 800–1 000 m may provide adequate air-cooling through fans only and installing surface and underground cooling systems may not be necessary. Deep-level gold mines sometimes include energy recovery devices, three-chamber pipe feeder systems and/or high-pressure U-tube systems.

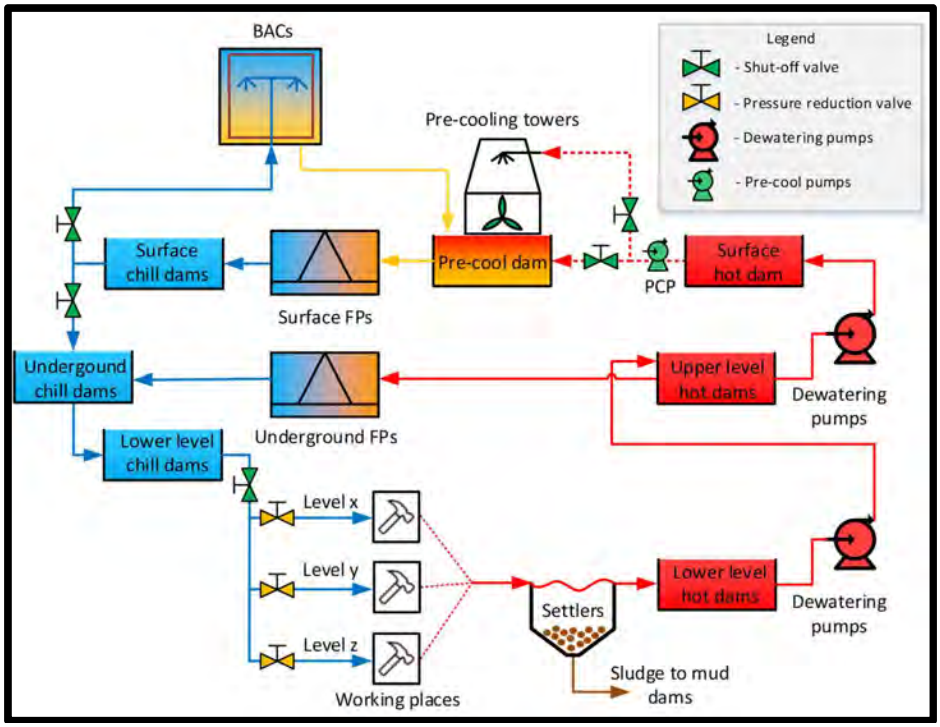

Figure 16: Overview of a typical mine WRS

SA has eight of the ten deepest gold mines in the world, with the remaining two in Ontario, Canada. These deep SA mines are as follows [22]:

Table 3: 8 deepest gold mines in SA [22]

Mine name	Mining group	Depth
Mponeng	AngloGold Ashanti	4.0 km
TauTona	AngloGold Ashanti	3.9 km
Savuka	AngloGold Ashanti	3.7 km
Driefontein	Sibanye Gold	3.4 km
Kusasalethu	Harmony Gold	3.3 km
Moab Khotsong	AngloGold Ashanti	3.1 km
South Deep	Gold Fields	3.0 km
Great Noligwa	AngloGold Ashanti	2.6 km

In shallow mines, water is predominantly used during the drilling shift and to supress dust after blasting has occurred. For deep mines, water is cooled and then used predominantly for ventilation air-cooling and cooling of rock after blasting shifts. The VRT in gold mines in the Johannesburg region of SA increase by 10–12°C per vertical kilometre. At depths of 1–3 km, the VRT vary from 35–80°C [14] [15].

Heat is radiated from the rockface into the surrounding air and a large heat load is generated [14]. This heat load needs to be reduced by transporting cooled air underground through ventilation fans and removing heated air through extraction fans. Cooling of ventilation air is predominantly done at surface FPs. Deep mines, however, may also have FPs installed underground.

As shown in Figure 16, hot water is transferred from underground dams to underground and surface FPs through dewatering pumps. FPs work on the principle of the vapour-compression cycle, which consists of an evaporator, condenser, compressor and expansion valve [23]. Further literature for the vapour-compression cycle is included in Section 2.2.2.

After water is cooled at FPs, it is stored in chill dams. Surface and underground BACs use this water to cool and dehumidify ambient air. The cooled air is then forced down the ventilation shaft by using forced draught ventilation fans. Cold water is also distributed to underground mining activities such as rock drilling, cleaning, sweeping and dust suppression.

SA gold mines typically consume on average 200–600 ℓ/s of cold water per day for underground air-cooling and mining activities. This results in 17–52 Mℓ cold water demand per day, depending on the size of operations [14].

After cold water has been used for underground mining services, it is discarded on the ground of the haulage and flows to the lower level settlers. Sludge drifts down to the bottom of the settlers, where it is removed and deposited into mud dams. Clear water overflows at the top into a water channel [24]. This water then flows into the lower level clear water dams. This water is pumped to underground and surface cooling systems by the dewatering system.

2.2.2 Water- and air-cooling systems

As mentioned, water temperatures are reduced at FPs. Water fed to the FPs include mining water that has been pumped from underground and potable water that has been added to the WRS. Potable water is purchased from the local water board and added to the WRS if dam levels are low [25]. FPs are mainly located on the surface; however, in deep mines they may also exist underground [18].

Figure 17 shows the typical layout of a mine's water-cooling system. It consists of pre-cooling towers (PCTs), FPs, BACs and a variety of dams. Note that analysis and calculations for temperature changes fall beyond the scope of this research.

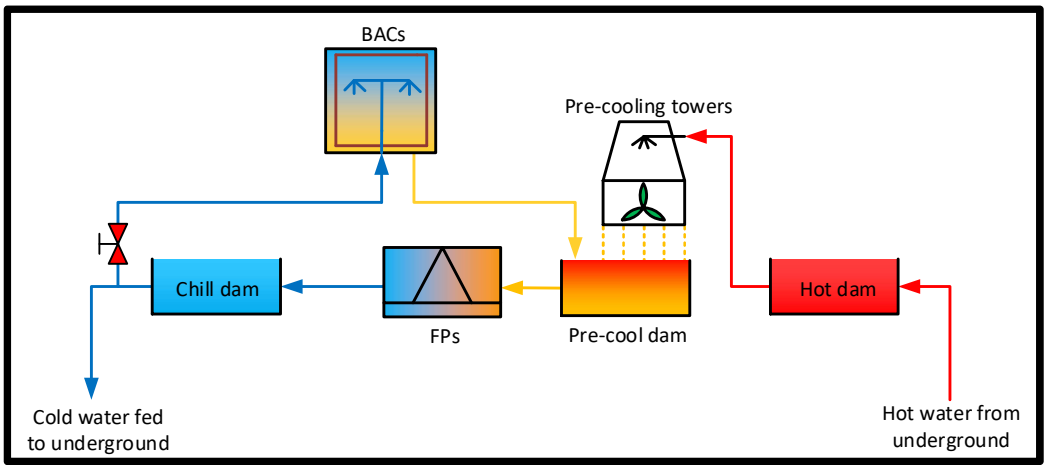

Figure 17: General refrigeration process of a mine

Water-cooling systems

Hot water, pumped by dewatering pumps, accumulates in hot storage dams. This water typically has temperatures of 28–33°C. Water is then pumped through PCTs by low powered centrifugal pumps. The pre-cooled water falls into a pre-cool dam (PCD), where the water temperature is approximately 2°C higher than the ambient wet-bulb (WB) air temperature. On the surface, the ambient WB air temperature in winter is normally 15–20°C and in summer 22–27°C. This results in PCD water temperatures of 17–22°C and 20–25°C for winter and summer months respectively.

From the PCD, water is fed through FPs. At these cooling systems, water is further cooled to a desired outlet temperature of 3–6°C [25]. The refrigeration process works on the principle of the vapour-compression cycle, which will be discussed in more detail in the following paragraph.

Figure 18 shows a flow diagram of the working principle of the vapour-compression cycle.

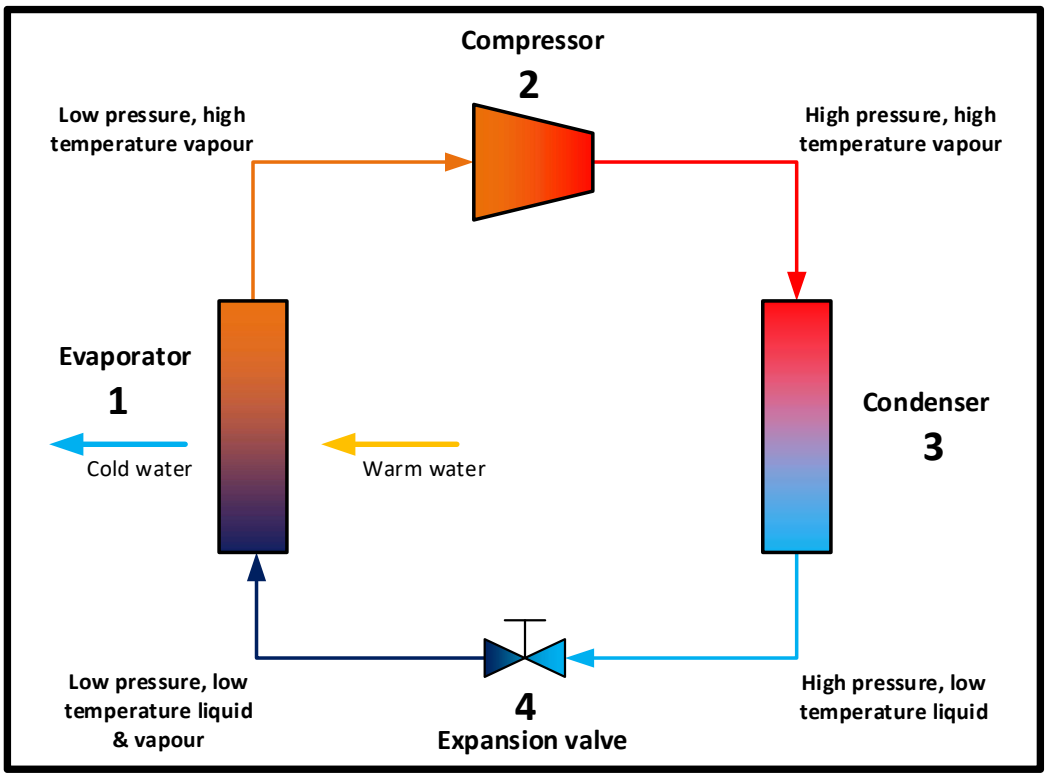

Figure 18: Vapour-compression cycle

The **evaporator** (point 1) is a shell-and-tube type HX. The refrigerant flows inside finned tubes. Hot water is fed over the tubes, where it transfers heat to the refrigerant. Mechanical work is brought into the cycle through a **compressor** (point 2). The cooling duty of the system can be regulated by varying compressor speed. The flow rate of refrigerant through the compressor affects the heat transfer rate, which is controlled by inlet guide vanes. When the refrigerant exits the compressor, it enters the **condenser** (point 3), which is also a shell-and-tube HX. Heat is removed from the refrigerant at the condenser. The condensed refrigerant then passes through an **expansion valve** (point 4). This valve decreases the pressure of the refrigerant to suitable levels upon entering the evaporator [23].

Air-cooling systems

After water has been cooled at FPs, it is deposited into chill dams. Cold water is then pumped through BACs to cool ventilation air. Within a BAC structure, heat is transferred from the air to the cold water. This results in air temperatures of 6–8°C WB [14]. It should be noted that cold water utilisation of surface BACs has no influence on the EC of a dewatering system. Circulation of water between surface BACs and FPs forms a loop, which is isolated from the water that is sent underground.

As discussed in Section 1.3, there are two types of HXs used in BACs: DC spray HX, and CC cooling-coil HX banks. Figure 19 represents a vertical surface BAC, which is of the DC spray HX type [26].

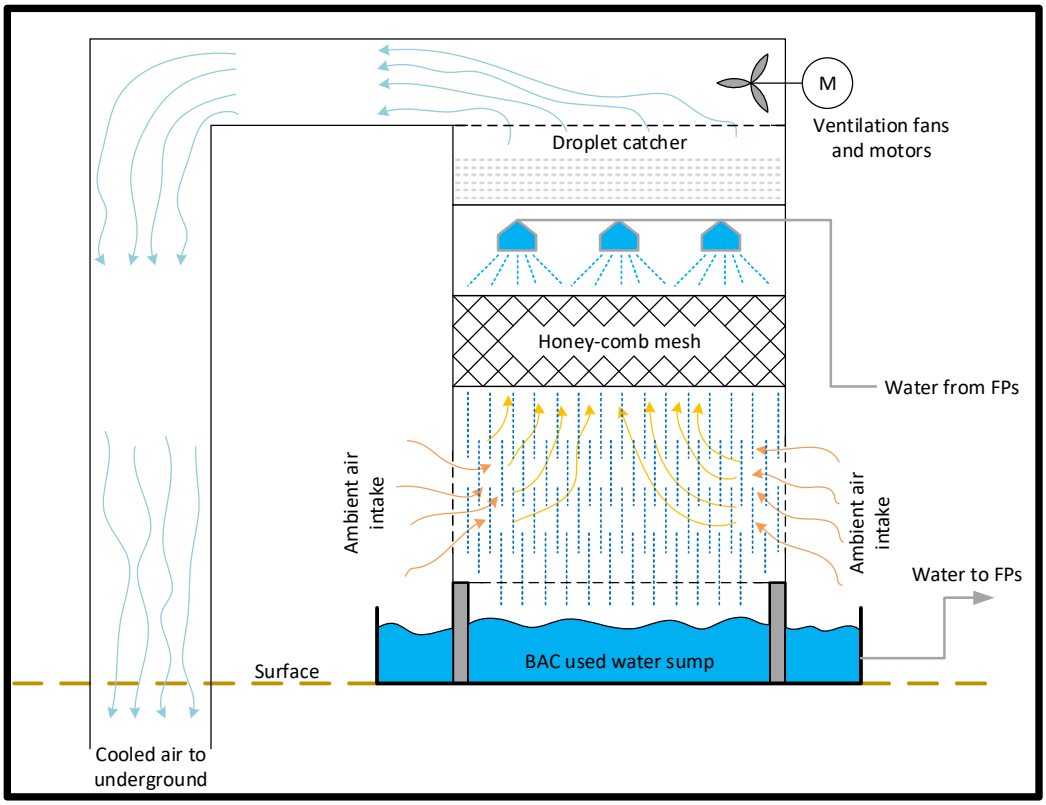

Figure 19: Surface vertical DC sprayer type BAC

A forced draft fan at the top of the structure ensures ambient air is sucked in at the bottom of the structure. Sprayer nozzles at the top half of the structure create small cold-water droplets. As the ambient air moves upwards through a honey-comb mesh, the droplets fall onto the mesh. Heat is transferred from the ambient air to the cold water. Heat exchange takes place through convection and condensation if the ambient air has a WB temperature higher than the temperature of the water [23]. Once heat has been transferred, the water is deposited into the BAC sump. Water is then pumped from the BAC sump to the FPs to be re-cooled.

Efficiencies and cooling duties of PCTs and BACs are influenced by several variables [23]:

- Water and air mass flow rate.
- Supply temperature of water.
- Inlet air psychometric conditions.
- Duration and contact area between the air and water droplets.

Figure 20 shows a horizontal underground DC spray chamber BAC.

[3]

Figure 20: Underground horizontal DC spray chamber

Most mines prefer to use horizontal spray chambers underground, because they can be installed in existing airways. Figure 21 represents a single stage of air-cooling at horizontal spray chambers.

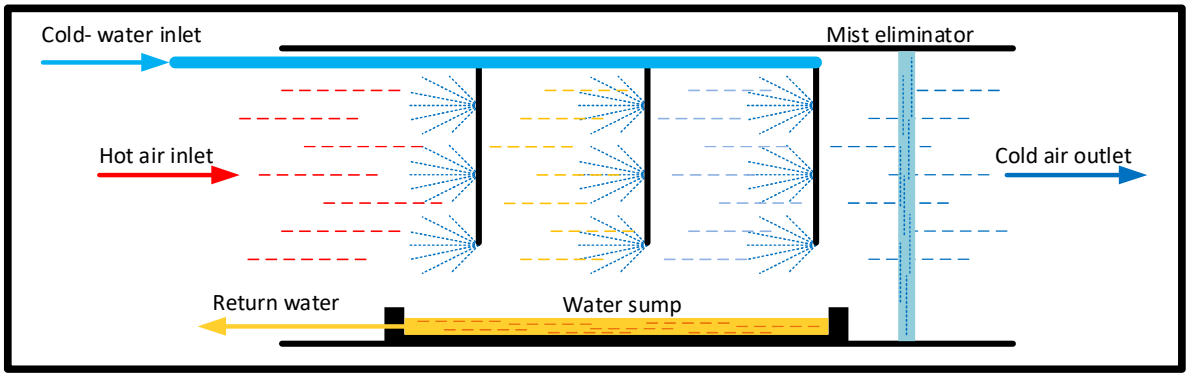

Figure 21: Single stage process of underground horizontal spray chamber

Cold water is forced through nozzles and water droplets are sprayed into the incoming air. Heat is removed from the air and the heated water falls into a sump underneath the nozzles. Typical horizontal spray chambers include two stages, where return water from the water sump is pumped through a second set of nozzles. When the cold air exits the spray chamber, it moves through a mist eliminator. It is then mixed with surface-ventilated air, while it moves to deeper mining levels. The used hot water in the sump is pumped to FPs to be re-cooled [26].

[3] Photo courtesy of www.bbegroup.ca.

One disadvantage of horizontal spray chambers is their limited maximum cooling capacity. Highly efficient horizontal systems achieve cooling capacities of about 3.5 MW, while vertical systems can achieve more than 20 MW [23]. A BAC's cooling duty can be determined by using Equation 1:

$$q = \dot{m}_w \times Cp_w \times \Delta T_w$$

Equation 1: BAC cooling duty

Where: $\dot{m}_w$ = mass flow rate of water $\left[\frac{kg}{s}\right]$

Cp_w = heat capacity of water $\left[\frac{kJ}{kg\ °C}\right]$

ΔT_w = change in water temperature $[°C]$

Figure 22 shows the design layout of an underground CBAC, which uses CC cooling-coil HX banks.

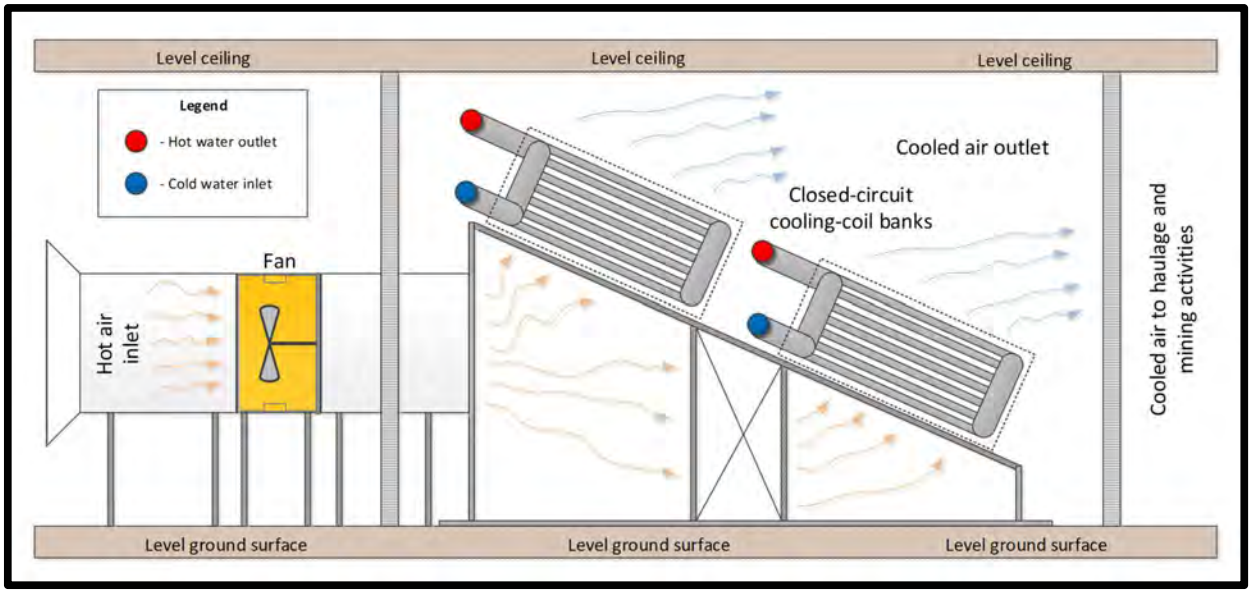

Figure 22: Design layout of CBAC with CC cooling-coil HX banks

At underground CBACs, air-cooling is achieved by using cold water at normal hydro-power pressure. Multiple cooling-coil banks can be installed to increase the surface area for heat transfer. An average cold-water flow rate of 40 ℓ/s results in a cooling duty of 2 000 kW per CBAC unit.

These modular CBACs, which use closed-coil technology, have an advantage over conventional DC spray-type BACs: they can be installed in a closed-loop system. CBAC water outlet pressures are high enough to be used for mining activities. Cooling duties of these modular units can reach up to 10 000 kW [27].

As discussed in Section 1.3 (see Figure 9), primary air-cooling from surface BACs may not provide effective cooling for mining levels deeper than 1.4 km. Secondary cooling solutions installed underground, which include horizontal spray chambers, can assist with cooling of levels deeper than this. However, there are working areas, typically on the furthest ends of the lowest levels, where even secondary cooling does not provide a safe and productive working environment. At cross-cuts where additional cooling is needed, tertiary cooling solutions are applied [28].

An example of a tertiary cooling system is shown in Figure 23, which is known as a CWC. The cooling capacity of these units vary from 100 kW to 500 kW, with operating pressures of up to 19 MPa [27]. A CWC consists of a CC cooling-coil HX bank, fan, and silencer [28]. It also has wheels to enable it to be moved on underground railway tracks.

[4]

Figure 23: Closed-circuit CWC

2.2.3 Underground water distribution

Water distribution is one of the most important processes that enables a gold mine to effectively extract ore. The amount of gold produced is directly proportional to cold water consumption [29] [16]; thus, if production increases, so does the water usage.

[4] Photo courtesy of www.manos.co.za.

Figure 24 shows a simplified layout of the chill water distribution network of gold mines. As mentioned, water is cooled at surface FPs and stored in surface chill water dams. Cold water is typically gravity-fed in pipe columns down the mineshaft.

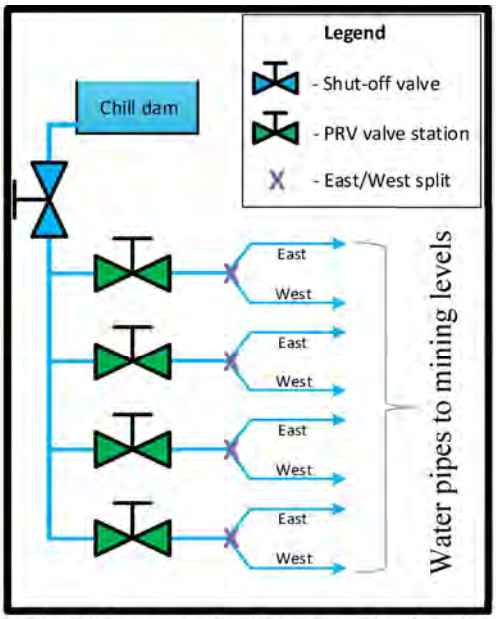

Figure 24: Simple layout of cold-water distribution network

The mining levels of deep-level gold mines can reach depths of up to 4 km. Water column pressure increases by approximately 1 000 kPa for every 100 m of vertical head [16]. Equation 2 can be used to prove this:

$$P_h = \rho \times g \times H$$

Equation 2: Hydrostatic pressure inside a vertical column

The density of water $\left(\rho_w \approx 1000 \frac{kg}{m^3}\right)$ and the gravitational acceleration $\left(g \approx 9.81 \frac{m}{s^2}\right)$ stay approximately the same with a change in *H*. Hydrostatic pressure only depends on vertical height; thus, if *H* increases, hydrostatic pressure increases [30]. Figure 25 shows the correlation between water pressure and vertical head.

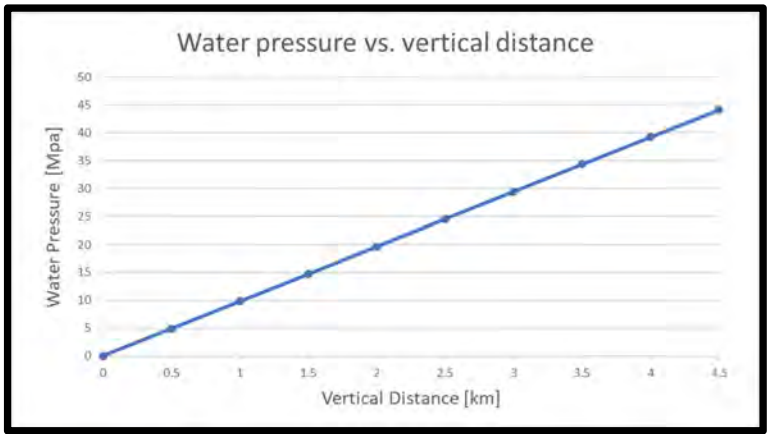

Figure 25: Vertical pressure compared to vertical distance (*H*)

If no pressure reducing strategy is applied as water descends to deeper levels, the pressure inside pipes will become too excessive and may burst them. Water pressure reduction methods include cascading dams, energy recovery systems, and pressure reducing valves (PRVs) [16]. High-pressure pipes are typically made of steel and insulated with materials such as expanded polystyrene and glass fibre [23].

As the water is fed down the mineshaft from surface chill dams, it either moves through a turbine (if installed) or through a pressure dissipater before it is deposited into underground chill dams. The turbine can either be used to generate electricity or be directly connected to the shaft of a pump to aid in transferring water from hot dams to the surface [24].

Figure 26 shows a simplified layout of a chill water distribution network, with a Pelton turbine and pressure dissipater installed. Heat is added to the water if it is fed through the pressure dissipater. Feeding water through the turbine does not affect water temperatures, which reduces refrigeration costs [24].

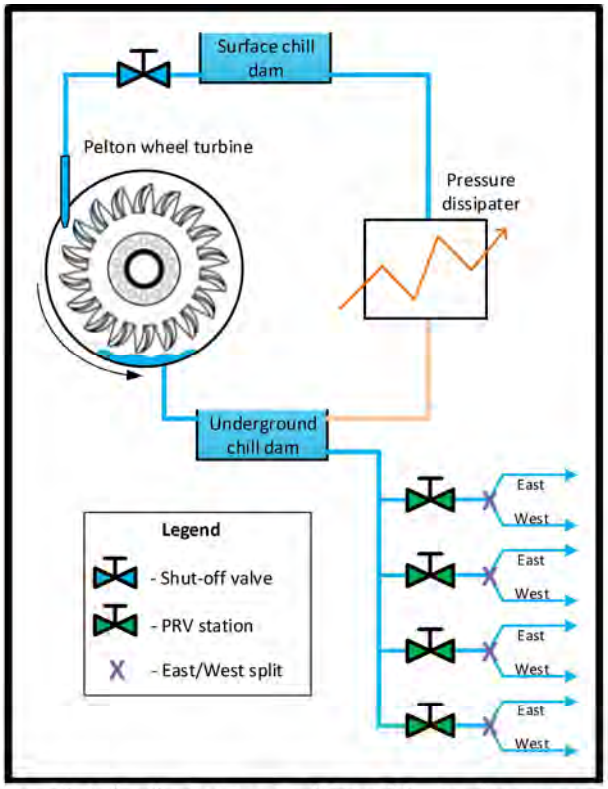

Figure 26: Cold-water distribution system, with turbine and pressure dissipater installed

In Figure 26, PRVs are installed on the entering main-line of each mining level. The water pressure within columns increases with depth. Lower mining levels may experience water pressures of up to 10 MPa. These excessive pressures can cause mining equipment that uses cold water to break. PRVs are installed to reduce the hydraulic pressure. To achieve this, energy is dissipated to the environment in the form of heat. This causes an increase in ambient air temperature around a PRV [31].

Figure 27 shows that several PRVs can be connected in series to create a PRV station. This system allows water pressures to be decreased in stages. Modern PRVs ensure a constant downstream pressure, irrespective of a fluctuating upstream pressure [31].

[5]

Figure 27: PRV station

Other energy recovery technologies used in a WRS in gold mines include three-chamber pipe feeder systems (3CPFS) and high-pressure U-tube systems. 3CPFSs are installed in horizontally excavated underground chambers. Figure 28 shows a photograph of a 3CPFS's piping in an excavated space.

[6]

Figure 28: 3CPFS hydro-lift chamber excavated space and pipes

[5] Photo courtesy of www.gaindustries.com.

[6] Image courtesy of Bluhm, Burton Engineering.

Figure 29 shows a simple component layout of a 3CPFS.

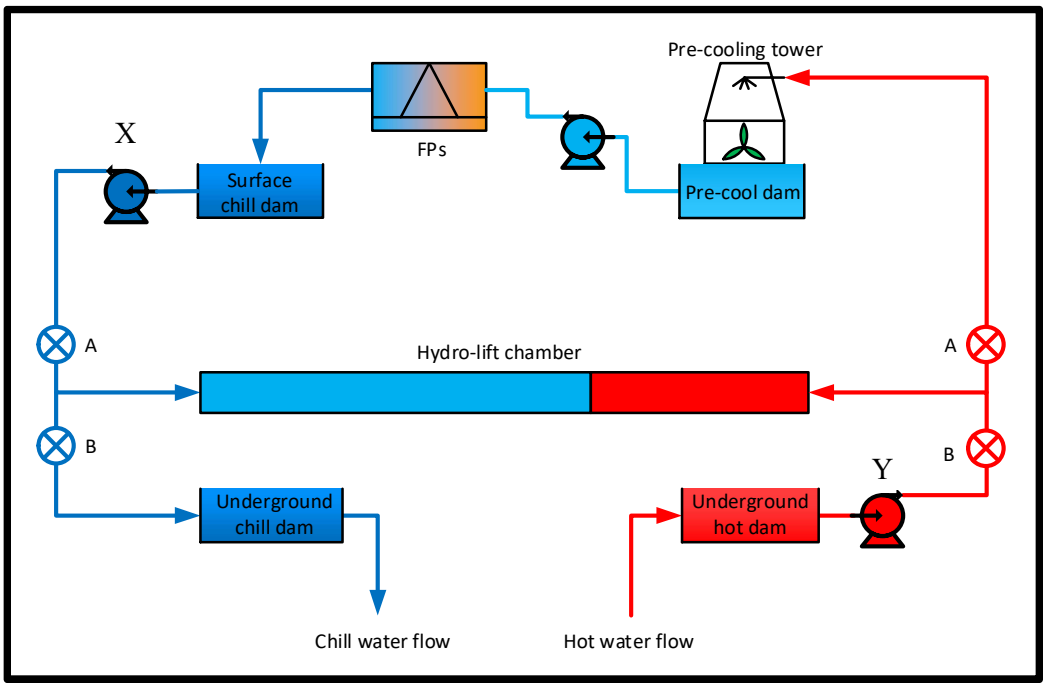

Figure 29: Simple component layout and operating principle of a 3CPFS

The following can be observed in Figure 29:

- There is no head component between the surface chill dam and surface PCD.
- Pump X is used to overcome pipe friction and is known as the booster pump.
- Pump Y is used to fill the chamber with hot water and is known as the filler pump.

The following points summarise the working principles of a 3CPFS:

1. Assume the chamber is initially filled with warm water.
2. Initially, both valves at positions A are open and both at B are closed. Pump X feeds cold water down the main shaft pipes and into the chamber.
3. This forces hot water out to the right, causing hot water to move upwards in the return shaft pipes.
4. With the chamber now filled with cold water, both valves at A close and both at B open. Pump Y forces hot return water into the chamber, ejecting the cold water into the underground chill dam.

The back-and-forth motion of hot and cold water is cancelled out by installing two additional hydro-lift chambers (see Figure 28). Valve sets are phased to open and close automatically. This enables a continuous flow into and out of the respective water dams [23].

A high-pressure (HP) U-tube system is the third type of energy recovery technology discussed in this dissertation. Figure 30 shows a simple component layout of an HP U-tube system. Cold water is fed from chill dam X to CC cooling-coil HX banks. It can be observed that dam X is at a higher elevation than dam Y. This causes water to flow through the HX banks and into dam Y. Water is then pumped to dam Z. Feasibility studies of HP U-tube systems concluded that it is not viable to use this technology if the height difference is greater than 1 km [18].

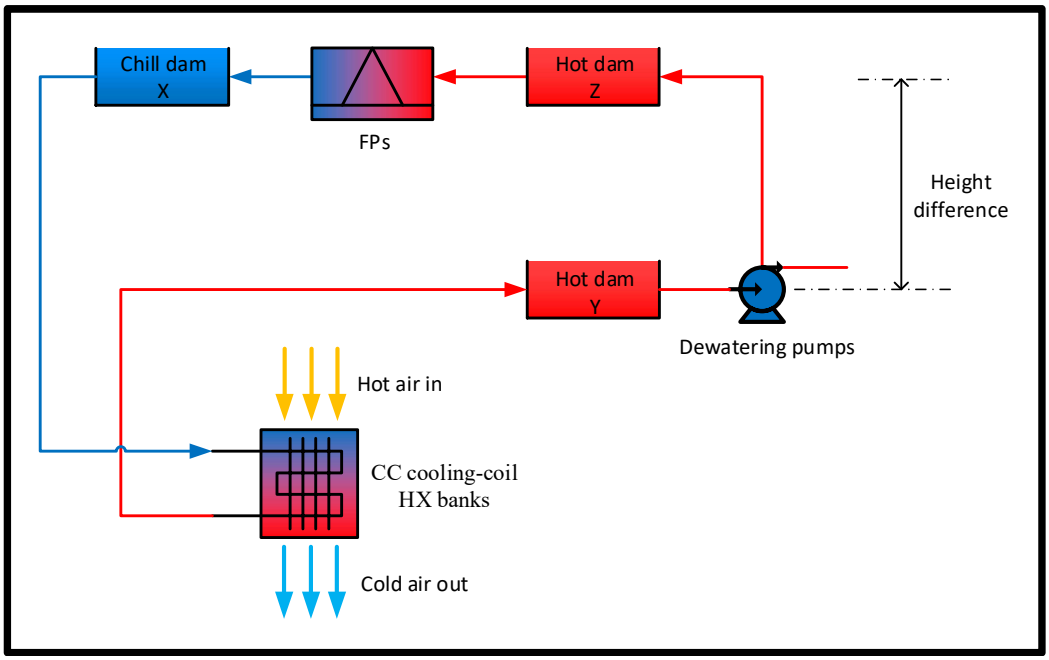

Figure 30: Simple component layout and operating principle of a HP U-tube system

2.2.4 Cold-water consumers

As mentioned, cold water is the predominant method used for air-cooling at BACs and CWCs. The following paragraphs discuss other mining activities that also consume cold water.

During the drilling shift, holes are drilled at the stoping areas. At the next shift, called the blasting shift, miners insert explosives in the holes. The shift then clears the mine and each shift-boss must confirm that all employees have been evacuated from underground. The explosives are then triggered, which causes the ore to shatter.

HP cold water is used as working fluid for hydro-power rock drills. Cold water sprays out at the front of the drill. This helps to cool the drill-bit and aid dust suppression during drilling. Figure 31 shows miners drilling holes to position explosives into mine walls.

[7]

Figure 31: Miners drilling holes with hydro-power equipment

The cleaning shift starts after the blasting shift. Figure 32 shows a miner spraying water into the air to suppress dust. This enables miners to enter a zone where blasting has recently occurred. As newly blasted rock temperatures are too high for human handling, water is also used to cool down the blasted rock. The ore can then be moved by hand, winches and loaders into loading boxes, for extraction to the surface.

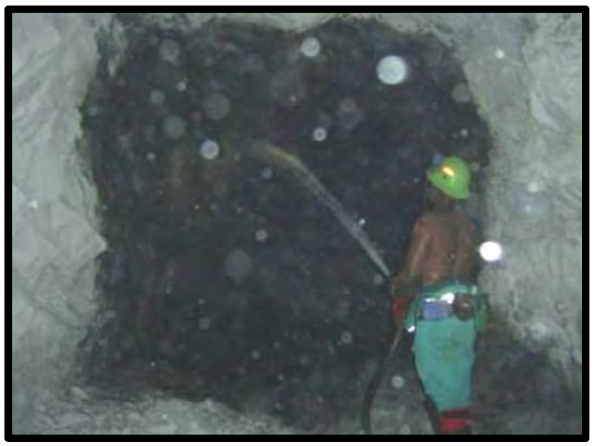

[8]

Figure 32: Miner cooling newly blasted rock

Fine pieces of rock, which are too small to pick up by hand after blasting, also need to be collected and moved into loading boxes. HP water is utilised by water cannons to sweep these rocks and fine gold particles to a central location. From this location, it is easily scraped up and moved into loading boxes.

[7] Photo courtesy of www.miningsafety.co.za.

[8] Photo from Master's dissertation of F.G. Taljaard, 2012.

Figure 33 shows a miner using an HP water cannon to sweep fine particles, which consist of gold and rock, to loading boxes.

[9]

Figure 33: Miner using an HP water cannon

After cold water has been used for mining activities and air-cooling at CWCs, it is discarded onto the ground of the haulage. It then flows into channels, which divert the water into settlers on the lower pumping levels. Figure 34 shows a picture of the top of a cylindrical-conical settler, with murky water flowing into it. This water consists of used mining water and fissure water.

[10]

Figure 34: Murky water flowing into a cylindrical-conical settler

[9] Photo from Master's dissertation of F.G. Taljaard, 2012.

[10] Photo courtesy from PhD thesis of J.C. Vosloo, [25].

Figure 35 is a representation of the working principles of a cylindrical-conical settler.

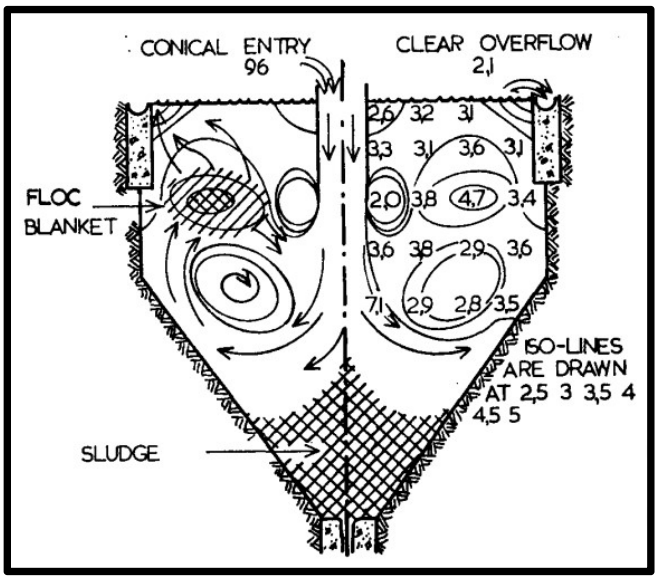

[11]

Figure 35: Working principles of cylindrical-conical settler

The purpose of a settler is to remove sludge, which contains solid particles such as mud, small rocks and fine gold particles, from water. Flocculent and lime is added to the water, causing suspended particles to bind to each other and accumulate at the bottom of the settler [32]. From here, it is drained and stored in mud dams. Clear water overflows into channels at the periphery of the settler and gets deposited into clear water hot dams.

Sludge is pumped by means of mud pumps to a surface metallurgical plant, where the gold is extracted from the mud. The remaining solid mass is then deposited into evaporation slime dams.

The clear water that accumulates in underground hot water dams are pumped to underground and surface cooling systems by dewatering pumps.

[11] Image courtesy of the Journal of South African Institute of Mining and Metallurgy

2.2.5 Dewatering systems

Mine dewatering systems house dewatering pumps and include hot storage dams, valves and return water piping. Cascading pump stations, consisting of hot dams and pumps connected in parallel, are used to transfer water from underground. Figure 2 on page 3 shows that a typical dewatering system can consume more than 24% of the total electricity demand on gold mines.

Installing multiple levels of pump stations result in smaller heads which pumps need to overcome. This decreases pump power consumption and increases station flow rates because pumps can operate in parallel. Multi-stage centrifugal pumps, with typical power consumptions of 1–3.5 MW, are used to pump water to the hot dams of the next pump station, with heads of 500–1000 m.

Centrifugal pumps can be connected in two configurations: series or parallel. A series configuration achieves a greater head, whereas connecting pumps in parallel results in an increased flow rate [33]. Figure 36 shows a basic layout of a typical cascading dewatering system, which displays the characteristics discussed in the previous paragraph.

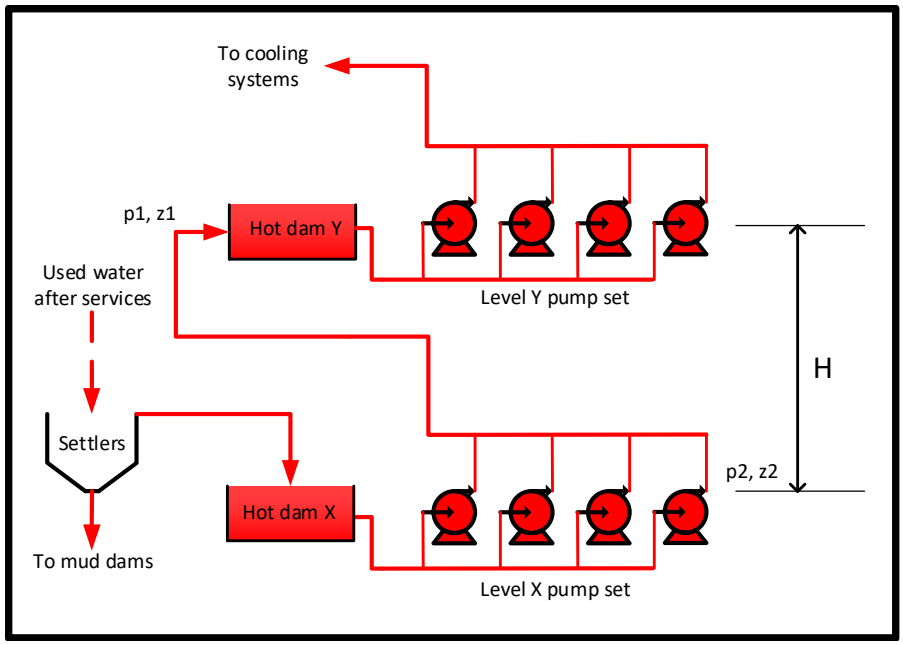

Figure 36: A typical cascaded pumping process of a gold mine dewatering system

Figure 37 shows a cut-out view of the inner workings of a multi-stage centrifugal pump. A typical dewatering pump consists of five to ten stages and can achieve static heads of 120–1800 m and flow rates of 36–278 ℓ/s [34].

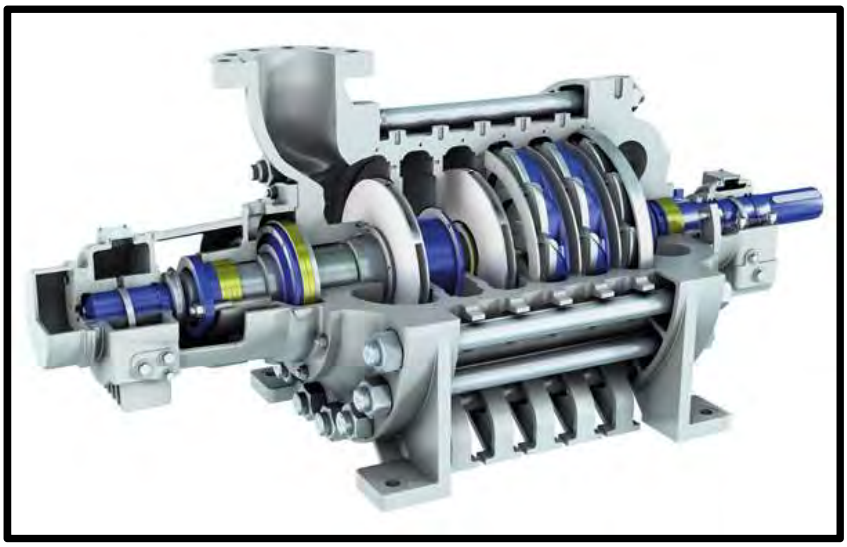

[12]

Figure 37: Inner workings of a multi-stage centrifugal pump (cut-out view)

The fundamentals of fluid mechanics can be applied to calculate pump characteristics such as flow rate and power consumption. The following paragraphs discuss pump performance curves and equations for calculating pump power consumption.

Pump characteristics

Pump characteristics are usually obtained from data sheets. Figure 38 displays an example of a data sheet that contains information about the pump head (H) at different volume flow rates (Q). The shape of these curves is determined by the design and physical attributes of the pump. The head and flow rate the pump needs to achieve determine its dimensions [35].

[12] Image courtesy of www.sulzer.com.

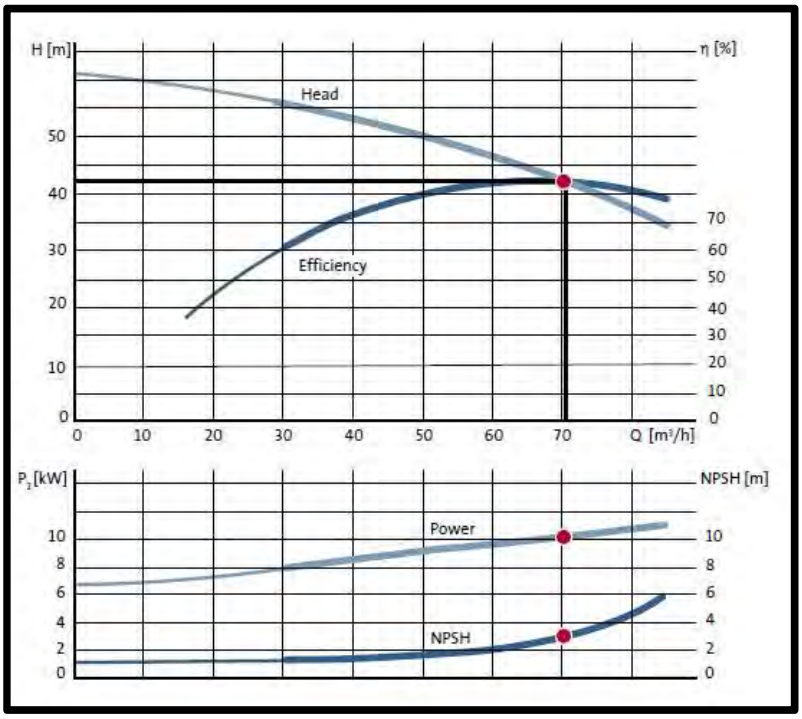

[13]

Figure 38: Example of pump data sheet

In Figure 38, head (H) is shown as a function of volume flow rate (Q). Head can be calculated by Equation 3 below (refer to Figure 36) [35] [36] [24]:

$$\boldsymbol{H = z_1 - z_2 = \frac{\Delta p_{tot}}{\rho_{fluid} \times g} = \frac{p_2 - p_1}{\rho_w \times g} \quad [m]}$$

Equation 3: Head from differential pressure

Where: p_1, z_1 = pressure and elevation of level Y $[Pa]$

p_2, z_2 = pressure and elevation of level X $[Pa]$

g = gravitational constant $\left[\frac{m}{s^2}\right]$

ρ_w = water density $\left[\frac{kg}{m^3}\right]$

[13] Graph courtesy of net.grundfos.com.

Pump power consumption depends on the density of the fluid being pumped. Fluid density is a function of temperature. Power curves are generally based on a standard fluid density of 1000 kg/m^3, which corresponds to the density of water at 4°C [37].

Pump power consumption can be calculated by using Equation 4 [35] [36] [24]:

$$\boldsymbol{P = \frac{\dot{m} \times g \times H}{\eta_p}} \quad [\boldsymbol{W}]$$

or

$$\boldsymbol{P = \frac{\rho_w \times g \times H \times Q}{\eta_P}} \quad [\boldsymbol{W}]$$

Equation 4: Pump power consumption

Where: $\dot{m} = \rho_w \times Q \quad \left[\frac{kg}{s}\right]$

$Q =$ volume flow rate of water $\left[\frac{m^3}{s}\right]$

$\eta_p =$ total efficiency of entire pump system $[\%]$

Pumps in a parallel configuration

Gold mines in SA circulate approximately 200–600 ℓ/s, or 17–52 Mℓ per day, depending on the number of operations [14]. Continuous adjustment of water supply is needed to ensure demand is met and that dam levels fluctuate within pre-defined ranges.

Figure 39 shows an example of dewatering pumps connected in a parallel configuration.

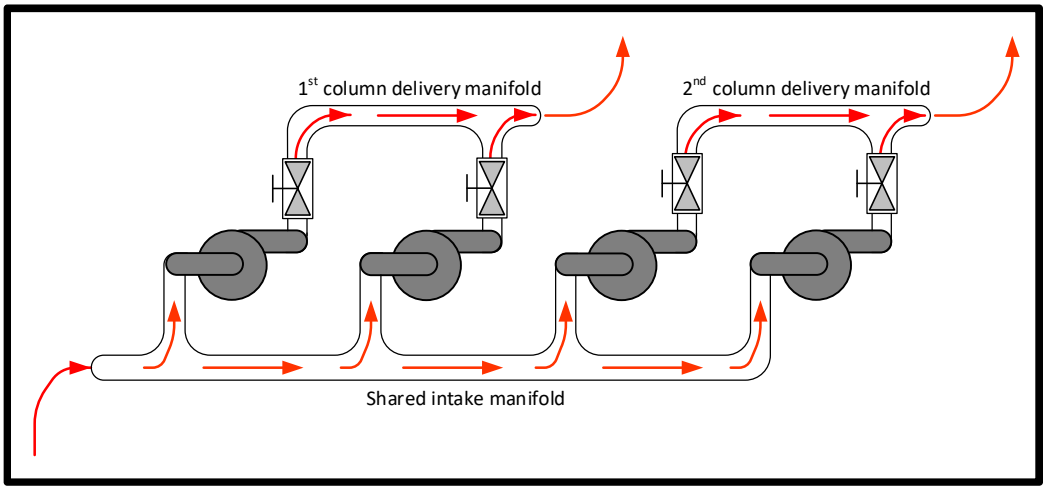

Figure 39: Pumps operating in parallel with two delivery columns

It can be observed that all pumps are connected to a single intake manifold. Two pumps are connected to a shared delivery manifold, which means two pumps are installed per discharge column. A non-return valve is installed at the outlet of each pump.

It is not necessary to install pumps with identical characteristics; however, it is important for all pumps connected to a shared discharge column to have matching heads. This is to prevent pump block-in at low flow conditions [38]. If specified pressures of non-return valves are lower than the delivery pressure of a pump, a valve may close and hydraulic shut-off will occur [24].

When adding pumps to a single discharge column, the flow rate within that column will increase with each start-up of a pump. An increase in flow rate results in an increase in frictional force on the inner wall of the pipe column. This results in an increase in water pressure drop over the length of the column.

The Darcy-Weisbach equation can be used to calculate a relationship between pressure and flow rate:

$$\frac{\boldsymbol{\Delta p}}{\boldsymbol{L}} = \boldsymbol{f_D} \times \frac{\boldsymbol{\rho_w}}{\boldsymbol{2}} \times \frac{(\boldsymbol{v})^{\boldsymbol{2}}}{\boldsymbol{D}}$$

Equation 5: Darcy-Weisbach equation

Where: $\frac{\Delta p}{L} =$ pressure drop per unit length $\left[\frac{Pa}{m}\right]$

$f_D =$ Darcy friction factor $[-]$

$v =$ flow velocity – direct relation to flow rate $\left[\frac{m}{s}\right]$

$D =$ hydraulic diameter of the pipe $[m]$

By using Equation 5, the following can be observed for real-world application for two pumps running on a single column:

- The variables that stay constant are L, ρ_w and D.
- Δp increases.
- $f_D = \frac{64}{Re}$ decreases, because the Reynolds number (Re) increases with an increase in frictional force on the pipe inner wall.
- With a decrease in f_D and an increase in Δp, v must increase to validate Equation 5.

Figure 40 shows a combined characteristic curve for pumps connected in parallel. It visually represents the effects discussed above by using the Darcy-Weisbach equation. It can be observed that if two pumps are running simultaneously on one column, the maximum flow rate will not be achieved. This is due to the Darcy friction factor being present in real-world application of pumps operating in parallel. It is recommended that the pumps run on separate columns to maximise the flow rate.

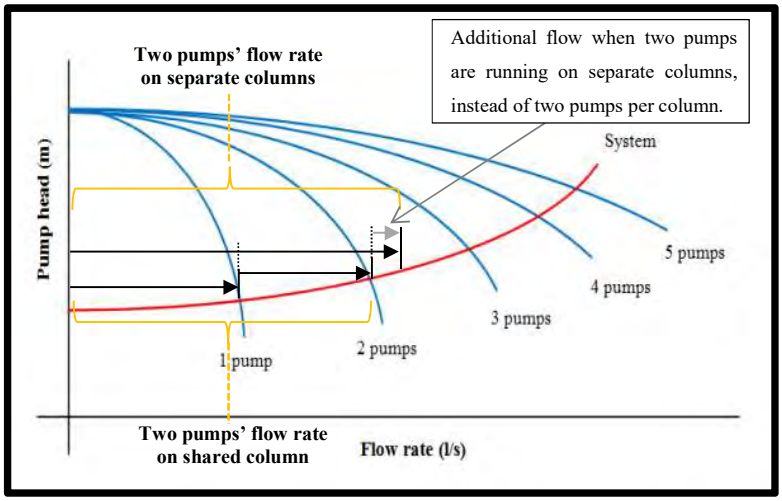

[14]

Figure 40: Combined pump characteristic curve for pumps connected in parallel

2.3 Techniques to reduce water consumption

As mentioned, cold water is used for cooling of ventilation air and mining activities. The scale of mining operations determines the amount of water consumption. A direct relationship exists between water consumption and gold production.

[14] Graph from the Master's dissertation of A.P. van Niekerk.

Figure 41 shows an example of a scatter plot for water pumped through the dewatering system versus gold production.

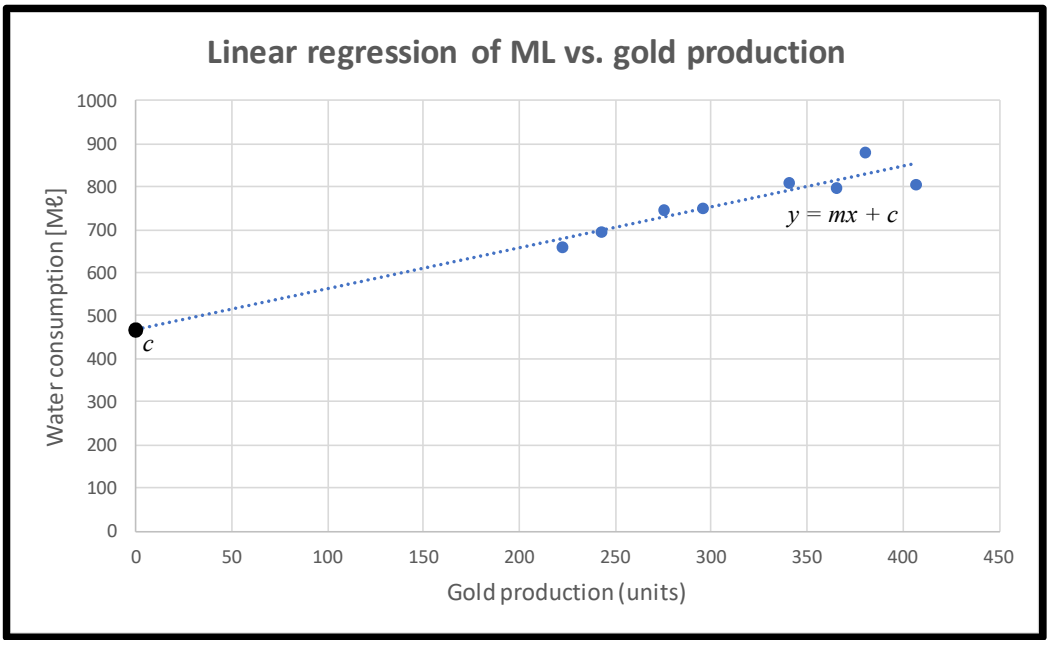

Figure 41: Example of water consumption versus units of gold produced, with regression line

It can be observed that the regression line plotted on Figure 41 does not intersect at the origin. This is because there is a baseload water consumption aspect on gold mines. This is where water is only used for cooling of ventilation air and no gold is produced. This baseload can be estimated by the value "*c*" from the regression line equation. In this example, the baseload water consumption should be approximately 480 Mℓ per month.

WSO techniques were developed to minimise water supply to underground. Effective implementation of these techniques will decrease the baseload water consumption, which means the regression line will be shifted downwards. The effect of this is a decrease in water consumption per unit of gold produced. These techniques are discussed in the following sections.

2.3.1 Water leak management

Water leakage is one of the largest problems a mine WRS experiences. The underground water distribution network consists of kilometres of pipes, which are generally made of steel. Pipes are exposed to humid air and over time they start to rust. If maintenance on the pipe network is neglected and rust becomes excessive, cracks can form on the pipe walls. This eventually leads to water leakage [31].

Leaks can also be caused by high water pressures within a pipe or manufacturing defects. Cold water column leaks result in decreased refrigeration efficiency, while leaks on hot water columns result in pumping energy losses. Valve- and gasket leaks exist due to incorrect installation. Miners may also forget to turn of the cold-water supply to hoses when they are finished working. Figure 42 shows water leaks on a pipe and Figure 43 shows cold water being wasted through an open hose [31].

[15]

Figure 42: Water leaks on pipe

[16]

Figure 43: Cold water hose left open

The best way to identify leaks is by conducting a leak audit. Mining employees and/or personnel from an ESCO needs to physically check every section of the mine to find water leaks. Notes should be taken to describe the type, size and location of each leak. It is recommended that boilermakers fix the largest leaks first, which will result in an immediate increase in the EE of water supply [31].

[15] Photo courtesy of www.climatetechwiki.org.

[16] Photo from Master's dissertation of A. Botha, 2010.

The volume flow rate of a water leak can be quantified by using Bernoulli's theorem:

$$Q = \alpha A_t \sqrt{\frac{2(P_{inside} - P_{outside})}{\rho_{water}}}$$

Equation 6: Bernoulli's Theorem

Where: Q = volumetric flow rate $\left(\frac{m^3}{s}\right)$

P_{inside} = pressure inside pipe (Pa)

$P_{outside}$ = pressure outside pipe (Pa)

A_t = area of leak through which flow occurs (m^2)

α = fluid flow coefficient (-)

ρ = fluid density $\left(\frac{kg}{m^3}\right)$

For example, the flow rate of a 20 mm-diameter hole in a pipe, flow coefficient of 0.7, inner water pressure of 1400 kPa and outside air pressure of 110 kPa:

$$Q = 0.7 \left(\pi \times \left(\frac{0.02}{2}\right)^2\right) \sqrt{\frac{2(1400000 - 110000)}{1000}} \approx 11.2 \frac{l}{s} \approx 965 \frac{kl}{day}$$

Figure 44 shows the flow rate of a water leak versus the diameter of the hole, with the physical parameters above.

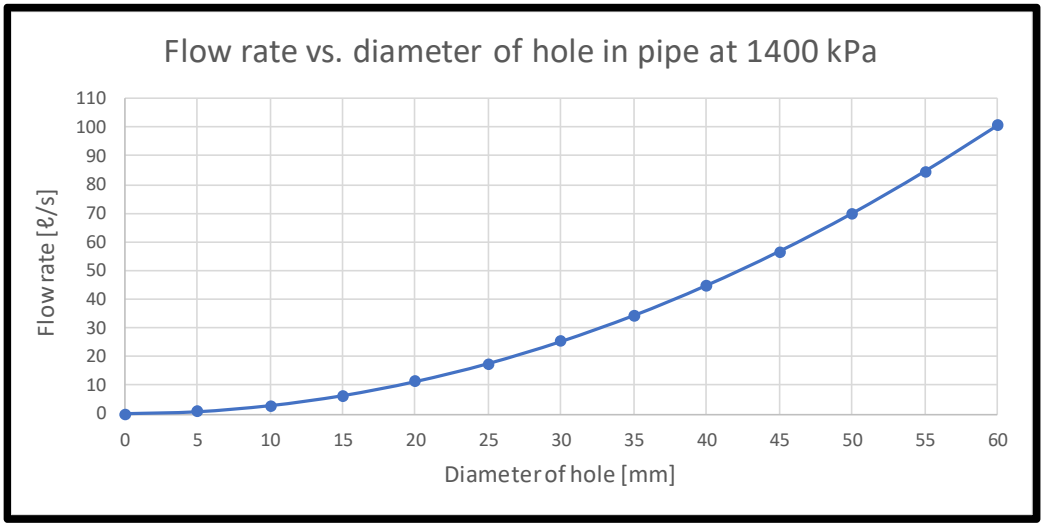

Figure 44: Flow rate vs. size of water leak

2.3.2 Stope isolation control

A stope is a space left open once the ore extraction process is done. As mining activities progress, the stope is often filled with tailings (backfilling) or, when strength is needed, a mixture of tailings and cement. The stopes are accessed by branches that extend from main underground walkways. The cold-water pipes are located along the walkways and tap-offs to each cross-cut are installed to supply cold water to the stopes with pressures of 1000–1600 kPa.

Cold water is utilised at the stopes for air-cooling and mining activities, which includes drilling, cleaning, sweeping, and dust suppression. Mining activities take place in the following daily shifts [31]:

- **Morning – drilling shift:** Holes are drilled in rock surfaces, so that explosives can be placed in them.
- **Afternoon – blasting shift:** After the holes have been drilled, all miners are cleared from underground and explosives are triggered.
- **Evening – cleaning shift:** After the hot virgin rock has been blasted, the ore is cooled and moved to loading boxes for extraction to surface.

Cold water is only used during drilling and cleaning shifts. Water supply can be shut off to mining activities during blasting shift. The supply of cold water to air-cooling systems should not be stopped because a continuous supply of cooled air should be ventilated through the underground levels.

The following types of stope isolation control methods can be installed:

- Manual stope isolation valve control.
- Automatic stope isolation control method.

The manual stope isolation method does not require a large amount of initial cost expenditure and no actuators have to be installed on the valves. The operating principle for manual isolation valves is as follows:

1. After the drilling shift, the last miner that exists the stoping area closes the valve.
2. When the cleaning shift starts, the first miner entering the stoping area opens the valve.

The effective application of manual valve control depends entirely on the discipline of the miners. Miners often forget to turn off the water supply when they are finished with the morning shift. This method is therefore not recommended [31].

The automatic control stope isolation method requires additional installation of actuators on the valves and the necessary control instrumentation to regulate these valves. Automatic stope isolation valves can be controlled as follows:

- Through timers that regulate according to shift schedules.
- By using the mine's centralised blasting system.

Timers automatically switch the cold-water supply on and off at pre-defined times. Most mines have a time schedule for the aforementioned three shifts. The timers switch off cold-water supply at the end of the morning shift period and switch on again at the start of the cleaning shift. This technique can sometimes cause problems, because some mines do not consistently follow their schedules [31].

The second technique is to make use of the mine's centralised blasting system. When a section is cleared for the blasting shift, each section's shift-boss has a clearance key that is inserted into a clearance box. This triggers a valve solenoid which switches off the water supply. The key is removed when the cleaning shift starts, restoring water supply to that section. The advantage of this method is that it is not dependent on a pre-defined time schedule [31].

The stope isolation method results in a significant water supply reduction within the blasting shift. The blasting shift period is normally from 14:00 to 22:00, which results in eight hours of water reduction.

2.4 Previous studies on mine water reticulation systems

The following studies were previously conducted on mine WRSs:

- Applying LS techniques to dewatering pumps.
- Increasing LS performance of a mine dewatering system.
- Analysing the effects of constraints on LS performance of a mine dewatering system.
- Analysing the effects of WSO on a mine WRS.

Previous studies are described per the following criteria:

- Objectives.
- Methodology.
- Results.

The studies discussed in the following sections investigated better management strategies of TOU schedules.

Study 1: [39]

As mentioned in Chapter 1 , energy tariffs are not the same throughout the day. Schoeman et al. investigated cost savings of a mine dewatering system when reducing peak TOU load. An optimised control philosophy was developed, which enabled better pump automation and scheduling.

The LS control philosophy was implemented on dewatering pumps and the system was tested for several months. The predicted cost saving per annum was calculated. Energy management software (EMS) was used to monitor and control the dewatering pumps. Automatic starting and stopping of pumps was implemented in the EMS programme according to pre-determined dam levels [39].

Table 4: Study 1 results

	TOU optimisation for Study 1		
	Scaled baseline average load [kW]	Optimised average load [kW]	Difference [kW]
Off-peak	14 369	16 153	-1 784
Standard	13 291	14 544	-1 253
Peak	9 536	3 394	6 142

Figure 45 shows the optimised power profile versus the baseline for Study 1.

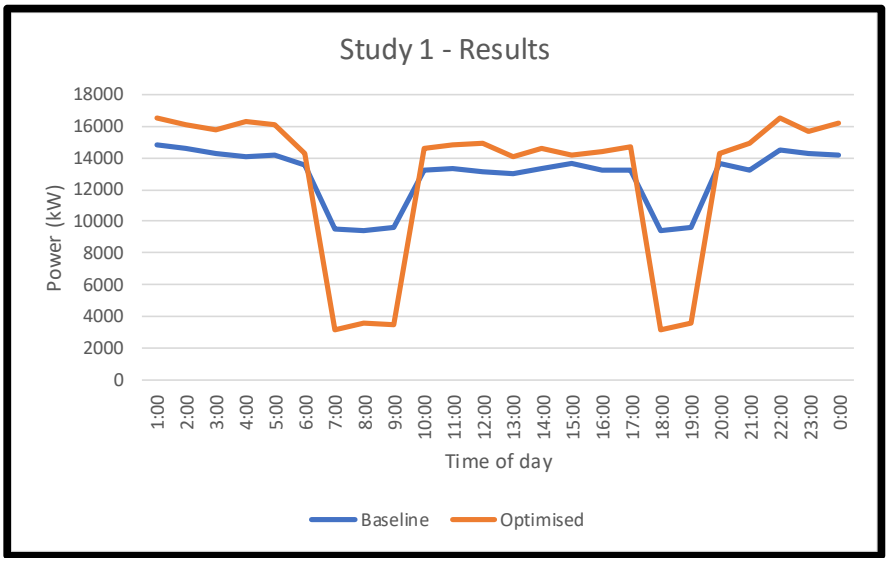

Figure 45: Optimised power profile for Study 1

Table 4 includes the results of this study. An average LS of **6 142 kW** for morning and evening peak periods was achieved, with an increase of 1 784 kW load to the off-peak period and 1 253 kW to the standard period. The scaled baseline versus the optimised power profile is shown in Figure 45. According to 2017–2018 Megaflex tariffs (see Appendix B), the total cost saving predicted per year was **R7.4 million**.

Study 1 did not focus on optimising preparation and comeback load. TOU standard time was not taken into consideration during optimisation and when LS was performed. Standard time tariffs are almost double that of the off-peak rates, which means the LS can be optimised when more load is shifted to off-peak periods, rather than standard periods [16] [39]. Study 2 addresses this problem.

Study 2: [16]

Cilliers *et al.* considered the results in Study 1 and optimised existing LS strategies to maximise savings achievable from LS on the dewatering pumps. The study focused on optimising preparation and comeback load of LS on mine dewatering systems. Two case studies were investigated for re-optimisation.

The results of Study 2, case study A, are included in Table 5:

Table 5: Optimised power profile for Study 2, case study A

	TOU optimisation for Study 2, case study A		
	Scaled baseline average load [kW]	Optimised average load [kW]	Difference [kW]
Off-peak	8 948	12 158	-3 210
Standard	10 110	7 691	2 419
Peak	38	221	-183

Figure 46 shows the optimised power profile versus the baseline for Study 2, case study A.

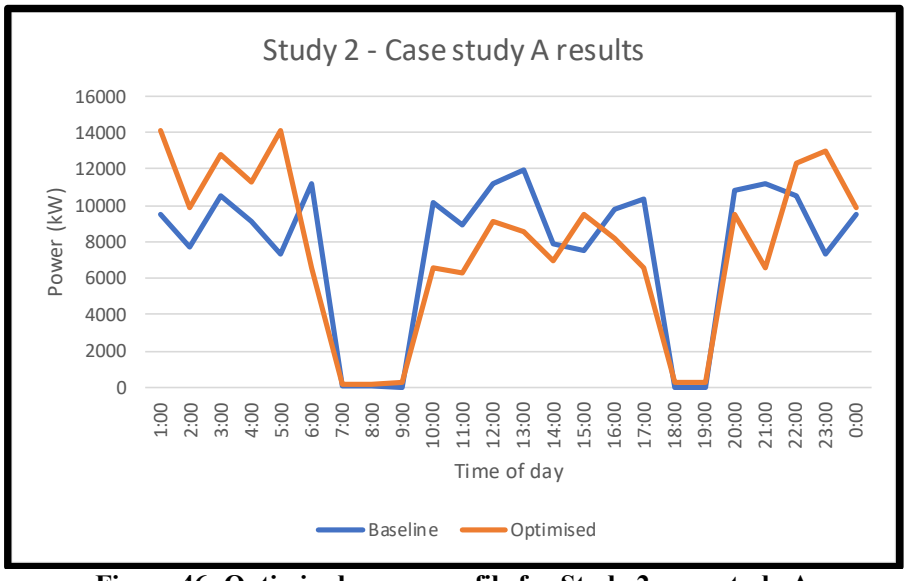

Figure 46: Optimised power profile for Study 2, case study A

The average peak LS for case study A decreased when further optimisation was completed. However, this difference is small compared to the total daily power consumption. The scaled baseline versus the optimised power profile for case study A is shown in Figure 46. According to 2017–2018 Megaflex tariffs, which are included in Appendix B, the total cost saving predicted per year is **R1.59 million**, even if the LS decreased after optimisation.

The results of Study 2, case study B, are included in Table 6:

Table 6: Optimised power consumption results for Study 2, case study B

	TOU optimisation for Study 2, case study B		
	Scaled baseline average load [kW]	Optimised average load [kW]	Difference [kW]
Off-peak	2605	3605	-1000
Standard	3382	2655	727
Peak	0	0	0

Figure 47 shows the optimised power profile versus the baseline for Study 2, case study B.

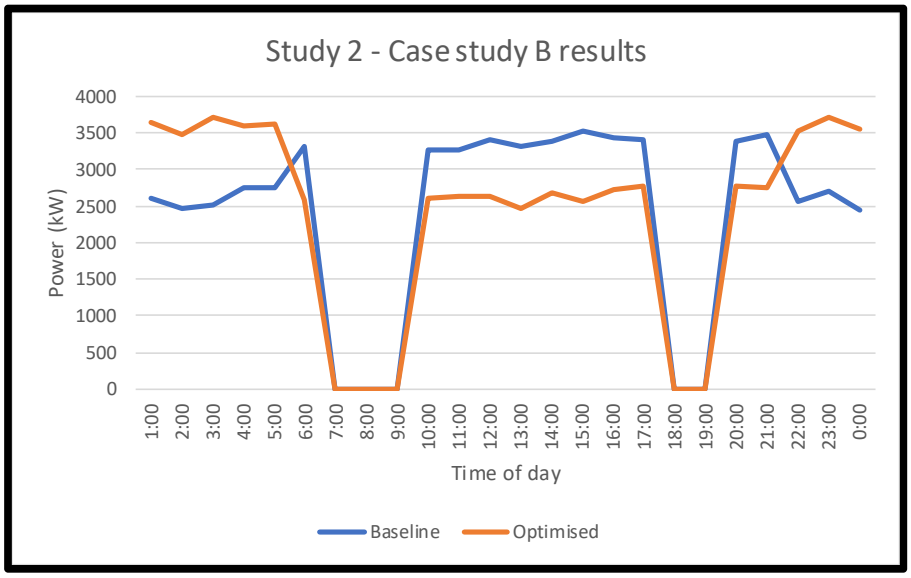

Figure 47: Optimised power profile for Study 2, case study B

The average peak LS for case study B stayed the same after further optimisation. An average of 727 kW load was shifted from standard time to off-peak periods. The scaled baseline versus the optimised power profile for case study B is shown in Figure 47. According to 2017–2018 Megaflex tariffs, the total cost saving for shifting **8 MWh** of electrical energy out of standard periods to off-peak periods is predicted to be **R536 660** per annum.

Study 3: [40]

Stols *et al.* investigated the effects of dewatering system constraints on energy costs of running dewatering pumps. Simulations were included to determine the cost saving potential of reducing these constraints. Manual LS was completed to obtain actual data and to compare it to simulations to verify the accuracy of the data.

The aim of this study was to use simulations to predict cost savings for the following improvements on constraints of the dewatering system:

- Cleaning of hot dams to increase volume capacity.
- Increasing pump efficiencies.
- Implementing LS procedures for morning and evening peak periods.
- Applying a 10% WSO process to decrease water consumption.

The predicted cost savings results are included in Table 7:

Table 7: Predicted annual cost savings for simulated improvements of Study 3

Constraint improvement	Individual annual predicted saving	Cumulative annual savings
Normal operation	R0	R0
Increase dam capacities	R514 570	R514 570
Increase pump efficiencies	R8 317 821	R8 832 391
Enable evening LS	R2 350 672	R11 183 063
Enable morning LS	R2 752 131	R13 935 194
Optimise water supply	R7 637 545	**Total = R21 572 739**

The studies 4 and 5, discussed below, investigated WSO techniques on a mine WRS.

Study 4: [29]

Vosloo *et al.* conducted a study on WSO of a mine WRS. The objectives of this study were to reduce energy use through WSO. LS on the dewatering system and FPs were applied to achieve additional cost savings.

EMS software was used to control and optimise the dewatering system and FPs in combination, instead of individually. FPs were used to generate a surplus of cold water before peak periods, enabling increased LS performance. A combination of pump scheduling and turbine utilisation enabled better performance of pump LS [29].

A 2.43 MW morning-peak LS and 3.15 MW evening peak LS were realised. Based on the 2017–2018 Megaflex tariffs (see Appendix B), the total cost saving for the LS of Study 4 was predicted as R1.74 million per annum. LS on FPs resulted in an average peak load reduction of 1.71 MW, amounting to a cost saving of R1.57 million per year.

WSO was also implemented during blasting shifts and an average daily energy saving of 4.8 MWh was achieved, which amounts to a predicted yearly cost saving of R1.38 million [29]. The total predicted cost saving for this study amounted to approximately **R4.7 million** per annum.

Table 8 includes the results for LS on the dewatering system and FPs.

Table 8: Results of Study 4 [29]

	Dewatering system & FPs optimisation					
	Dewatering scaled baseline average load [kW]	Dewatering optimised average load [kW]	Difference for dewatering [kW]	Refrigeration scaled baseline average load [kW]	Refrigeration optimised average load [kW]	Difference for refrigeration [kW]
Off-peak	3 816	2 282	1 534	6506	7114	-608
Standard	3 238	5 619	-2 381	6772	7268	-496
Peak	3 046	261	2 785	6593	4883	1 710

Study 5: [31]

Botha investigated the optimisation of mine water supply. WSO was achieved by controlling supply valves on various mining levels [31]. The objective of the study was to minimise water usage during periods of the day when less water is required, such as during the blasting shift. By reducing the amount of water sent down the mineshaft during these periods, less water needs to be pumped through the dewatering system. Cost savings were achieved by reducing the daily electricity consumption for the dewatering system, due to a decrease in pump operational time.

EMS was used to monitor and evaluate control valve data, such as pressures and flow rates. PID controllers adjusted the control valve positions according to a desired pressure set-point, as required by machinery.

Botha investigated two case studies. Case study A resulted in an average power reduction of 400 kW over the course of a day. This resulted in an energy saving of **9.6 MWh per day** [31]. For case study B, a mine was identified with a substantial number of water leaks in the WRS. By completing underground leak audits, most of the large leaks were repaired and a decrease of 7 Mℓ of daily water consumption was achieved. This resulted in a decrease in EC of around **73 MWh per day** [31].

The studies discussed in this section, which focused on LS of dewatering pumps, created optimised LS control strategies to achieve increased cost savings. The aforementioned studies, which focused on WSO techniques, used WSO methods to increase energy and cost savings on mine WRSs.

The limitations of these investigations are that they only create savings opportunities for a limited period of the day. LS achieves the greatest cost saving within peak periods, and mostly in winter months. WSO methods also only decrease water supply for a limited period of 5–8 hours during the blasting shift. There is a need to decrease the overall daily water demand for a WRS. This will result in increased energy and cost savings, compared to the traditional methods investigated in Studies 1–5.

2.5 Chapter summary

WRSs house the FPs, which typically consume more than 30–35% of a typical SA mine's total energy demand. Water that has been pumped from underground is cooled at FPs and then diverted to air-cooling systems and underground mining activities. The purpose of BACs is to cool down and dehumidify ambient air. This cooled air is forced into the mineshaft through ventilation and extraction fans. This ensures a safe and productive underground working environment for the mine's employees.

A mine's water distribution network transfers cold water to air-cooling systems and mining activities. These mining activities make use of specialised equipment that use water at a specific pressure. If water pressures are excessive, the equipment can be damaged. For this reason, PRVs are installed on the main-line of each level in a mine.

Used mining water and fissure water flows into lower level hot dams. This water is pumped back to surface and underground FPs by a dewatering system. The dewatering system's centrifugal pumps are energy intensive, creating opportunities for potential energy and cost saving strategies to be applied.

Techniques to reduce water consumption on in gold mines include water leak management and stope isolation control. The humidity underground causes steel pipes to rust over time and if no maintenance work is performed, these pipes may start to leak. The best way to find leaks is by conducting a leak audit, in which personnel inspects each level of a mine to identify water leaks. Stope isolation valves are installed to turn off water supply to mining activities when there is no water demand. This is typically done after the morning shift because blasting does not require water. The valves are opened again when the cleaning shift starts.

These studies achieved their outcomes of reducing EC of components in the WRS. Observing the methods these studies used to evaluate energy and cost savings indicate a need for an improved methodology. The following chapter will describe the processes and steps taken to create such a methodology.

CHAPTER 3 METHODOLOGY TO EVALUATE RECONFIGURED MINE WATER RETICULATION SYSTEMS

[17]

"The ones who are crazy enough to think that they can change the world, are the ones who do"

- Steve Jobs

[17] Courtesy of IvanoeMines.com, March 2017.

3.1 Preamble

SA is home to the deepest gold mines on earth. Most of these mines are situated in the Johannesburg, North-West and Welkom regions. The VRT increases by 10-12°C per kilometre of vertical depth at these locations. Energy intensive FPs are installed to cool down the water pumped from underground.

Cold water is supplied to air-cooling systems and underground mining activities. A mine's WRS includes water cooling, distribution and dewatering from underground. Cooled water is mainly used for air-cooling and mining activities.

Electricity prices increased approximately 17% from 2007 to 2016. This forces gold mines to minimise their EC, because it negatively affects their gold sales. ESCOs develop energy and cost savings strategies to improve system efficiency and save on operational costs. DSM strategies, which include WSO and LS, can be applied on energy intensive systems such as the WRS.

A literature study on mine WRSs is included in the previous chapter. This included information about the water supply and demand on SA gold mines. Techniques to reduce water demand and previous studies on mine WRSs were also discussed.

This chapter includes the methodology developed to accurately evaluate energy and cost savings of the dewatering system for a reconfigured WRS. The reconfiguration entailed removing CWCs and replacing them with CBACs. This enables more efficient cold-water usage for tertiary air-cooling on active mining levels.

The methodology includes evaluation methods such as analysis, calculations and simulations. These methods will be used to accurately predict energy and cost savings of a dewatering system on a gold mine in SA, which has this type of reconfiguration implemented on the WRS.

3.2 Summary of developed methodology

Figure 48 displays a summary of the developed methodology in a flow diagram.

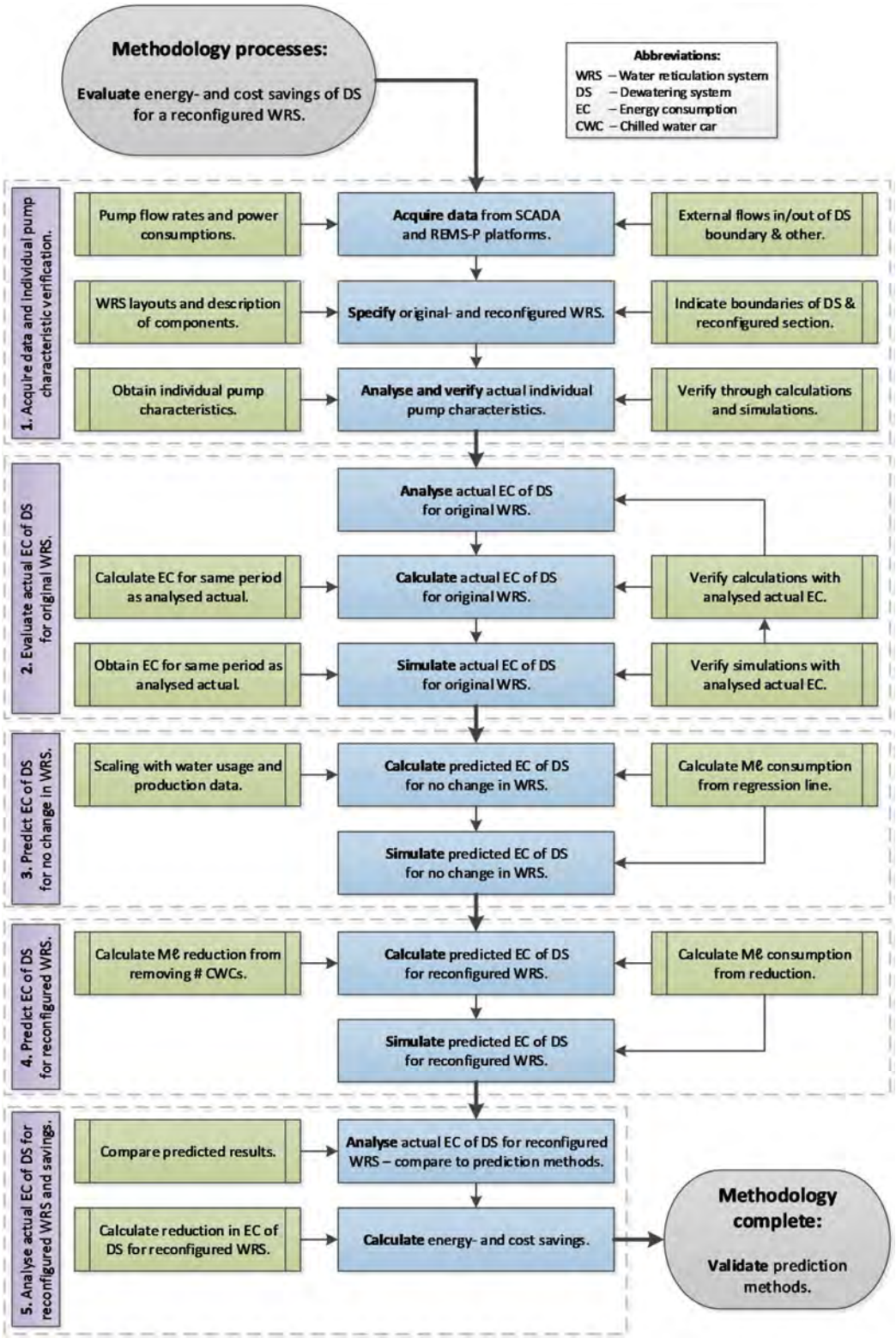

Figure 48: Summary of the developed methodology

As mentioned, the objective of this study was to accurately evaluate energy and cost savings of a dewatering system for a reconfigured WRS. The methodology in this chapter was developed to achieve this objective.

The methodology consists of five processes:

1. Data acquisition and verification of individual pump characteristics.
2. Evaluation of actual EC of the dewatering system for the original WRS.
3. Prediction of EC of the dewatering system for no change in the WRS.
4. Prediction of EC of the dewatering system for the reconfigured WRS.
5. Analysis of actual EC of the dewatering system for the original WRS and savings calculations.

These processes are discussed in the following sections.

3.3 Process 1: Data acquisition and verification

The objective of this process was to gather the necessary data and information. To accurately evaluate energy and cost savings of the dewatering system of a reconfigured WRS, this data had to be verified.

Data acquisition phase

Most gold mines make use of a supervisory control and data acquisition (SCADA) system, which logs data from sensors on mine machinery. These logs are known as *tags*. The data is stored on the mine's *historian* for future use. These tags can be logged on third-party energy management software (EMS). The EMS platform used for the logging of pump characteristics is known as Real-time Energy Management System for Pumps (REMS-P).

Data is logged in two-minute intervals in REMS-P and saved in a comma separated value (CSV) data structure. The data stored on the historian mainly consists of daily totals or averages. The historian thus stores values with a lower resolution compared to the data stored on the REMS-P platform.

The use of data from REMS-P is recommended for evaluation purposes. This is due to the increased resolution of the data points, while data from the historian acts as a layer of redundancy for data availability. If REMS-P loses connection to the SCADA server or fails to log for a certain period, data can be recovered from the historian.

Calculations included in this dissertation were done using Microsoft's Excel software. Data obtained from the historian and REMS-P is in raw format and should be converted into a more manageable format.

The following data needed to be gathered for future evaluation procedures discussed later in this dissertation:

- Flow rate of each individual pump.
- Power consumption of each individual pump.
- Additional flow rates entering and exiting the dewatering system boundary.
- Other information, including pump efficiencies, heads, and the number of CWCs removed.

After the relevant data was obtained and converted, the original and reconfigured WRSs needed to be described. Component layouts were drawn to visually present differences between these WRSs. Specifications of all components housed in the WRSs were also included. The following paragraphs will summarise the steps taken to acquire the relevant information for the original and reconfigured WRSs.

The following components are housed in a mining WRS:

- Cooling towers
- Refrigeration plants
- Bulk air-coolers
- Chilled water cars
- Centrifugal pumps
- Water and mud storage dams
- Valves
- Settlers

Figure 49 shows a typical layout of these components in a basic mining WRS. A blue boundary is drawn for the dewatering system, which includes all centrifugal pumps evaluated for energy and cost savings. The green boundary displays the tertiary cooling and mining activities boundary. This boundary is where the reconfiguration was implemented to decrease cold-water consumption of the WRS.

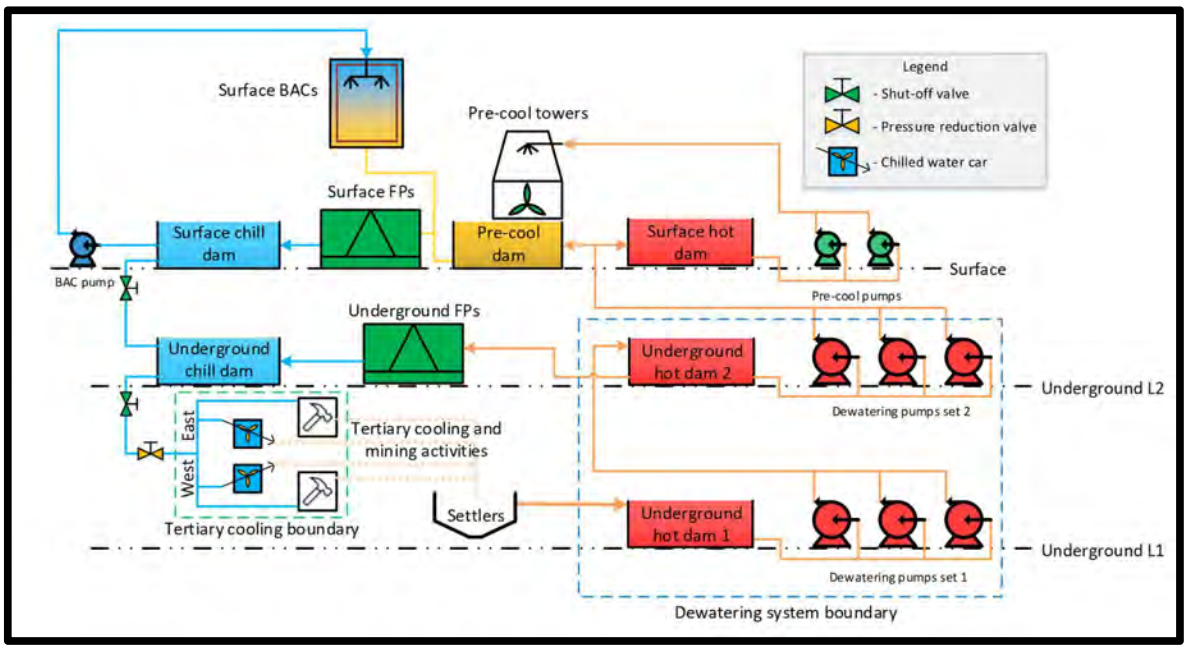

Figure 49: Typical layout of components in basic original mine WRS

A WRS distributes cold water to air-cooling systems such as BACs and CWCs. The cooling of water is achieved in FPs and the heat removed is dissipated in cooling towers. After the cold water has been used for mining activities, it is discarded on the ground and flows into settlers. Sludge, which consists of mud and other solid particles, is removed from the settlers and clear water overflows into hot water dams. Cascaded dewatering pump stations transfer water from underground hot dams to underground and surface FPs to be re-cooled.

Some mines have three-way pressure control valves installed on CWCs, through which outlet water is fed to mining activities. The water can only be effectively used for these activities when outlet water pressures are sufficient. However, many mines do not have these valves installed because water pressure upon exiting a CWC is not adequate for effective use at mining equipment.

This means multiple tap-off pipes exist, which extend from the main-line into a cross-cut. One pipe feeds a CWC located at the entrance of the cross-cut and the other extends further into the cross-cut to supply water to mining activities. The outlet water from the CWCs and mining activities is discarded onto the ground.

The original WRS may have many underground CWCs installed. Figure 50 displays the typical design of a CWC used in gold mines in SA. These units range from 100 kW–500 kW, where cold water is consumed at approximately 10–14°C with flow rates of 2–10 ℓ/s.

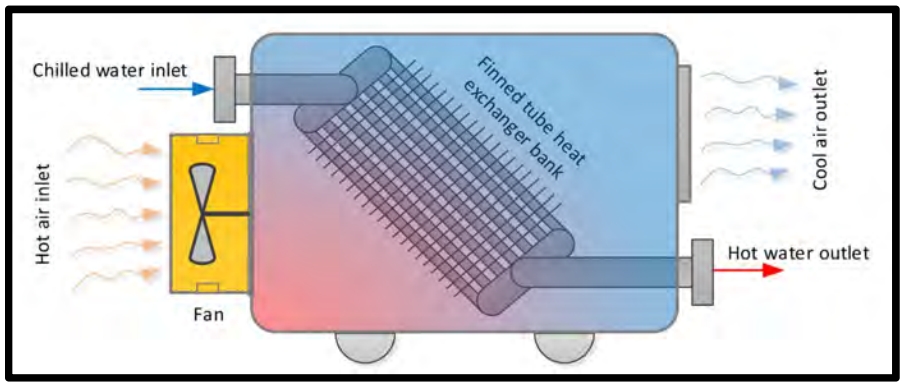

Figure 50: Typical CWC design

Heat transfer takes place from the hot air to the cold water through conduction and convection. Cold water is fed into the CWC, which then moves through a finned tube bank. A forced draft fan sucks in air and blows it over the fins on the outside of the tubes. Upon exiting the CWC, the air is cooled and dehumidified.

The information acquired for the original WRS needed to be obtained for the reconfigured WRS as well. Boundaries for the dewatering system and reconfigured section are displayed in the component layout of the reconfigured WRS. Figure 51 shows the typical component layout of a basic reconfigured WRS. The main difference between the original and reconfigured WRS is displayed in the green boundary.

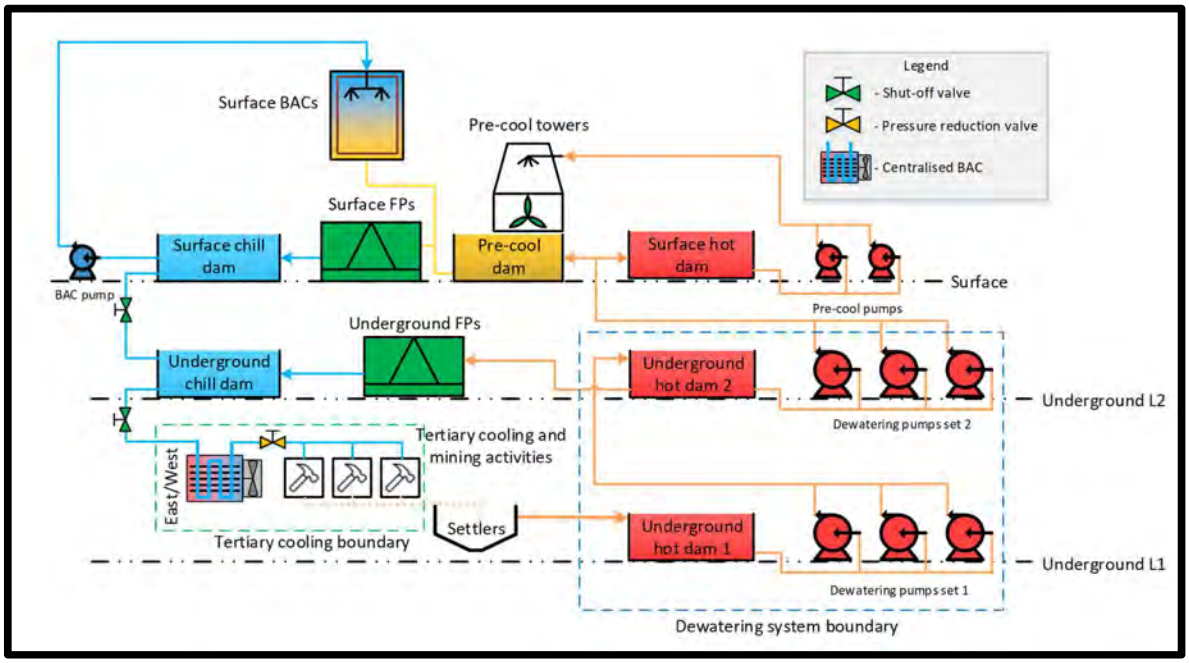

Figure 51: Typical layout of components in basic reconfigured mine WRS

It can be observed that CWCs were removed and replaced with CBACs. A single CBAC is located on the entrance of each active mining level's east and west side. A CBAC unit is significantly larger than a CWC; however, only one CBAC is needed for effective cooling of one side of a level. It can also be noted that the outlet water is used to feed mining activities. The water pressure on the outlet pipe is sufficient for utilisation at mining equipment.

Note that the component layout of the dewatering system did not change from the original to the reconfiguring WRS. The reconfiguration resulted in a reduction in water demand for tertiary cooling. The effects of this influence the power consumption of dewatering pumps. The blue dewatering system boundary indicates the section where the effects of the water reduction were evaluated. The outcome of this evaluation was in the form of energy and cost savings of only the centrifugal dewatering pumps.

Figure 52 shows a typical water balance for the basic dewatering system displayed in Figure 49 and Figure 51.

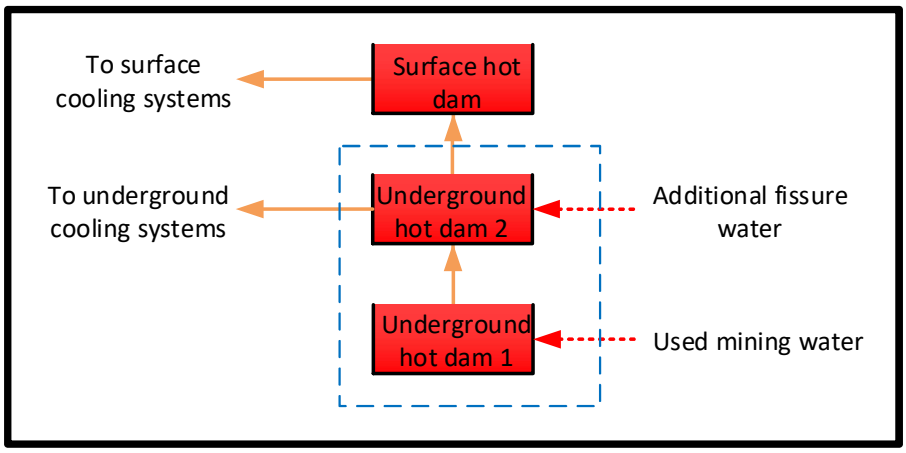

Figure 52: Typical water balance of dewatering system

Flow rates from pump stations into hot dams needed to be analysed and a flow balance like the above needed to be developed. This was done to determine whether there was additional fissure water entering the WRS. These external water effects needed to be included in evaluation processes to ensure accurate prediction of energy and cost saving results.

After the necessary data for evaluation was acquired, individual pump characteristics needed to be analysed and verified. This is discussed in the following sections.

Verification of analysed individual pump characteristics

Before any pump EC predictions could be made, individual pump characteristics needed to be verified. To achieve this, individual pump power consumption and flow rate needed to be analysed. The results were used as inputs in calculations and simulations to verify these actual analysed characteristics.

Figure 53 shows a basic layout of pumps connected in parallel. For the purposes of this explanation, pumps are connected to a single inlet and discharge column. Note that all pumps exert the same individual characteristics, which means their individual power consumption and flow rate does not differ.

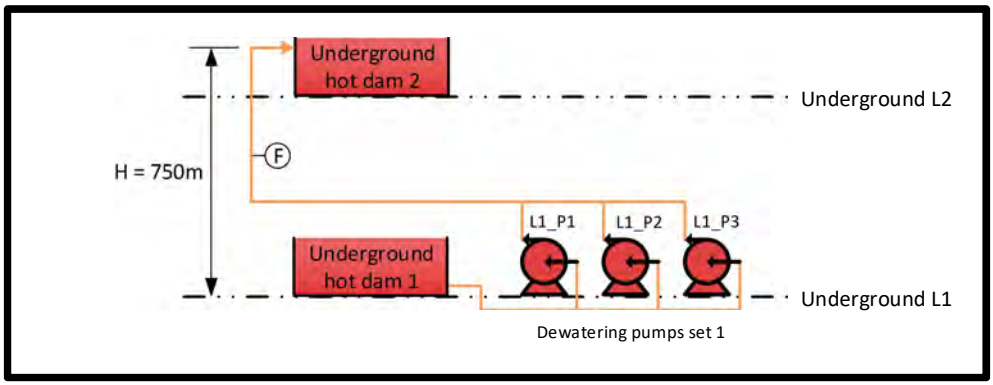

Figure 53: Basic parallel pump configuration

Table 9 displays an example of pump power consumption and flow rate data obtained from an EMS server. It includes 12 data points for the three pumps displayed above. Water flow rate within the discharge column was measured with a flow measuring device. The data needed to analyse pump characteristics including measured column flow rate, pump status, and pump power consumption.

Table 9: Theoretical example data of pump characteristics

Data point	Time of day	Column flow rate [ℓ/s]	L1_P1 Status [1/0]	L1_P2 Status [1/0]	L1_P3 Status [1/0]	L1_P1 Power [kW]	L1_P2 Power [kW]	L1_P3 Power [kW]	L1 Station Power [kW]
1	10:00	0	0	0	0	0	0	0	0
2	10:02	0	0	0	0	0	0	0	0
3	10:04	208	1	0	0	2 080	0	0	2 080
4	10:06	192	1	0	0	1 920	0	0	1 920
5	10:08	392	1	1	0	1 950	1 970	0	3 920
6	10:10	388	1	1	0	1 930	1 950	0	3 880
7	10:12	204	0	1	0	0	2 040	0	2 040
8	10:14	196	0	1	0	0	1 960	0	1 960
9	10:16	390	0	1	1	0	1 930	1 970	3 900
10	10:18	390	0	1	1	0	1 960	1 940	3 900
11	10:20	198	0	0	1	0	0	1 980	1 980
12	10:22	202	0	0	1	0	0	2 020	2 020

Only one pump should be running in a column to obtain its individual characteristics. It can be observed in Table 9 that initially there were no pumps running and all pump statuses and power consumptions were zero.

Table 10 includes the analysis of average pump characteristics. It can be seen at data points 3–4 that L1_P1 was running individually on the column. Its individual power consumption and flow rate were obtained by taking the average of the two data points. The same applies for L1_P2 at data points 7–8 and for L1_P3 at 11–12.

Table 10: Theoretical analysis of average pump characteristics

Data points [#]	Period running	Pump(s) running	Average power consumption of pumps [kW]	Average flow rate of pumps [ℓ/s]
3–4	10:04–10:08	L1_P1	2 000	200
5–6	10:08–10:12	L1_P1 & L1_P2	3 900	390
7–8	10:12–10:16	L1_P2	2 000	200
9–10	10:16–10:20	L1_P2 & L1_P3	3 900	390
11–12	10:20–10:24	L1_P3	2 000	200

It can be observed that two pumps are running in the column at data points 5–6 and 9–10. Taking the average of these values results in the pumps' combined characteristics. The result of running multiple pumps in one column is slightly different to using multiple columns and running one pump per column. The combined flow rate and power consumption of multiple pumps running in one column are lower than if the pumps run on separate columns.

Figure 54 shows an example of a combined pump characteristic curve for pumps connected in parallel.

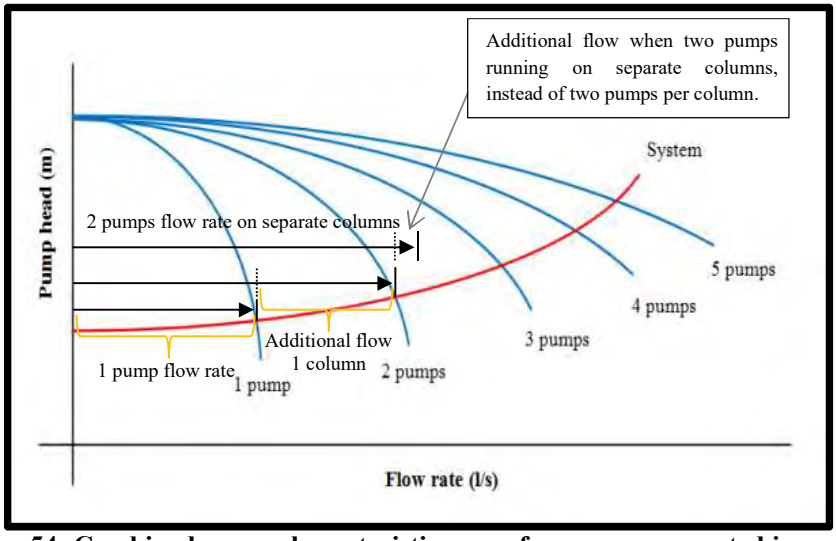

Figure 54: Combined pump characteristic curve for pumps connected in parallel

The pump system will follow the red line in this curve. It can be observed that additional flow can be achieved when running pumps on separate columns. This is not always possible, because installing a column for each pump can be very expensive and maintenance on all pipes will also become costly over time.

Many mines have two columns per pump station if more than three pumps are installed. The flow rate can be maximised by running the first two pumps in separate columns. The rest of the pumps can then be started when needed. Note that running more than two pumps per column can cause excessive pressure build-up within the pipes which may lead to bursting. Additionally, no two pumps should be started at the same time in a shared column. This can also cause an extreme discharge of pressure, which could damage the column.

After analysing individual characteristics, pump power calculations, and dewatering system simulations were used to verify the actual analysed results.

Equation 7 shows the theoretical pump power formula to calculate the individual power consumption of a pump for a required head and volume flow rate.

$$P_{Calc.\,Indiv.} = \frac{\rho_w \times g \times Q_{Ana.\,Indiv.} \times H}{\eta_o} \quad [W]$$

Equation 7: Individual pump power consumption

Where: ρ_w = water density $[kg/m^3]$ → 1000 kg/m^3

g = gravitational acceleration $[m/s^2]$ → 9.81 m/s^2

$Q_{Ana.\,Indiv.}$ = individual pump volume flow rate $[m^3/s]$

H = pumping head $[m]$

η_o = overall pump efficiency [%]

Theoretical pump power calculations can be used to verify the analysed individual pump power consumptions.

Example: In Figure 53, the pumps transfer water from underground hot dam 1 to hot dam 2. Each pump's individual characteristics were analysed, and the results are included in Table 10. All pumps achieved an individual flow rate of 200 ℓ/s, or 0.2 m^3/s, at a head of 750 m. The overall pump efficiency was assumed to be 75%.

By using Equation 7, a pump's power consumption can be calculated as:

$$P_{Calc.\ Indiv.} = \frac{1000 \times 9.81 \times 0.2 \times 750}{0.75} \quad [W]$$

Thus: $$\boldsymbol{P_{Calc.\ Indiv.} = 1\,962\,000\ W \approx 1\,962\ kW}$$

The calculated individual pump power consumption can be compared to the individual analysed results.

Equation 8 includes the formula for the percentage difference between calculated and analysed power consumption results:

$$Difference_{\ Calc.\ Indiv.} = \left(1 - \frac{P_{Ana.\ Indiv.}}{P_{Calc.\ Indiv.}}\right) \times 100 \quad [\%]$$

Equation 8: Difference between calculated and analysed individual power consumption

Verification of actual analysed pump power consumption can be obtained if the calculated percentage difference is smaller than 10%, where the difference for a pump in the example is:

$$Difference_{\ Calc.\ Indiv.} = \left(1 - \frac{2\,000}{1\,962}\right) \times 100\% = 1.94\%$$

Simulations were conducted to verify the analysed individual pump flow rate. REMS-P has a built-in simulation function that automatically controls pumps according to pre-defined dam levels.

All dewatering system simulation components are described in Appendix E. The simulation dewatering system layout and setup process are included in Appendix F and Appendix G, respectively.

Actual analysed individual pump characteristics obtained in Table 10 were used as pump specification inputs in the setup process. Note that, in general, at least five days of data should be simulated, and an average value should be calculated from the daily results for more accurate results.

To obtain the percentage error between simulated and analysed results, the total daily EC of the dewatering system also needed to be analysed from actual power consumption data. Equation 9 can be used to calculate the total daily EC after the average daily power consumption has been analysed.

$$\frac{EC_{\ Ana.\ Daily.}}{day}\ \left[\frac{kWh}{day}\right] = P_{Av\ \ Ana.\ Daily.}\ [kW] \times \frac{24\ h}{day}$$

Equation 9: Total daily analysed actual EC of the dewatering system

Hourly power consumptions can then be obtained from the simulated data, from which the average daily power consumption is calculated. The results are then multiplied by 24 hours to calculate the total daily EC of the dewatering system.

Equation 10 can then be used to calculate the percentage error between simulated and analysed dewatering system EC results:

$$Error_{Sim.\,Daily.} = \left(1 - \frac{EC_{Avg\ Ana.\,Daily.}}{EC_{Avg\ Sim.\,Daily.}}\right) \times 100 \quad [\%]$$

Equation 10: Error for simulated individual power consumption of dewatering system

Verification of actual analysed individual pump power consumption can be obtained if the simulated percentage error for the average value is smaller than 5%.

After verification of individual pump characteristics through simulation, the next process in the methodology can start.

3.4 Process 2: Evaluation of actual EC of the dewatering system for the original WRS

This process includes analysis, calculations and simulations to obtain the EC of the dewatering system of the original WRS.

The first part in this process was to analyse the total monthly EC of the dewatering system for the original WRS. These results were already verified, because all data necessary to achieve this was verified in Process 1. Note that data for at least three months needs to be evaluated. An average EC for the evaluated months was calculated to obtain accurate energy and cost savings.

EC is analysed by converting average monthly pump power consumptions into total monthly EC. As mentioned in the previous process, data is logged on an EMS server in two-minute intervals. Raw pump power consumption data was needed for this analysis.

Monthly averages were analysed from this data in Microsoft Excel. Appendix D includes an example of a dataset acquired from the REMS-P server. This sample only includes several minutes of power consumption data; however, an entire month's data needed to be analysed to obtain the average monthly consumption. If there is data loss for a small period within the month, averaging of power consumption will still give accurate results.

Note that when excessive data loss exists, where more than half of the month's power data is lost, the month should be marked as condonable and a different month should be analysed.

The results of the dewatering system's monthly average power consumption can be converted into EC by using Equation 11.

$$\frac{EC_{Ana.\,Orig.}}{day}\left[\frac{kWh}{day}\right] = P_{Avg\,Ana.\,Orig.}\,[kW] \times \frac{24\,h}{day}$$

$$EC_{Ana.\,Orig.}\left[\frac{MWh}{month}\right] = \frac{EC_{Ana.\,Orig.}}{day}\left[\frac{kWh}{day}\right] \times \frac{30.4\,day}{month} \times \frac{MW}{1000\,kW}$$

Equation 11: Total monthly analysed actual EC of the dewatering system for the original WRS

The total daily EC is calculated by using the average daily dewatering system's power consumption multiplied by the number of hours per day. The total monthly EC is calculated by using the total daily EC multiplied by the average number of days in a month. There are 12 months in a year of 365 days; thus, 365 days divided by 12 months, gives an average of 30.4 days per month. The conversion from kWh to MWh is also included to obtain a more readable unit for highly energy intensive dewatering systems.

As mentioned, there were two methods evaluated for predicting dewatering system EC for a reconfigured WRS. The theoretical pump power calculation method was investigated for accurate prediction of EC. The second method was by simulating the dewatering system.

The same months' data used in the analysis was used for the calculation method to obtain the EC of the dewatering system for the original WRS. Equation 12 displays an adapted form of Equation 7 on page 63, which can be used to calculate the average power consumption of an entire pump station per month.

$$P_{Av\ \ Calc.\,Orig.} = \frac{\rho_w \times g \times Q_{Avg\,Ana.\,Orig.} \times H}{\eta_o}\ [W]$$

Equation 12: Average pump power consumption calculation

The following information stayed unchanged from the calculation of individual pump characteristics:

- ρ_w = density of water
- g = gravitational acceleration
- H = pumping head
- η_o = overall pump efficiency

The only variable that changed was the individual volume flow rate ($Q_{Ana.\ Indiv.}$), which is now the analysed average monthly volume flow rate of the entire pump station ($Q_{Avg\ Ana.\ Orig.}$).

An entire pump station's average monthly flow rate (ℓ/s) can be obtained by analysing the average flow rate of water transferred through water columns. If multiple columns exist, the flow rates of all respective columns should be added together. This flow rate can then be divided by 1 000 to obtain volume flow rate (m^3/s).

Calculation of the total monthly EC can be obtained by converting the calculated average monthly power consumption. This can be achieved by adapting Equation 11 to obtain Equation 13:

$$EC_{Calc.\ Orig.}\left[\frac{MWh}{month}\right] = P_{Av\ \ Calc.\ Orig.}[kW] \times \frac{24\ h}{day} \times \frac{30.4\ day}{month} \times \frac{MW}{1000\ kW}$$

Equation 13: Total monthly calculated EC of the dewatering system for the original WRS

An average EC value is obtained for the analysed and calculated EC from the three or more months evaluated for the original WRS. The average calculated EC results can be compared to the average analysed results to obtain the percentage error for the calculated values by using Equation 14:

$$Error_{Calc.\ Orig.} = \left(1 - \frac{EC_{Avg\ Ana.\ Orig.}}{EC_{Avg\ Calc.\ Orig.}}\right) \times 100 \quad [\%]$$

Equation 14: Error for calculated EC of the dewatering system for the original WRS

Because of individual pump characteristics being verified in Process 1, analysed EC results act as verification for calculated results. EC calculations are deemed verified if the percentage error is less than 5% for the average of at least three evaluated months.

The second method to predict EC of the dewatering system for the original WRS is by simulations. The water balance shown in Figure 52 can be re-evaluated for each month's average flow rate through the pump stations. It is important to obtain all external flow rates which enter and exit the boundary of the dewatering system. These flows will influence the EC of the dewatering system. Note that nothing needs to be changed inside of the boundary, because all individual pump characteristics were already inserted at the simulation setup stage in Process 1.

The total monthly simulated EC can be obtained through converting the simulated average monthly power consumption by using Equation 15:

$$EC_{Sim.\,Orig.}\left[\frac{MWh}{month}\right] = P_{Avg\,Sim.\,Orig.}[kW] \times \frac{24\,h}{day} \times \frac{30.4\,day}{month} \times \frac{MW}{1000\,kW}$$

Equation 15: Total monthly simulated EC of the dewatering system for the original WRS

The simulated EC results can be compared to the analysed results to obtain the percentage error for the simulated values.

$$Error_{Sim.\,Orig.} = \left(1 - \frac{EC_{Avg\;Ana.\,Orig.}}{EC_{Avg\;Sim.\,Orig.}}\right) \times 100 \quad [\%]$$

Equation 16: Error for simulated EC of the dewatering system for the original WRS

For verification of the simulation method, the percentage error of simulated EC results needs to be less than 5% for the average of the three or more evaluated months. The prediction method that results in the lowest percentage error will be the best method to use for accurately predicting energy and cost savings of the dewatering system for a reconfigured WRS.

Note that the total monthly water consumption of the dewatering system for the original WRS needed to be obtained for the next process. This was done by converting average flow rate (ℓ/s) to water consumption per month ($M\ell/month$) by using Equation 17:

$$M\ell_{\,Orig.}\left[\frac{M\ell}{month}\right] = Q_{Avg\;Ana.\,Orig.}\left[\frac{m^3}{s}\right] \times \frac{3600 \times 24 \times 30.4\,s}{month} \times \frac{M\ell}{1\,000\ \mathrm{m^3}}$$

Equation 17: Total water consumption per month

After the prediction methods were verified and the monthly water consumption was obtained for the original WRS, the next process could start.

3.5 Process 3: Prediction of EC of the dewatering system for no change in WRS

The methods discussed and verified in the previous process can be used to predict the EC of the dewatering system if no change was made to the WRS. This step is important because a reference energy consumption (REC) needs to be obtained. Scaling needs to be applied to obtain the REC.

Scaling with energy neutrality will not achieve accurate results, because EE is achieved for the reconfigured WRS due to the reduction in cold-water consumption. A scaling factor needs to be investigated which has a good correlation to the water consumption of the dewatering system.

Scaling according to gold production was investigated. Each gold mine has its own water consumption per kilogram of gold produced. Cold-water demand is dependent on the amount of underground air-cooling and gold production. If there is a good linear relationship for water consumption versus gold production, scaling can be done according to this factor, given that there is no increase or decrease in workforce.

A scatter plot, with a linear regression line, can be plotted for water consumption versus gold production. Figure 55 displays an example linear regression of this. It can be observed that there is a strong correlation between water consumption and gold production, with a coefficient of determination (R^2) greater than 80%.

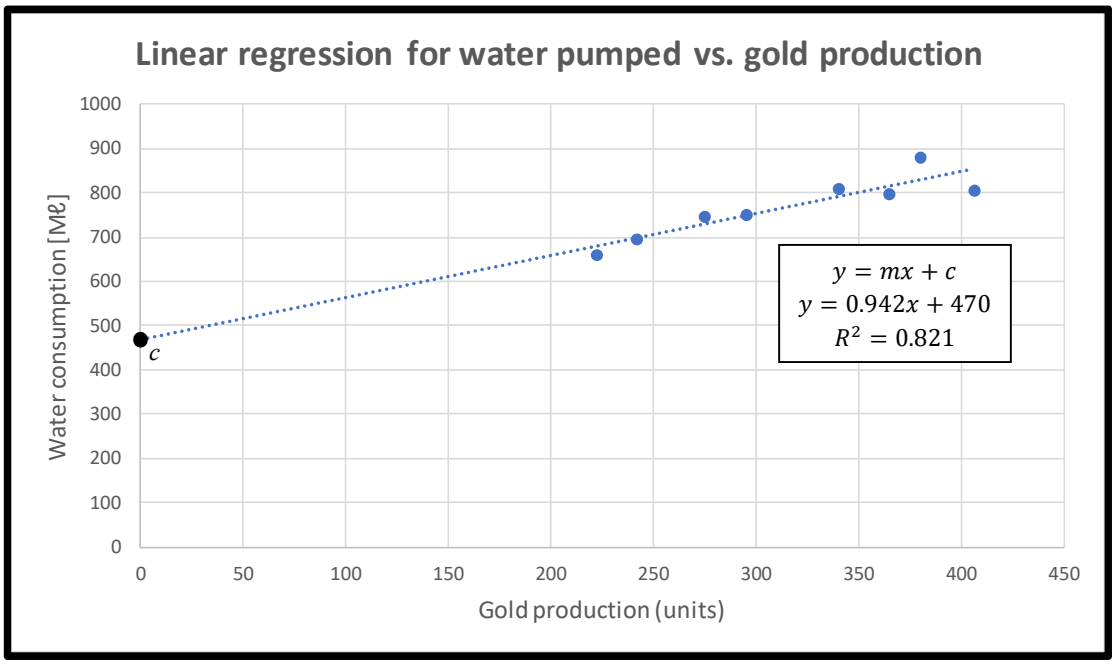

Figure 55: Example of linear regression line for Mℓ of water pumped versus gold production

The baseload water consumption of the WRS is dependent on water demand of the underground air-cooling systems. It can be observed that the baseload for this example (c) is 470 Mℓ. This is the theoretical water consumption (Mℓ) when no gold is produced. This consumption will only be for underground air-cooling systems and not for any mining activities. The reconfiguration of the WRS will decrease the baseload water consumption and/or increase the amount of gold production.

Note that it is necessary to predict the REC to evaluate energy and cost savings of the reconfigured WRS. The reference water consumption (RWC) needed to firstly be predicted, which was done by using the slope of the regression line. Scaling was applied according to the original WRS's water consumption per unit of gold produced. Equation 18 displays the relationship for scaling between the original and predicted reference WRS.

$$\left[\frac{M\ell}{gold_{\,units}}\right]_{Orig.} = \frac{M\ell_{\,Ref.}}{gold_{\,units\,Reconf.}}$$

Equation 18: Scaling of water consumption according to gold production

The predicted RWC can be calculated by using Equation 19:

$$M\ell_{\,Ref.} = Avg\left[\frac{M\ell}{gold_{\,units}}\right]_{Orig.} \times gold_{\,unit\;\;Reconf.}$$

Equation 19: Calculation of predicted RWC

The water consumption of the original WRS ($M\ell_{\,Orig.}$) was obtained in Process 2. Gold production data of the original and reconfigured WRS for the evaluation period needed to be acquired. The RWC is the result when no changes were made to the WRS, however, for gold produced after the WRS was reconfigured.

After results of the reference water consumption were obtained, calculations could then be done. It is important to convert total water consumption ($M\ell_{\,Ref.}$) back into average monthly volume flow rate ($Q_{Av\;\;Ref.}$).

Equation 20 shows the formula for the conversion:

$$Q_{Av\;\;Ref.}\left[\frac{m^3}{s}\right] = \frac{M\ell_{\,Ref.}}{month} \times \frac{month}{3600 \times 24 \times 30.4\;s} \times \frac{1\,000\;\mathrm{m}^3}{M\ell}$$

Equation 20: Average reference volume flow rate

The results for average reference volume flow rate can be used to calculate the predicted EC of the dewatering system for no change in the WRS at the achieved production. Equation 21 can be used to calculate the average power consumption of a pump station.

$$P_{Avg\ Calc.\ Ref.} = \frac{\rho_w \times g \times Q_{Avg\ Ref.} \times H}{\eta_o} \quad [W]$$

Equation 21: Average pump station power consumption for the reference WRS

The total monthly calculated REC of the dewatering system can be obtained by using Equation 22:

$$EC_{Calc.\ Ref.} \left[\frac{MWh}{month}\right] = P_{Avg\ Calc.\ Ref.}[kW] \times \frac{24\ h}{day} \times \frac{30.4\ day}{month} \times \frac{MW}{1000\ kW}$$

Equation 22: Total monthly calculated REC of the dewatering system

Because the total monthly EC of the dewatering system for the original WRS was verified with calculations and simulations in Process 2, the predicted REC results were deemed valid.

The average reference volume flow rate ($Q_{Avg\ Ref.}$) can be used in simulations of the dewatering system. Water flowing into and out of the dewatering system's boundary (see Figure 51 and Figure 52) can be obtained from this flow rate. These flow rates can be inserted as input values into simulations, by specifying it in dam editor windows.

The total monthly simulated REC of the dewatering system was obtained by converting the simulated dewatering system power consumption results. To achieve this, Equation 23 was used:

$$EC_{Sim.\ Ref.} \left[\frac{MWh}{month}\right] = P_{Avg\ Sim.\ Ref.}[kW] \times \frac{24\ h}{day} \times \frac{30.4\ day}{month} \times \frac{MW}{1000\ kW}$$

Equation 23: Total monthly simulated REC of the dewatering system

Note that again, at least three months' REC needs to be evaluated where the average thereof is used for validation and to predict energy and cost savings. After this average was calculated, the next process could start.

3.6 Process 4: Prediction of EC of the dewatering system for the reconfigured WRS

As mentioned, reconfiguring a WRS entails removing CWCs and replacing them with CBACs. An assumption was made for mines that do not have three-way valves installed on CWCs. This is that the number of CWCs removed from the WRS determines the reduction in water demand for underground tertiary cooling. This is because the water exiting the CWCs was not utilised for mining activities; whereas after the reconfiguration, the outlet water from the CBACs flowed to mining equipment.

Equation 24 displays the formula to calculate the predicted average reduction in water flow rate. It is calculated by multiplying the specified water consumption of a single CWC with the number of CWCs removed.

$$Reduction\ in\ Q_{Avg\ Reconf.}\left[\frac{m^3}{s}\right] = (Water\ consumption\ per\ CWC\ \times\ \#CWCs)\left[\frac{\ell}{s}\right] \times \frac{m^3}{1000\ \ell}$$

Equation 24: Predicted average reduction in water volume flow rate for the reconfigured WRS

Equation 25 displays the formula to obtain the predicted water volume flow rate of the dewatering system for the reconfigured WRS. The predicted reduction is subtracted from the predicted RWC.

$$Q_{Avg\ Reconf.}\left[\frac{m^3}{s}\right] = Q_{Av\ \ Ref.} - Reduction\ in\ Q_{Avg\ Reconf.}$$

Equation 25: Predicted average water volume flow rate for the reconfigured WRS

The predicted volume flow rate results ($Q_{Av\ \ Reconf.}$) can now be used to calculate and predict the EC of the dewatering system for the reconfigured WRS. Equation 26 displays the formula for predicting the average power consumption of the dewatering system for a reconfigured WRS:

$$P_{Av\ \ Calc.\ Reconf.} = \frac{\rho_w\ \times\ g\ \times\ Q_{Avg\ Reconf.}\ \times\ H}{\eta_o}\ \ [W]$$

Equation 26: Average pump power consumption of dewatering system for the reconfigured WRS

The total monthly calculated EC of the dewatering system for the reconfigured WRS can be obtained by using Equation 27:

$$EC_{Calc.\ Reconf.} = P_{Av\ \ Calc.\ Reconf.}[kW]\ \times \frac{24\ h}{day} \times \frac{30.4\ day}{month} \times \frac{MW}{1000\ kW} \qquad \left[\frac{MWh}{month}\right]$$

Equation 27: Total monthly calculated EC of the dewatering system for the reconfigured WRS

The average reconfigured WRS's volume flow rate ($Q_{Avg\ Reconf.}$) can be used in dewatering system simulations. No design change to the dewatering system was made for the reconfigured WRS. As mentioned, the reduction in cold-water consumption for tertiary underground air-cooling systems affects the EC of the dewatering system.

It can be observed in Figure 52 that there are three flows entering or exiting the dewatering system boundary. These flows needed to be obtained to use as flow rate inputs into and out of the dam components included in REMS-P simulations. Appendix G describes the process of inserting these flow rates into simulations conducted in this dissertation.

The total monthly simulated EC of the dewatering system for the reconfigured WRS can be obtained by using Equation 28:

$$EC_{Sim.\ Recon\ .}\left[\frac{MWh}{month}\right] = P_{Av\ \ Sim.\ Reconf.}[kW] \times \frac{24\ h}{day} \times \frac{30.4\ day}{month} \times \frac{MW}{1000\ kW}$$

Equation 28: Total monthly simulated EC of the dewatering system for the reconfigured WRS

After predicting EC of the dewatering system for the reconfigured WRS, the results needed to be compared to actual analysed EC results. This process is discussed in the following section.

3.7 Process 5: Analysis of actual EC of the dewatering system for the reconfigured WRS.

This process follows the same steps discussed in Process 1 to analyse EC of the dewatering system for the reconfigured WRS. A summary of these steps is included in the following paragraphs. The results from this process will validate the prediction models developed in the methodology.

The raw pump power data acquired from the REMS-P server is converted from 2-minute intervals into average dewatering system power consumption for the three or more months evaluated in previous processes. The total monthly analysed EC of the dewatering system for the reconfigured WRS can be obtained by using Equation 29:

$$EC_{Ana.\ Reconf.}\left[\frac{MWh}{month}\right] = P_{Avg\ Ana.\ Reconf.}[kW] \times \frac{24\ h}{day} \times \frac{30.4\ day}{month} \times \frac{MW}{1000\ kW}$$

Equation 29: Total analysed EC of the dewatering system per month for the reconfigured WRS

An average value is obtained for the analysed and calculated EC from the three or more months evaluated for the reconfigured WRS. This average value can be compared to the predicted results obtained in Process 4. The percentage error for the calculation and simulation prediction methods is displayed in Equation 30 and Equation 31, respectively:

$$Error_{Calc._{Reconf.}} = \left(1 - \frac{EC_{Avg\ Ana._{Reconf.}}}{EC_{Avg\ Calc._{Reconf.}}}\right) \times 100 \quad [\%]$$

Equation 30: Error for calculated EC of the dewatering system for the reconfigured WRS

$$Error_{Sim._{Reconf.}} = \left(1 - \frac{EC_{Avg\ Ana._{Reconf.}}}{EC_{Avg\ Sim._{Reconf.}}}\right) \times 100 \quad [\%]$$

Equation 31: Error for simulated EC of the dewatering system for the reconfigured WRS

If the percentage error of these methods is less than 5%, the methodology is validated. More on the validation of the methodology is included in the next chapter, after a real-world reconfigured WRS is evaluated.

3.8 Energy and cost savings quantification

The last step in achieving the objective of this study is to calculate energy and cost savings.

The average monthly energy saving from the decreased power consumption of the dewatering system for the reconfigured WRS can be calculated by using Equation 33 or Equation 32:

$$\frac{EE_{Sa\quad Avg}}{month}\left[\frac{MWh}{month}\right] = EC_{Avg\ Calc._{Ref.}} - EC_{Avg\ Ana._{Recon\ .}}$$

Equation 32: Average monthly energy saving according to calculated REC

$$\frac{EE_{Saving_{Avg}}}{month}\left[\frac{MWh}{month}\right] = EC_{Avg\ Sim._{Ref.}} - EC_{Avg\ Ana._{Reconf.}}$$

Equation 33: Average monthly energy saving according to simulated REC

The method which achieves the smallest percentage error will predict energy and cost savings more accurately than the other. The average monthly cost saving can be calculated by using Equation 34:

$$\frac{Cost_{Saving}}{month}\left[\frac{R}{month}\right] = \frac{EE_{Saving_{Avg}}}{month}\left[\frac{MWh}{month}\right] \times \frac{1000\ kWh}{MWh} \times E_{Tariff_{Avg}}\left[\frac{R}{kWh}\right]$$

Equation 34: Predicted monthly cost saving for reconfigured WRS

For annual prediction of cost savings, Equation 34 can be multiplied by the number of months per year. Equation 35 displays the formula for calculating the predicted yearly cost saving:

$$\frac{Cost_{Saving}}{year}\left[\frac{R}{year}\right] = \frac{Cost_{Saving}}{month}\left[\frac{R}{month}\right] \times \frac{12\,months}{year}$$

Equation 35: Predicted annual cost saving for reconfigured WRS

If all processes of the methodology are applied correctly on a reconfigured WRS, the predicted energy and cost savings should be at least 95% accurate. This is because the prediction methods investigated provide accurate EC results when compared to actual analysed results.

The methodology processes were applied on a reconfigured WRS on a gold mine in SA. Proof for validation of the developed methodology is included and discussed throughout the next chapter.

3.9 Chapter summary

The methodology developed in this chapter can be used to accurately predict energy and cost savings of a dewatering system for a reconfigured WRS. Evaluation with analysis, theoretical calculations and simulations were discussed in this chapter.

Individual pump characteristics were analysed and verified with calculations and simulations. These characteristics are then used as inputs for further evaluation of EC of the dewatering system for the original and reconfigured WRS. Predictions are then made to obtain the REC of the dewatering system for scaling according to production for the reconfigured WRS.

For mines that have CWCs installed without three-way valves, the predicted water consumption of the reconfigured WRS can be obtained by subtracting the total removed CWC water reduction from the RWC. This predicted water consumption can then be used to predict the EC of the dewatering system for the reconfigured WRS by using pump power calculations and simulations.

Analysis for the actual EC of the dewatering system for the reconfigured WRS needs to be done. This result will then be compared to the predicted result, which will give an indication of the validity of the methodology. Note that the average EC of the dewatering system from at least three months needs to be evaluated to obtain accurate prediction results. It the percentage error from the predicted and actual analysed EC of the dewatering system for the reconfigured WRS is less than 5%, the methodology is validated.

The total energy savings is calculated as the predicted REC minus the predicted EC of the dewatering system for the reconfigured WRS. Cost savings can then be calculated by taking the average energy tariff per year and multiplying it with the energy saving result. The prediction methods provide accurate energy and cost saving results. This is because these methods were verified throughout the entire evaluation and their percentage errors are less than 5% when compared to actual analysed results.

CHAPTER 4 RESULTS

[18]

"The future depends on what we do in the present"

- Mahatma Gandhi

[18] Courtesy of Mining Review Africa, January 2017.

4.1 Preamble

A WRS was reconfigured on a deep-level gold mine near Carletonville in SA. The reconfiguration entailed removing CWCs and replacing them with CBACs. This results in decreased water demand for tertiary underground air-cooling. The reduced cold-water demand influences the EC of the dewatering system.

A methodology was developed in Chapter 3 to accurately evaluate energy and cost savings of the dewatering system after the WRS was reconfigured. Methods were investigated for prediction of EC of the dewatering system, which included calculations and simulations. Verification of these methods are discussed throughout this chapter.

The developed methodology can only be applied for mines that do not have three-way valves installed on CWCs. This is due to the cold-water distribution to CWCs and mining activities in the original WRS, where two tap-off pipes extend from the main-line into a cross-cut. After the reconfiguration, outlet water from the CBACs is utilised for mining activities. This ensures that only one tap-off pipe enters the cross-cuts, where the pipes to previously-installed CWCs are removed. The result is an increase in EE for the dewatering system, where significant cost savings can be realised.

The methodology consists of five processes to accurately predict energy and cost savings of the dewatering system for the reconfigured WRS. These processes include:

1. Data acquisition and verification of actual data.
2. Evaluation of actual EC of the dewatering system for the original WRS.
3. Prediction of EC of the dewatering system for no change in the WRS.
4. Prediction of EC of the dewatering system for the reconfigured WRS.
5. Analysis of actual EC of the dewatering system for the reconfigured WRS.

The result from Process 3 is considered as the REC for the original WRS. This is the scaled predicted EC of the dewatering system for the original WRS. Scaling is done according to water consumption per unit of gold produced. The REC can be used to predict energy and cost savings of the dewatering system for the specified reconfigured WRS investigated in this chapter.

The reduction in water consumption is calculated from the number of CWCs removed from underground. This reduction is subtracted from the predicted reference water consumption obtained in Process 3, which results in the water demand for the reconfigured WRS. The decreased water demand can then be used as inputs to the methods predicting the EC of the dewatering system for the reconfigured WRS.

After the five processes are completed for the specified reconfigured WRS, the energy and cost savings of the dewatering system can be calculated. The accuracy of the prediction methods will depend on the correctness of the acquired data. If the analysed individual pump characteristics do not differ more than 10% from the predicted results, the prediction models will predict savings accurately.

The results from the processes applied on the specified reconfigured WRS are discussed in the following sections.

4.2 Process 1 results: Acquired data and verification

The outcome of this process was to acquire data and information for the original and reconfigured WRS. Layouts of these WRSs are included within this section, to visually present the changes made after the reconfiguration was implemented.

4.2.1 Data acquired for evaluation

As mentioned, data is obtained by logging SCADA tags on an EMS server. The specific EMS platform used for data logging and simulations is known as REMS-P. Data is logged in 2-minute intervals and is saved in a CSV file format. This data can be converted to a more manageable format by using Microsoft's Excel software.

The following data was acquired from REMS-P:

- Flow rate of each individual pump.
- Power consumption of each individual pump.
- Average monthly flow rates entering and exiting the dewatering system boundary.
- Other information including pump efficiencies, heads and the number of CWCs removed.

Table 61 in Appendix D includes example data of pump data logged in 2-minute intervals, which was acquired from the REMS-P server installed on the mine. This data can be used to analyse the individual pump characteristics listed above. Flow rate measurement devices are installed on the discharge columns of each pump station. The locations of these devices are displayed on the dewatering system's component layout diagram, which is included later in this section. Power measuring devices are connected to the power supply cable of each centrifugal pump.

Note that all pumps on their respective pumping level are of the same design and they should exert approximately the same characteristics. The specifications for dewatering pumps are included when the specified mine's dewatering system is specified in this section.

As mentioned, when two pumps are running simultaneously on a single shared column, their combined flow rate will be slightly less than that of each pump running on its own column. The explanation for this phenomenon can be found in Section 3.3; however, only individual pump characteristics were analysed and used as inputs for calculations and simulations.

Refer to Table 61 in Appendix D for the following explanation on how to analyse the dewatering pumps' individual power consumption and flow rate. It can be observed that all pumps on 52L are off from 13:50 to 14:02 (points 1-7), where the first pump was started at 14:04 (point 8). This pump corresponds to 52L_P3, where it was the only pump active until 14:34 (point 23) in column B. It can be observed that when 52L_P1 was switched on at 14:36 (point 24), the flow rate in this column almost doubled. This means that these two pumps were sharing column B.

As mentioned, only the individual pump characteristics were used for evaluation; thus, only points 8-23 were used to analyse the individual flow rate and power consumption of 52L_P3. The average for these data points are calculated to obtain the individual characteristics. The individual characteristics could not be analysed for 52L_P1 from the data included in Table 61, because it was not running on its own in the column.

It can be observed that 52L_P2 was turned on at 14:20 (point 16) and it ran individually in column A until the end of the example data range. Individual pump characteristics for 52L_P2 were analysed by averaging the values from points 16-38. 52L_P4 was not switched on at any stage, according to the data in Table 61.

To obtain the individual characteristics for 52L_P1 and 52L_P4, other data ranges needed to be used where they ran individually in their respective columns. If there had not existed a data range where this occurred, an assumption could have been made that its individual characteristics are the same as for the other pumps. Note that this assumption can only be made if the pumps are of the same design and specification.

The results of the individual characteristics are included after the component layout of the original and reconfigured WRS is included. As mentioned, there was no change in the component layout of the dewatering system for the reconfigured WRS; thus, only one dewatering system layout was included. Component specifications are also provided. The following paragraphs will summarise the information acquired for the original and reconfigured WRS's component layout and the specification thereof.

4.2.2 Specification of original WRS on investigated SA gold mine

Figure 56 shows the component layout of the original WRS on the investigated gold mine in SA.

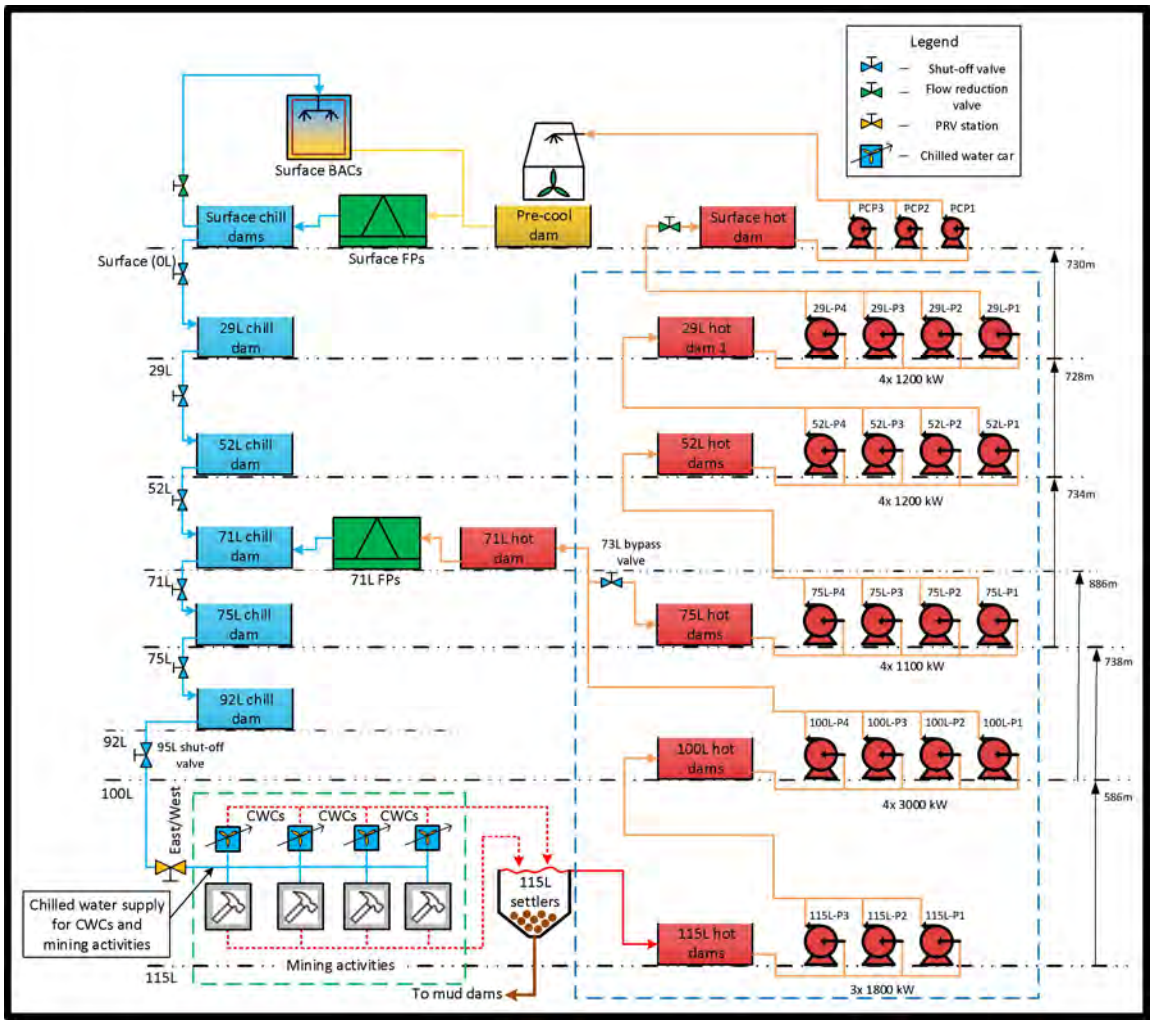

Figure 56: Overview layout of original WRS on gold mine near Carletonville, SA

The green dotted boundary displays a simplified layout for chilled water distribution to underground CWCs and mining activities. Note that this representation is only for one side of a single active mining level. There are typically two sides per level, which are the east and west sides. This layout is the same for the other side as well; thus, only one side is displayed for simplicity.

The blue dotted border displays the boundary for the dewatering system. All centrifugal dewatering pumps evaluated for energy and cost savings are included in this boundary. It can be observed that the cold-water demand for CWCs has a direct effect on the amount of water to be pumped back to FPs. This means that a decrease in cold-water demand will decrease the EC of dewatering pumps, if cold-water demand for mining activities stay constant.

Figure 57 displays the chilled water distribution to active mining levels in the original WRS.

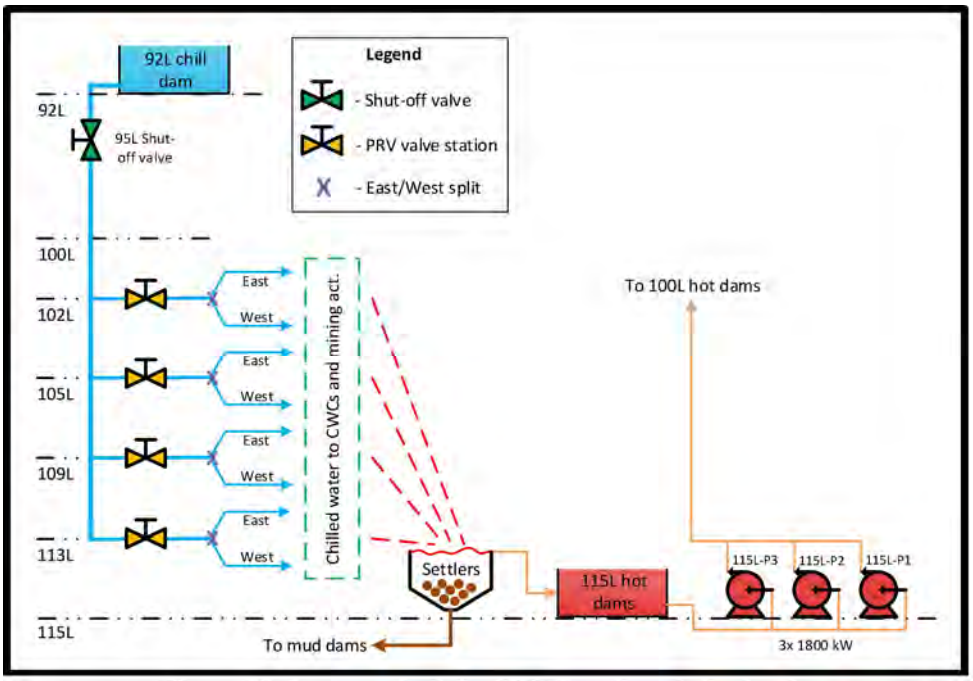

Figure 57: Layout of original WRS active mining levels

The active mining levels are 102L, 105L, 109L and 113L. A cold-water pipe enters each active mining level, where PRV stations decrease the water pressure to approximately 1 400−1 600 kPa [41]. This pipe splits (indicated by an X) into two main-lines, where one feeds the east side and the other feeds the west side. These main-lines extend along the walls of the haulage to feed all tertiary air-cooling systems and mining activities.

Figure 58 shows a basic layout of an active mining level's east/west side CWCs and mining activities.

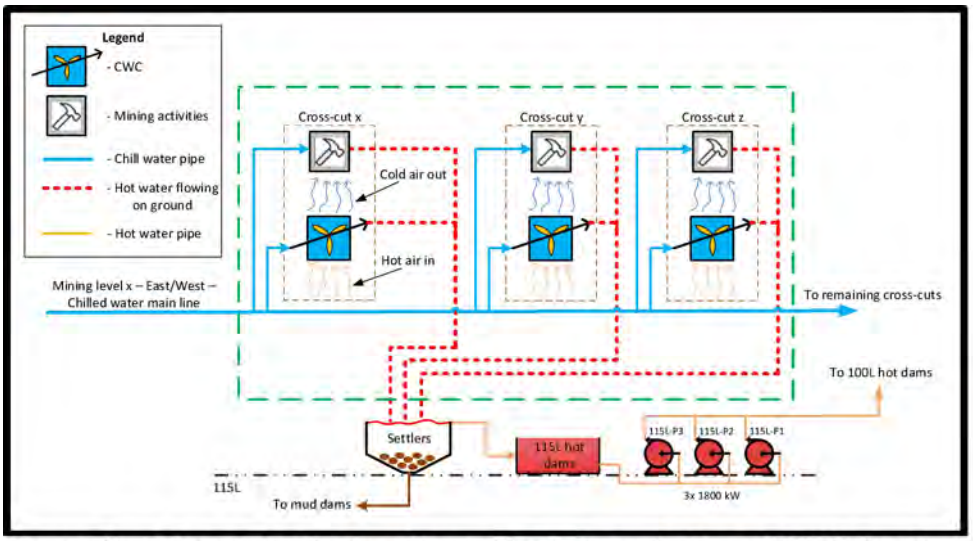

Figure 58: Active mining level east/west side mining activities and CWC locations

For the mine investigated in this research, it can be observed that two tap-off pipelines enter each cross-cut. This is because there are no three-way valves installed on CWCs. One pipe feeds cold water to a CWC and the other extends deeper into the cross-cut, which feeds mining activities. Note that the developed methodology can only be used for mines that do not have three-way valves installed on CWCs.

A representation of the typical design of a CWC is displayed in Figure 50 on page 59. The CWCs installed in the original WRS are 150 kW units. The specification for these CWCs include a cold-water flow rate of approximately 3 ℓ/s at 12–14°C WB. A total of 48 CWC units were installed on active mining levels in the original WRS. This amounted to a total water consumption of approximately 144 ℓ/s. This amount of water was used irrespective of the amount of water consumed for mining activities, because no three-way valves were installed.

The reconfigured WRS of the investigated mine is described in the following sections.

4.2.3 Specification of reconfigured WRS on investigated SA gold mine

Figure 59 shows the component layout of the reconfigured WRS on the investigated gold mine in SA.

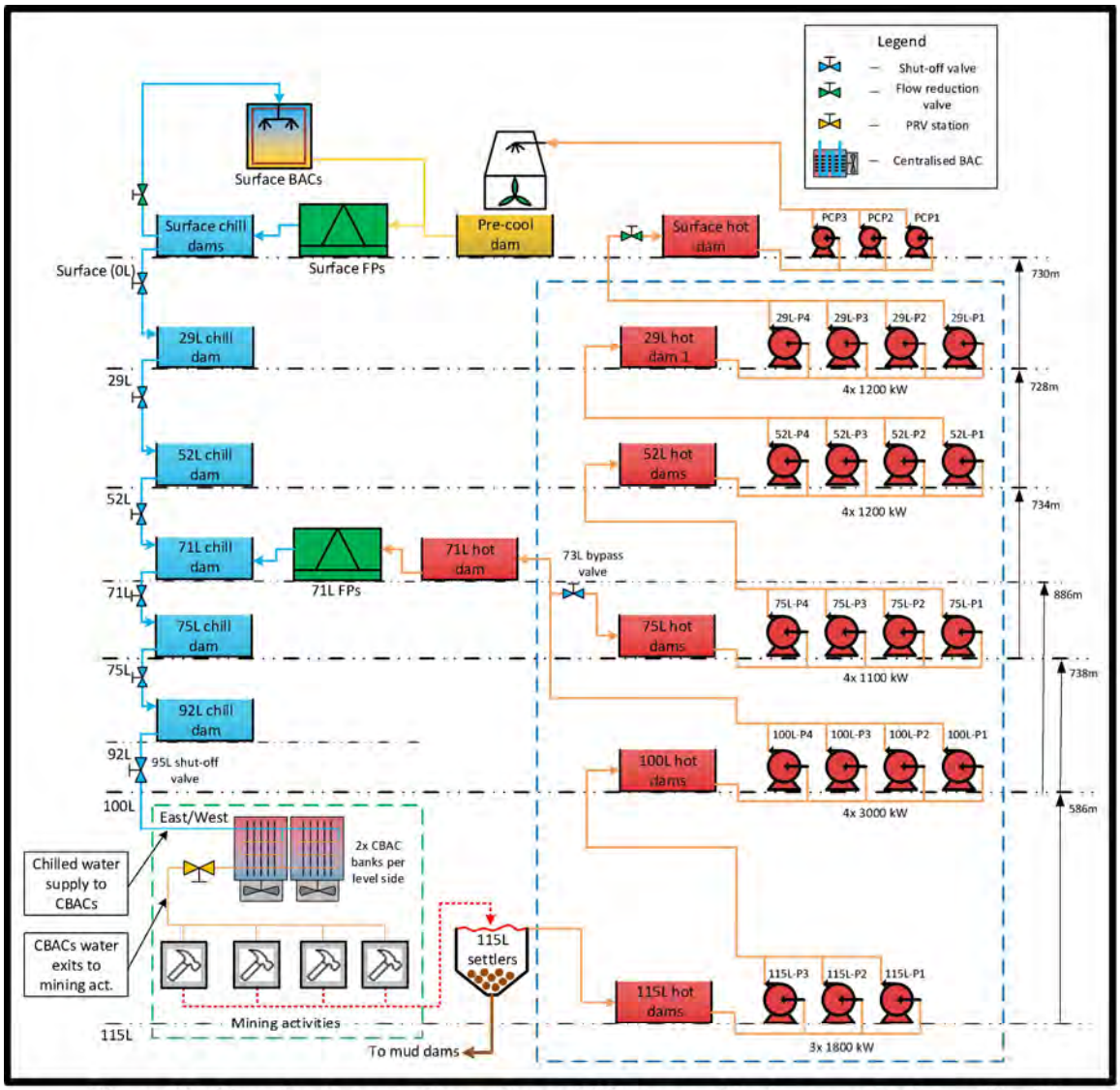

Figure 59: Overview layout of reconfigured WRS on gold mine near Carletonville, SA

The green dotted boundary displays a simplified layout for chilled water distribution to CBACs, where the outlet water is fed to mining activities. This representation is also only for one side of a single active mining level.

The blue dotted border is also shown in Figure 59. As mentioned, there were no change in the design of the dewatering system for the reconfigured WRS.

As mentioned, the reconfiguration entailed removing CWCs and replacing them with CBACs. Eight 2000 kW CBAC units were required to achieve the total tertiary cooling necessary for the active mining levels. Because there are four mining levels, two CBACs are installed per level. CBACs are located near the east/west split, at the entrance of each side. A total of 42 CWCs were removed after the CBACs were tested for several weeks.

Figure 60 displays the chilled water distribution to active mining levels in the reconfigured WRS. The PRV stations were removed from the cold-water pipes entering the active mining levels. High pressure water is needed at the inlet of CBACs to enable the water to be forced through the HX tube banks. The outlet water pressure also needs to be high enough to be utilised at mining activities.

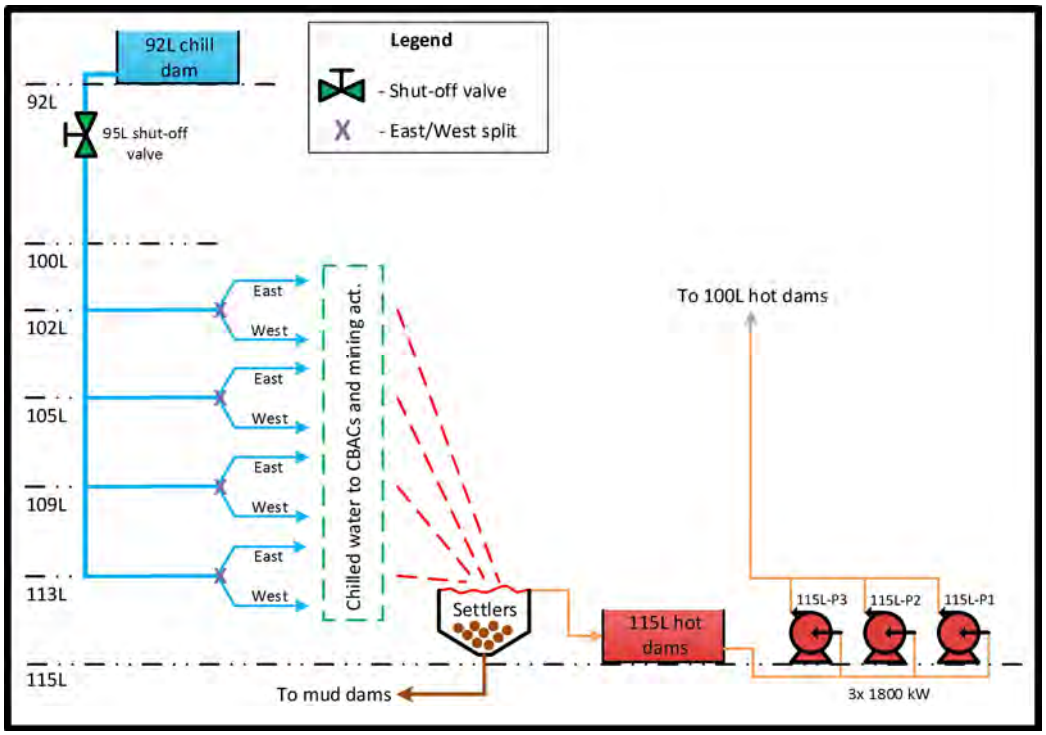

Figure 60: Layout of reconfigured WRS active mining levels

Water pressure increases as the mining depth increases. To calculate the main column water pressure, the active mining levels' elevation should be regarded from the elevation of 92L, which is 2.8 km underground. This is because 92L chill dam breaks the pressure created from the water columns above it. The head is thus the distance between the elevation of 92L and active mining levels.

Table 11 displays measured inlet water pressures at CBACs, with the main column water pressures calculated using Equation 2 in Section 2.2.3. It can be observed that the calculated results verified the measured pressure readings included in Appendix H.

Table 11: Cold-water pressure measurements in main-line of active mining levels

Mining level	Level elevation from 92L [m]	Calculated water pressure in main column at elevation [kPa]	Water pressure measured at CBAC inlet [kPa]
102L	306	3.0	2.9
105L	396	3.9	3.9
109L	516	5.1	5.0
113L	636	6.2	6.2

Figure 61 shows a basic layout of an active mining level's east/west side CBACs and mining activities.

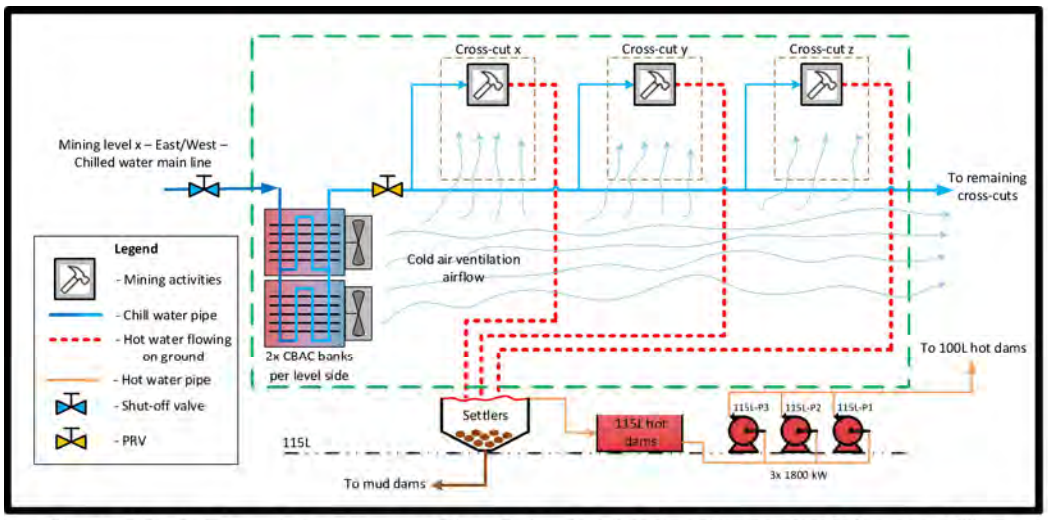

Figure 61: Active mining level east/west side CBAC location and mining activities

Cold water is fed from the main-line to the CBAC units. There are two HX banks installed per CBAC. The cooled ventilation air moves through the haulage and enters each cross-cut for cooling of working areas. Cold-water inlet temperatures for CBACs are approximately 12–14°C and the water outlet temperature is in the range of 16–20°C.

A shut-off valve is installed on the cold-water main-line before it enters a CBAC. Water supply can be closed on each level individually with the use of these valves. If a problem arises on a single level, that level's shut-off valve can be closed so that mining activities on the other levels can continue. PRVs are installed on the water pipe that exits a CBAC. These valves reduced the outlet water pressure to approximately 1400–1600 kPa to enable utilisation at mining equipment.

Figure 62 shows a picture of a CBAC unit being constructed on the investigated gold mine in SA.

Figure 62: Construction of a CC cooling-coil HX CBAC installed on investigated mine

A CBAC consists of two air intakes, two forced draught fans and ten CC cooling-coil banks. Each HX bank delivers approximately 200 kW of cooling power, which gives a total cooling duty of 2 000 kW per CBAC. Cold water, at a rate of about 40 ℓ/s per CBAC, is required to achieve this amount of cooling power.

The dewatering system of the investigated mine is described in the following sections.

4.2.4 Specification of dewatering system on investigated SA gold mine

As mentioned, the component layout of the dewatering system stayed constant during and after reconfiguration. The dewatering system's boundary is indicated by the blue dotted border in Figure 56 and Figure 59. Only pumps within this boundary were evaluated for energy and cost savings.

Figure 63 displays a detailed component layout of the dewatering system on the investigated gold mine. The shared discharge columns are indicated, where flow rate measuring devices are connected on each column.

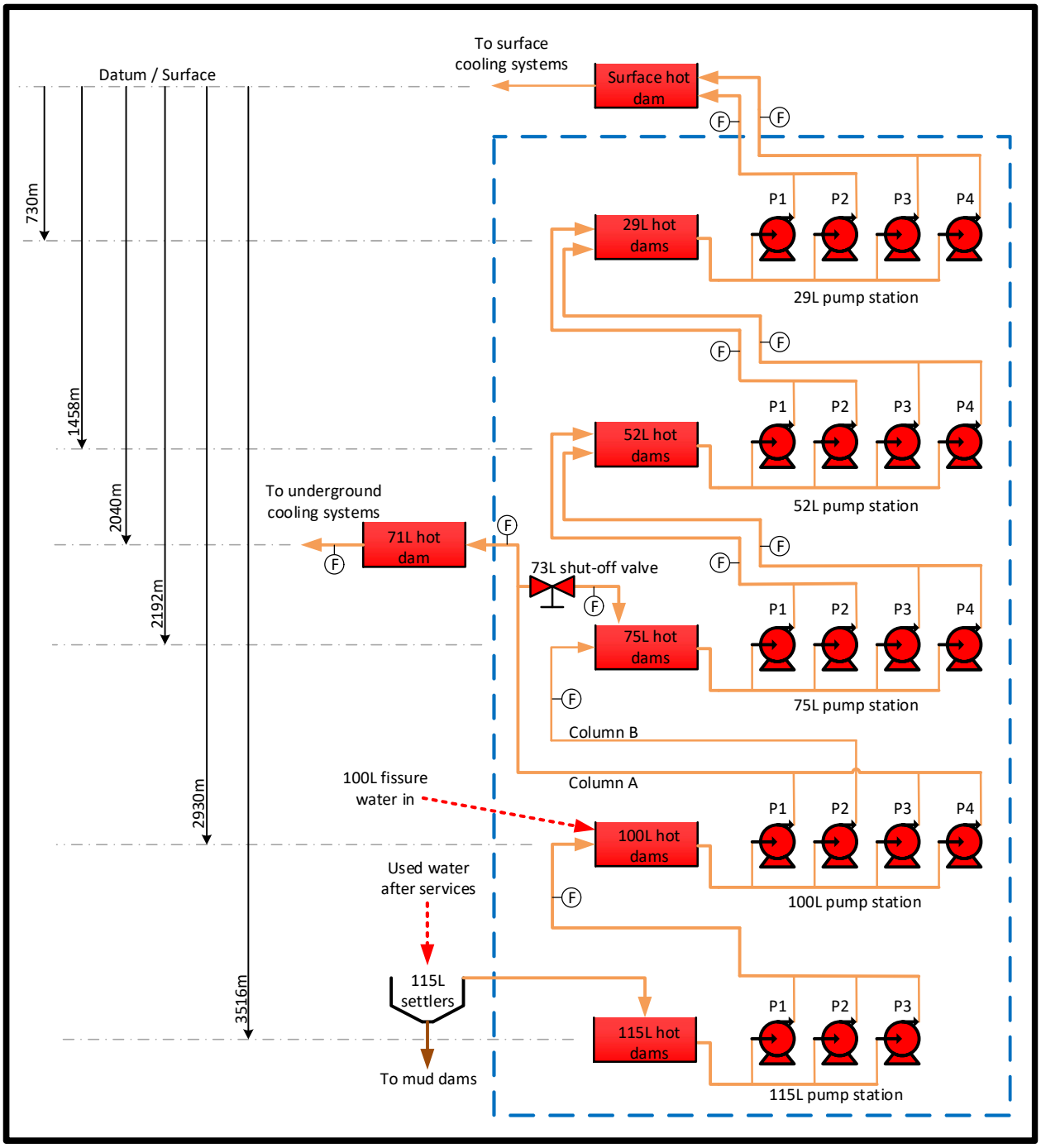

Figure 63: Layout of components in dewatering system on investigated mine

Figure 64 displays the water flow balance between hot dams of the dewatering system for the specified WRS.

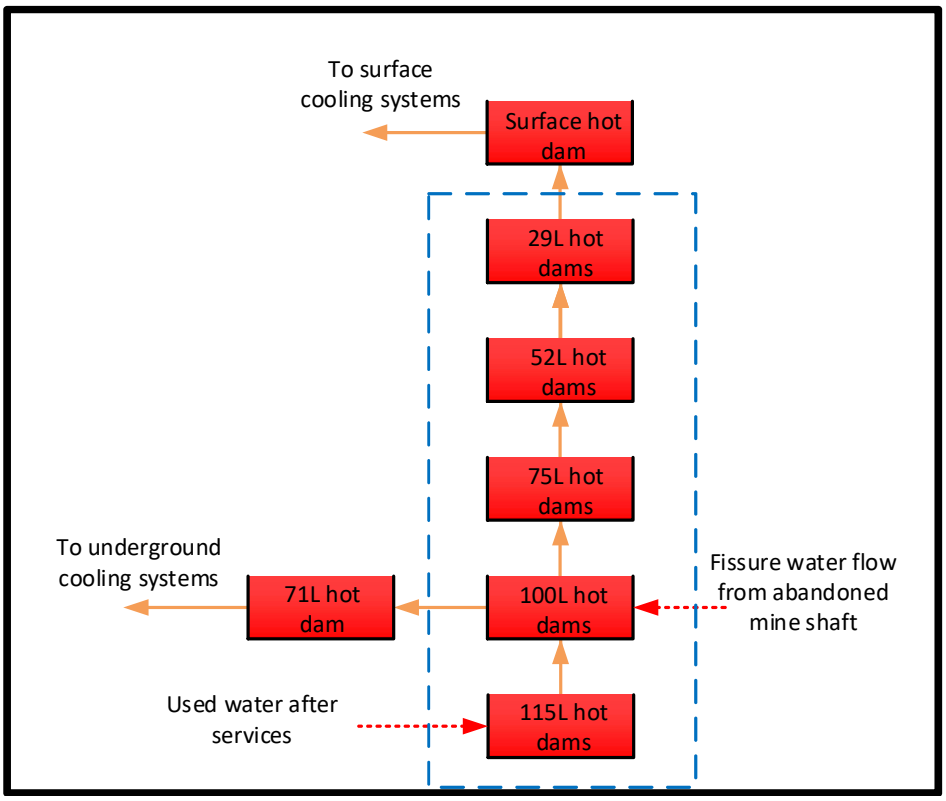

Figure 64: Dewatering system water balance

The water flow balance was obtained by analysing flow rate data through the pump stations and comparing it to flow directions displayed in Figure 63. The results indicated that there was an additional flow rate entering the WRS at 100L hot dams. This water came from an abandoned mineshaft that is interconnected to the 100L hot dams.

The following paragraphs explain the water flow balance shown in Figure 64.

115L flow balance:

After cold-water has been used for mining activities, it is discarded on the ground and flows into the 115L settlers. Sludge is drained from the bottom of the settlers and clear water overflows at the top into the 115L hot dams. This water is pumped from 115L hot dams in a single column and gets deposited into 100L hot dams. It can be observed from Figure 64 that the average monthly flow entering 115L hot dams are equal to the flow from the 115L pump station.

Equation 36 was used to calculate the average flow rate entering the 115L hot dams.

$$\mathbf{115}\boldsymbol{L\ Flow_{in}} = \mathbf{115}\boldsymbol{L\ Flow_{out}}$$

Equation 36: Average water flow into 115L hot dams

Note that there are three 115L pumps connected on the single column; however, only two may be running simultaneously. If three pumps are to be active at any given time, water discharge pressures will become excessively high, which may cause the pipe to burst.

100L flow balance:

Water pumped out of 100L hot dams consist of 115L outlet water and fissure water directly entering 100L hot dams. This water is deposited either into 71L or 75L hot dams. From Figure 63, it can be observed that the position of the 73L shut-off valve determines to which level water gets transferred. If the valve is open, the water is deposited into 75L hot dams. When the valve is closed, the water is pumped to a higher head into the 71L hot dam.

The control valve position can be changed by operators in the control room. The valve is closed when the 71L hot dam level is approximately 95% and it is opened when the level reaches 100%. Maintaining a high dam level ensures enough water is stored for at least a day to be cooled at 71L FPs, if a problem arises on the 100L pump station.

The 100L fissure water flow rate can be calculated by using Equation 37:

$$\mathbf{100}\boldsymbol{L\ Flow_{fissure}} = \mathbf{100}\boldsymbol{L\ Flow_{out}} - \mathbf{115}\boldsymbol{L\ Flow_{out}}$$

Or: $$\mathbf{100}\boldsymbol{L\ Flow_{fissure}} = \mathbf{75}\boldsymbol{L\ Flow_{in}} + \mathbf{71}\boldsymbol{L\ Flow_{in}} - \mathbf{115}\boldsymbol{L\ Flow_{out}}$$

Equation 37: Average 100L fissure water flow

It can be observed that the 73L valve is installed on column A. Three 100L pumps are connected on this column. The fourth pump is connected on column B, which only transfers water to 75L hot dams.

To ensure the transformer feeding 100L pumps is not overloaded, a maximum of three pumps may be active simultaneously. Note that a maximum of two pumps should be running simultaneously on column A. Water discharge pressures will be excessive if this maximum is exceeded, which could cause the pipe to burst. The fourth pump is on standby if one of the other pumps should fail.

71L flow balance:

It can be observed that there is a flow measuring device on the water column entering the 71L hot dam. The average monthly flow rate entering the 71L hot dam should equal the average flow rate exiting to the 71L FPs. This is displayed in Equation 37:

$$\boldsymbol{71L\ FPs_{flow} = 71L\ Flow_{in}}$$

Or:

$$\boldsymbol{71L\ Flow_{in} = 100L\ Flow_{out} - 75L\ Flow_{in}}$$

Equation 38: Average 71L FPs water flow

75L – 29L flow balance:

Figure 64 and Equation 39 shows that the flow into 75L hot dams are equal to the flow out.

$$\boldsymbol{75L\ Flow_{in} = 75L\ Flow_{out}}$$

Equation 39: Average flow into 75L hot dams

From Figure 64, it can be observed that the average monthly flow rate entering and exiting the 75L, 52L and 29L hot dams were equal. The confirmation of this water balance was obtained by looking at Table 71 and Table 72, where the average analysed flow rate for the four months included are approximately the same.

Table 12 to Table 14 include characteristics of components housed in the dewatering system shown in Figure 63. Table 12 includes name plate information for dewatering pumps, which is obtained from pump information sheets in Appendix C.

Table 12: Dewatering pump nameplate information

Dewatering pump information				
Level	**Pump ID**	**Name plate information**		
		Flow rate [ℓ/s]	**Static head [m]**	**Power consumption [kW]**
115L	HPH 54-25-7	174	700	1 575
100L	HPH 58-25-8	228	920	2 600
75L-29L	HPH 50-20-9	135	650	1 350

Table 13 includes information for the dams used in the dewatering system.

Table 13: Information of dewatering system dams

Dewatering system dam information			
Level	**Number of dams**	**Dams type**	**Total volume [m^3]**
29L	2	Horizontal	1 550
52L	2	Horizontal	2 300
71L	1	Horizontal	2 000
75L	2	Vertical	3 400
100L	3	Vertical	14 000
115L	2	Vertical	5 200

It can be observed that the total volume capacity of 100L hot dams is much larger than that of hot dams on the other levels. Natural factors affect the quantity of fissure water that enters the WRS; thus, sufficient storage capacity is needed on 100L during excessive rainfall seasons. As mentioned, 100L pumps feed water into 75L hot dams and to 71L FPs. This means there should also be enough water stored in 100L hot dams to supply the 71L FPs for an entire day if the 115L pumps fail to supply water to 100L hot dams.

Table 14 includes the number of pumps installed on each level's pump station.

Table 14: Pump installed capacities in dewatering system

Dewatering system pump installed capacities			
Level	**Number of pumps**	**Power per pump [kW]**	**Installed capacity [kW]**
29L	4	1 350	5 400
52L	4	1 350	5 400
75L	4	1 350	5 400
100L	4	2 600	10 400
115L	3	1 575	4 725
Total	**19**	**-**	**31 325**

The total installed capacity for a pump station is calculated by multiplying the number of pumps with the power consumption per pump. It can be observed that the total installed capacity for the 100L pump station is much larger than the rest of the pump stations. This is because water is transferred to 75L and 71L hot dams; therefore, the installed capacity is almost double that of the pumping stations on the other levels.

After the necessary data and information was gathered, the individual pump characteristics obtained by analysing actual data were verified. This is discussed in the following sections.

4.2.5 Results for verification of actual analysed individual pump characteristics

The process to analyse individual pump characteristics are discussed in Section 3.3. Appendix D includes a dataset obtained from REMS-P, which includes 2-minute interval logged data for 52L pumps. The data points include column flow rates, pump power consumptions, and pump statuses. Analysis of individual pump characteristics for the 52L are discussed in Section 4.2.1. This process was used to obtain the other levels' individual pump characteristics.

Table 15 to Table 20 includes the analysed results for individual flow rate for each pump.

Table 15: Analysed 115L pump flow rates

Analysed 115L pump flow rates		
Pump #	**Column**	**Flow (ℓ/s)**
Pump 1	A	256
Pump 2	A	230
Pump 3	A	221

Table 16: Analysed 100L pump flow rates to 75L

Analysed 100L pump flow rates to 75L		
Pump #	**Column**	**Flow (ℓ/s)**
Pump 1	A	260
Pump 2	B	252
Pump 3	A	224
Pump 4	A	224

Table 17: Analysed 100L pump flow rates to 71L

Analysed 100L pump flow rates to 71L		
Pump #	**Column**	**Flow (ℓ/s)**
Pump 1	A	116
Pump 2	B	N/A
Pump 3	A	135
Pump 4	A	124

Table 18: Analysed 75L pump flow rates

Analysed 75L pump flow rates		
Pump #	**Column**	**Flow (ℓ/s)**
Pump 1	B	137
Pump 2	A	122
Pump 3	B	123
Pump 4	A	118

Table 19: Analysed 52L pump flow rates

Analysed 52L pump flow rates		
Pump #	**Column**	**Flow (ℓ/s)**
Pump 1	B	127
Pump 2	A	112
Pump 3	B	126
Pump 4	A	130

Table 20: Analysed 29L pump flow rates

Analysed 29L pump flow rates		
Pump #	**Column**	**Flow (ℓ/s)**
Pump 1	A	142
Pump 2	B	143
Pump 3	A	110
Pump 4	B	115

To simplify individual pump flow rate inputs for calculations and simulations, the average flow rate per pump in its respective pump station was obtained. The results are included in Table 21.

Table 21: Average analysed individual pump flow rate

Average analysed flow rate per pump in station	
Pump station	**Flow per pump (ℓ/s)**
115L to 100L	236
100L to 75L	240
100L to 71L	125
75L to 52L	124
52L to 29L	125
29L to Surface	128

The method was applied to analyse individual pump power consumption. Table 22 includes the results for average analysed individual power consumption of each pump in its respective pump station.

Table 22: Average analysed individual pump power consumption

Average analysed power consumption per pump in station	
Level x to level y	**Power [kW]**
115L to 100L	1 587
100L to 75L	2 553
100L to 71L	1 411
75L to 52L	1 191
52L to 29L	1 201
29L to Surface	1 241

As mentioned, the pumps on 100L transfer water to 75L and 71L hot dams. Due to these dams being on different levels, the vertical distance varies that 100L pumps need to transfer water to. In Table 21 and Table 22, it can be observed that this affects the average individual pump flow rate and power consumption for the 100L pumps.

The individual pump power consumption for each pump on its respective level was calculated by using Equation 4 on page 39. Additional information was obtained that was needed to be inserted into Equation 4, which includes vertical head (H), overall pump efficiency (η_o) and volume flow rate (Q).

Table 23 displays the additional information obtained, as well as the results for theoretical pump power calculations.

Table 23: Theoretical pump power calculations for 2016 pump data

Pump power consumption calculations for 2016				
Description	**H [m]**	**η_o [-]**	**Q [m^3/s]**	**P_s [kW]**
115L to 100L	586	0.82	0.236	1 654
100L to 75L	738	0.74	0.240	2 348
100L to 71L	886	0.74	0.125	1 468
75L to 52L	734	0.72	0.124	1 240
52L to 29L	728	0.72	0.125	1 240
29L to Surface	730	0.72	0.128	1 273

The head (H) was obtained from Figure 59 and Figure 65. Overall pump efficiency (η_o) was obtained from information sheets such as the example sheet included in Appendix I. The volume flow rate (Q) was obtained from Table 21, however a conversion from ℓ/s to m^3/s was done to ensure correct use of units in Equation 4.

Table 24 includes the results for calculated and analysed individual pump power consumptions.

Table 24: Calculated and analysed pump power consumptions per level

Results for calculated and analysed pump power consumption			
Level	**Nameplate [kW] (X)**	**Analysed [kW] (Y)**	**Calculated [kW] (Z)**
115L to 100L	1 575	1 587	1 654
100L to 75L	2 600	2 553	2 348
100L to 71L	-	1 411	1 468
75L to 52L	1 350	1 191	1 240
52L to 29L	1 350	1 201	1 240
29L to Surface	1 350	1 241	1 273

From Table 24, the difference between the nameplate (X), analysed (Y), and calculated (Z) pump power consumptions can be obtained. The accuracy of the results can be verified if the analysed and calculated values are within 10% from each other.

The nameplate power consumption (X) may not correlate with Y and Z, because the values are results of tests with pre-determined heads, which may differ from the actual heads for the investigated dewatering system (see Table 12).

The percentage difference between the analysed and calculated individual power consumption results can be obtained by using Equation 8 on page 64. The results for the comparison between X, Y and Z are included in Table 25.

Table 25: Comparison between calculated, analysed and nameplate pump power consumption

Compare calculated, analysed and nameplate pump power consumption			
Level	**Nameplate vs Analysed (X/Y) [%]**	**Nameplate vs Calculated (X/Z) [%]**	**Analysed vs Calculated (Y/Z) [%]**
115L to 100L	0.8	4.8	**4.1**
100L to 75L	1.8	10.7	**8.7**
100L to 71L	-	-	**3.9**
75L to 52L	13.4	8.9	**4.0**
52L to 29L	12.4	8.9	**3.1**
29L to Surface	8.8	6.0	**2.5**

It can be observed that the analysed and calculated results are less than 15% from the nameplate values. This comparison however cannot be used to verify the actual analysed individual power consumption results. Note that the analysed (Y) versus calculated power consumptions (Z) differ with less than 10%. This percentage difference is low enough to verify the actual analysed individual pump power consumption results.

Simulations were conducted to verify analysed individual pump power consumptions and flow rates. The analysed individual characteristics were used as inputs when the simulation layout of the dewatering system was set up. The daily EC was then analysed for at least five randomly selected days for the original WRS. Because nothing was changed in the design of the dewatering system while the reconfiguration was implemented, the setup of the simulation platform only needed to be done once.

Figure 77 in Appendix F shows the component layout of the simulated dewatering system. All necessary setup information and pump control characteristics for these simulations can be found in Appendix G. The individual pump characteristics obtained in Table 21 and Table 22 are summarised in Table 62. Pump control characteristics can be found in Table 63.

Figure 65 shows a flow diagram of the algorithm used in simulations to obtain verifiable results for analysed individual pump characteristics. It consists of an iterative control philosophy that ensures a high degree of accuracy. Note that at least five days needed to be simulated to achieve an accuracy with percentage difference of less than 10%.

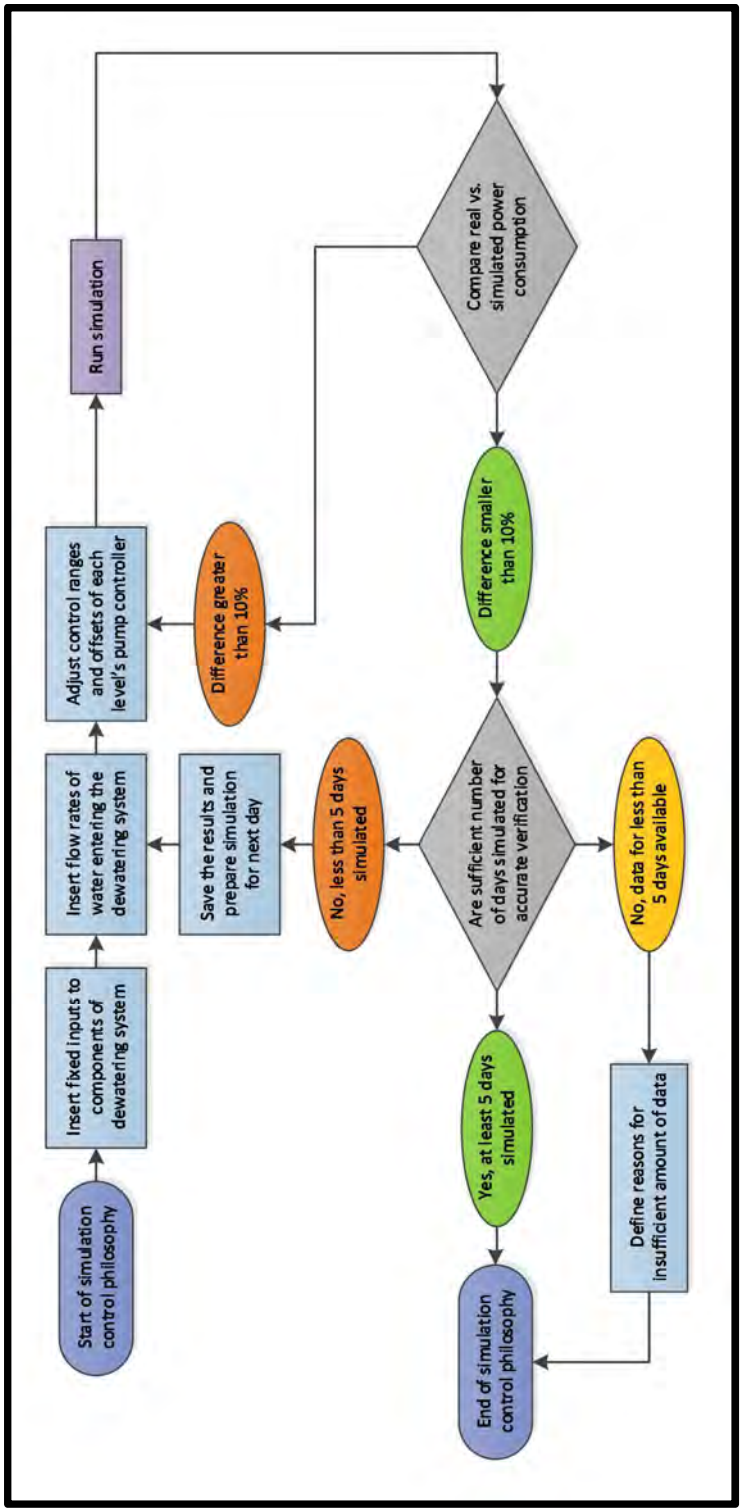

Figure 65: Control philosophy for simulation of the dewatering system

Note that results referring to 2016 comprise the results for the dewatering system of the **original WRS**. The reconfiguration was implemented at the beginning of 2017; thus, when reference is given to 2017 results, it is for the **reconfigured WRS**.

In Appendix J, Table 65 to Table 68 include results of the analysed and simulated power consumption of the dewatering system for six random days in 2016 and 2017. The average daily power consumption results were multiplied by 24 to obtain the total EC of the dewatering system for each day. Table 26 and Table 27 displays the results for the daily analysed and simulated EC of the dewatering system.

Table 26: Analysed- and simulated daily EC of the dewatering system in 2016

Evaluation of daily EC of the dewatering system for 6 days in 2016			
Day	**P_{total} analysed [kWh]**	**P_{total} simulated [kWh]**	**Error [%]**
2016/09/02	439 530	454 670	3.44
2016/09/05	415 370	402 292	-3.15
2016/09/06	363 962	338 927	-6.88
2016/09/19	414 141	431 751	4.25
2016/09/20	429 092	392 618	8.50
2016/09/26	441 454	430 487	-2.48
6-day average	**417 258**	**408 458**	**2.11**

Table 27: Analysed- and simulated daily EC of the dewatering system in 2017

Evaluation of daily EC of the dewatering system for 6 days in 2017			
Day	**P_{total} analysed [kWh]**	**P_{total} simulated [kWh]**	**Difference [%]**
2017/04/24	356 495	374 005	4.91
2017/05/02	382 169	406 694	6.42
2017/05/03	382 052	366 536	-4.06
2017/05/04	375 353	388 838	3.59
2017/05/17	438 864	427 497	-2.59
2017/05/18	380 602	368 522	-3.17
6-day average	**385 923**	**388 682**	**0.71**

It can be observed that no simulation for a single day had a percentage error greater than 10% from the analysed results. A 6-day average was calculated to obtain more reliable results.

Figure 66 visually displays the 6-day average results from Table 65 and Table 66 for 2016 in the form of power consumption profiles.

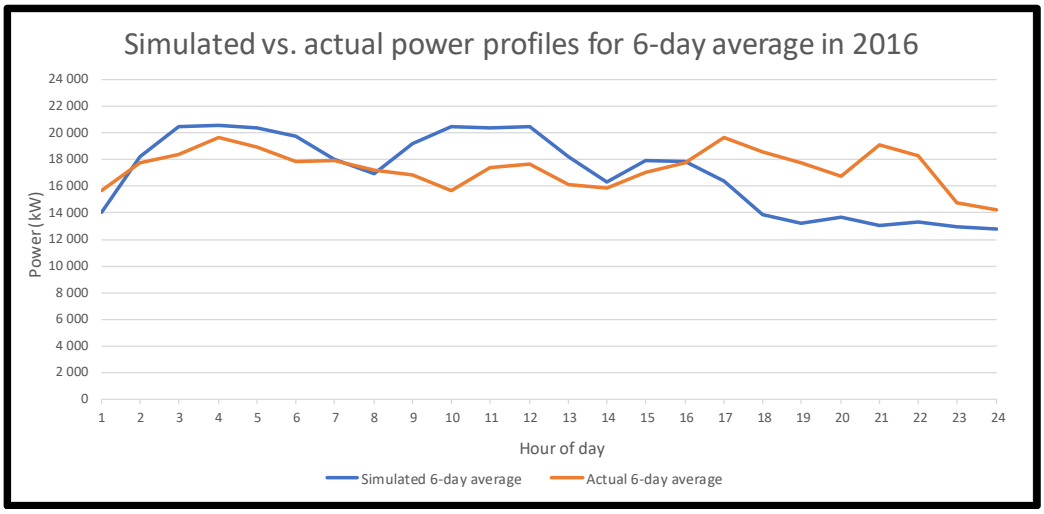

Figure 66: Actual analysed and simulated 6-day average power profiles for 2016

Figure 67 visually displays the 6-day average results from Table 67 and Table 68 for 2017 in the form of power consumption profiles.

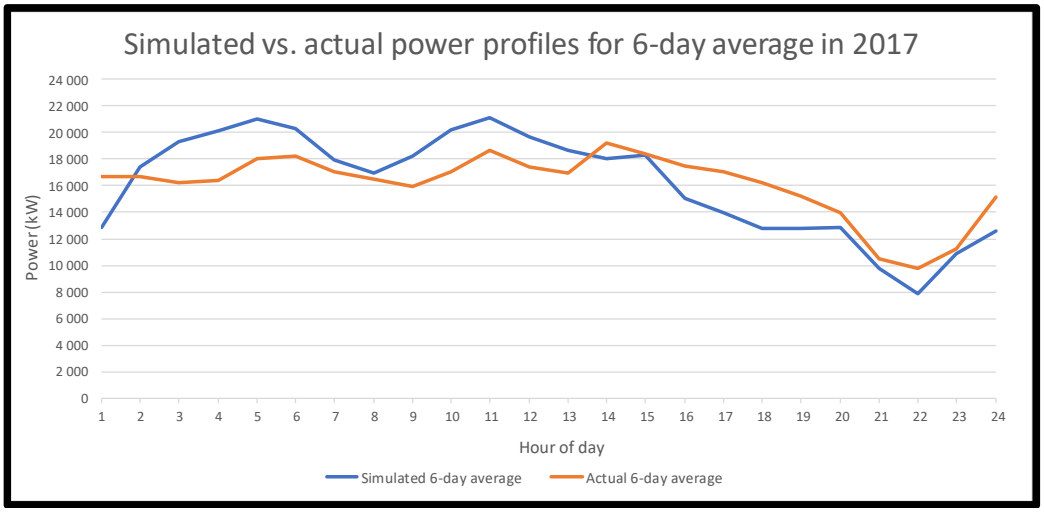

Figure 67: Actual analysed and simulated 6-day average power profiles for 2017

It can be observed that the simulated power profiles in Figure 66 and Figure 67 do not match the analysed profiles; however, verification of individual pump characteristics only requires the 6-day average percentage error to be less than 10%.

The percentage error for the 6-day average is 2.11% for 2016 and 0.71% for 2017 in Table 26 and Table 27, respectively. This is significantly less than the 10% needed for verification; thus, the verification of analysed individual pump power consumption and flow rate is confirmed.

After verification of individual pump characteristics was concluded, the remaining methodology processes were applied. The results for the next process are discussed in the following section. Refer to Chapter 3 for equations used to obtain results in the following sections.

4.3 Process 2 results: Evaluated actual EC of dewatering system for original WRS

The outcome of this process was to evaluate the EC of the dewatering system for the original WRS. The first step was to analyse actual power consumption data of dewatering pumps obtained from the REMS-P archive.

Table 69 in Appendix K includes results for the actual analysed power consumption of dewatering system for the original WRS in 2016. The results consist of average hourly data, which were analysed and converted from 2-minute data obtained from REMS-P. Note that a full set of data for the original WRS was only available for May to August 2016 and the reconfigured WRS for May to August 2017.

Table 28 includes the results for the analysed average power consumption of the dewatering system in 2016, which were obtained from Table 69 on page 141.

Table 28: Actual analysed power consumption of the dewatering system in 2016

Actual analysed power consumption of dewatering system in 2016 [kW]					
Pump station	**May**	**June**	**July**	**Aug**	**4-month average**
115L	2 142	2 611	2 262	2 497	**2 378**
100L	4 377	4 684	4 188	3 951	**4 300**
75L	2 455	3 388	2 921	2 968	**2 933**
52L	3 010	3 358	2 895	3 028	**3 073**
29L	2 884	3 165	2 814	2 936	**2 950**
Total	**14 868**	**17 206**	**15 080**	**15 380**	**15 634**

Table 29 includes the results for the analysed total monthly EC of the dewatering system for the original WRS in 2016, which were obtained by using Equation 11.

Table 29: Actual analysed EC of the dewatering system in 2016

Actual analysed EC of dewatering system in 2016 [MWh/month]					
Pump station	**May**	**June**	**July**	**Aug**	**4-month average**
115L	1 594	1 880	1 683	1 858	**1 754**
100L	3 256	3 372	3 116	2 940	**3 171**
75L	1 827	2 439	2 173	2 208	**2 162**
52L	2 239	2 418	2 154	2 253	**2 266**
29L	2 146	2 279	2 094	2 184	**2 176**
Total	**11 062**	**12 388**	**11 220**	**11 443**	**11 528**

After the analysis of actual power consumption data was completed, the prediction methods needed to be verified. The first method to achieve this is prediction through theoretical pump power calculations. Equation 12 was used to calculate the average daily power consumption of each pump station for 2016. Note that the average daily volume flow rate is needed for insertion into the equation.

The average daily flow rate for each pump station can be obtained from Table 71 in Appendix M. This was obtained by converting 2-minute flow rate data from REMS-P into average monthly values. Table 30 includes the results for the calculated average power consumption of the dewatering system in 2016, which were obtained by using Equation 12 and the data from Table 71.

Table 30: Calculated power consumption of the dewatering system in 2016

Calculated power consumption of dewatering system in 2016 [kW]					
Pump station	**May**	**June**	**July**	**Aug**	**4-month average**
115L	2 167	2 454	2 263	2 358	**2 311**
100L	4 457	4 801	4 448	3 799	**4 376**
75L	2 580	3 100	2 830	2 830	**2 835**
52L	2 879	3 307	3 087	3 109	**3 096**
29L	2 759	3 265	3 001	3 033	**3 015**
Total	**14 842**	**16 927**	**15 630**	**15 130**	**15 632**

Table 31 includes the results for the calculated total monthly EC of the dewatering system for 2016, which were obtained by using Equation 13.

Table 31: Calculated EC of the dewatering system in 2016

Calculated EC of dewatering system in 2016 [MWh/month]					
Pump station	**May**	**June**	**July**	**Aug**	**4-month average**
115L	1 612	1 767	1 683	1 755	**1 704**
100L	3 316	3 456	3 310	2 827	**3 227**
75L	1 920	2 232	2 106	2 106	**2 091**
52L	2 142	2 381	2 297	2 313	**2 283**
29L	2 053	2 351	2 233	2 257	**2 223**
Total	**11 042**	**12 187**	**11 629**	**11 257**	**11 529**

The second method investigated to predict EC of the dewatering system is by simulating the control of dewatering pumps. In Figure 63, it can be observed that the flow rates entering and exiting the dewatering system's boundary were the following:

- Flow rate into 115L hot dams.
- Fissure water flow rate into 100L hot dams.
- Flow rate entering the 71L hot dam.

The equations for obtaining the abovementioned flow rates are supplied in section 4.2.4. The results were used as inputs in simulation dam components. Automatic control of pumps was simulated to obtain the average power consumption of the dewatering system. Individual pump characteristics were already inserted and verified in section 4.2.5; thus, it did not have to be done again. The layout of the specified dewatering system and pump control characteristics are included in Appendix F and Appendix G, respectively.

The average simulated power consumption for each pump station are included in Table 32.

Table 32: Simulated power consumption of the dewatering system in 2016

Simulated power consumption of dewatering system in 2016 [kW]					
Pump station	**May**	**June**	**July**	**Aug**	**4-month average**
115L	2 037	2 384	2 112	2 223	**2 189**
100L	4 758	5 332	4 769	4 140	**4 750**
75L	2 632	3 158	2 816	2 836	**2 861**
52L	2 636	3 164	2 816	2 834	**2 862**
29L	2 663	3 197	2 844	2 862	**2 892**
Total	**14 725**	**17 235**	**15 358**	**14 895**	**15 553**

Table 33 includes the results for the simulated total monthly EC of the dewatering system for 2016.

Table 33: Simulated EC of the dewatering system in 2016

Simulated EC of dewatering system in 2016 [MWh/month]					
Pump station	**May**	**June**	**July**	**Aug**	**4-month average**
115L	1 516	1 716	1 571	1 654	**1 614**
100L	3 540	3 839	3 548	3 080	**3 502**
75L	1 958	2 274	2 095	2 110	**2 109**
52L	1 961	2 278	2 095	2 108	**2 111**
29L	1 981	2 302	2 116	2 130	**2 132**
Total	**10 956**	**12 409**	**11 426**	**11 082**	**11 468**

After results for EC of the dewatering system for the original WRS were analysed, calculated and simulated, the methods' percentage error could be calculated. Equation 14 and Equation 16 was used to obtain the results presented in Table 34.

Table 34: Percentage error of calculated- and simulated EC of dewatering system in 2016

Percentage error of calculated- and simulated EC results in 2016					
Pump station	**4-month average analysed**	**4-month average calculated**	**4-month average simulated**	**% error calculated**	**% error simulated**
115L	1 754	1 704	1 614	-2.93	-8.67
100L	3 171	3 227	3 502	1.74	9.45
75L	2 162	2 091	2 109	-3.40	-2.51
52L	2 266	2 283	2 111	0.74	7.34
29L	2 176	2 223	2 132	2.11	-2.06
Total	**11 528**	**11 529**	**11 468**	**0.01**	**0.52**

It can be observed that the percentage error for both prediction methods is smaller than 5%, which confirms verification of these methods. Both methods could now be used in the remaining processes to achieve the objective of this dissertation. The accuracy for these methods in predicting the EC of the dewatering system for the reconfigured WRS are compared in Process 5. The results for the most accurate prediction method was used to calculate energy and cost savings.

After the prediction methods were verified with actual data, the next process could be applied.

4.4 Process 3 results: Predicted EC of dewatering system for no change in WRS

The purpose of this process is to apply scaling to the power consumption of the dewatering system. This is a necessary step to accurately predict energy and cost savings.

Gold production data for the original WRS is needed to start this process. Table 35 includes the units of gold produced in the months of May to August 2016. Note that actual production data is not displayed. The actual kilograms of gold produced per month was multiplied by a randomly chosen factor to obtain *units* of gold produced. This was done because the actual production data obtained from employees on the mine is confidential.

Table 35: Gold production data for 2016

Gold production data for 2016											
Month	**Jan**	**Feb**	**Mar**	**Apr**	**May**	**Jun**	**Jul**	**Aug**	**Sep**	**Oct**	**Nov**
Amount [units]	400	340	236	212	303	351	354	289	338	299	350

Table 36 displays the analysed water consumption results for the 29L pump station in 2016.

Table 36: Analysed water consumption data of 29L pump station in 2016

Water consumption data of 29L pump station for 2016											
Month	**Jan**	**Feb**	**Mar**	**Apr**	**May**	**Jun**	**Jul**	**Aug**	**Sep**	**Oct**	**Nov**
Amount [Mℓ]	920	884	652	620	707	791	748	756	772	797	805

The data in Table 35 and Table 36 was used to calculate the amount of water consumed per unit of gold produced, where the results are displayed in Table 37.

Table 37: Water consumption per unit of gold produced in 2016

Water consumption per unit of gold produced in 2016											
Month	**Jan**	**Feb**	**Mar**	**Apr**	**May**	**Jun**	**Jul**	**Aug**	**Sep**	**Oct**	**Nov**
Amount [Mℓ/unit]	2.30	2.60	2.77	2.93	2.33	2.25	2.11	2.62	2.28	2.67	2.30

Figure 68 displays a scatter plot for water consumption versus units of gold produced in 2016. A regression line is drawn on the plot. It can be observed that the coefficient of determination (R^2) is approximately 74%, which is an effective correlation for the data.

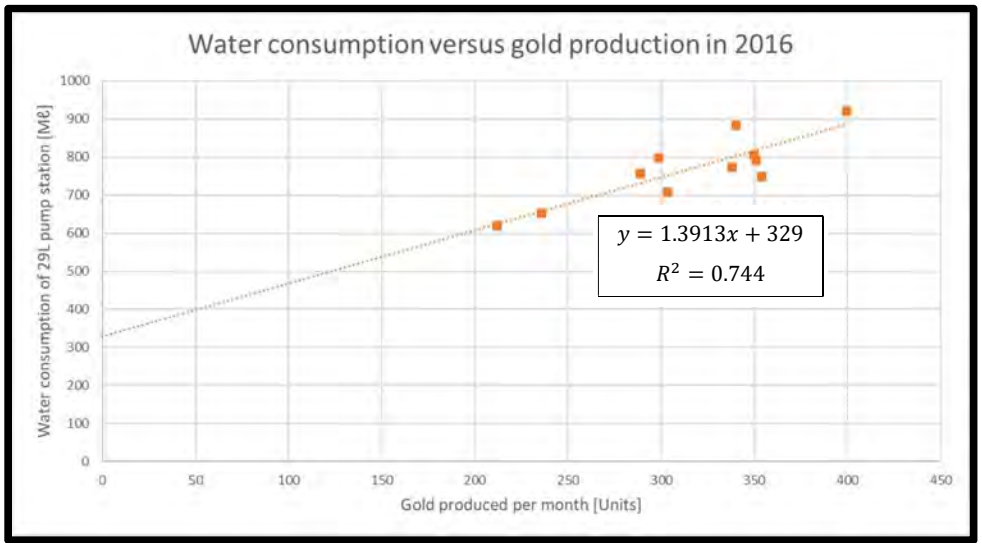

Figure 68: Scatter plot with regression line for water consumption versus gold produced in 2016

Equation 40 (adapted from Equation 19) can be obtained from Figure 68.

$$RWC\ \left[\frac{M\ell}{month}\right] = \left(1.3913\ \times\ gold_{\ unit\ \ Reconf.}\right) + 329$$

Equation 40: Predicted RWC for gold produced in 2017

Table 38 includes production data for the evaluated months of the reconfigured WRS in 2017.

Table 38: Gold production data for 2017

Gold production data for 2017				
Month	**May**	**Jun**	**Jul**	**Aug**
Amount [units]	573	479	400	353

By inserting the monthly gold production values from Table 38 into Equation 40, the RWC results were obtained and are displayed in Table 39.

Table 39: Calculated RWC

Calculated RWC for 2017				
Month	**May**	**Jun**	**Jul**	**Aug**
RWC [Mℓ]	1126	995	886	820

After the RWC was calculated for the evaluated months, it was used in calculations and simulations to obtain the REC. Note that the RWC firstly needs to be converted to an average volume flow rate for the reference WRS before it can be used for EC calculations and as inputs in simulations. Equation 20 on page 70 was used to convert water consumption into volume flow rate, where the results are displayed in Table 40.

Table 40: Calculated volume flow rate for the reference WRS in 2017

Volume flow rate for reference WRS in 2017				
Month	**May**	**Jun**	**Jul**	**Aug**
$Q\ [m^3/s]$	0.420	0.384	0.331	0.306

The average power consumption of each pump station for the reference WRS can be calculated by using Equation 21 on page 71, where the results are displayed in Table 41.

Table 41: Calculated power consumption of the dewatering system for the reference WRS

Calculated power consumption of dewatering system for reference WRS [kW]					
Pump station	**May**	**June**	**July**	**Aug**	**4-month average**
115L	3 244	2 963	2 555	2 363	2 781
100L	6 180	5 644	4 865	4 500	5 297
75L	4 008	3 660	3 155	2 918	3 435
52L	4 403	4 021	3 466	3 206	3 774
29L	4 220	3 854	3 323	3 073	3 618
Total	**22 056**	**20 143**	**17 365**	**16 059**	**18 905**

Equation 22 on page 71 was used to calculate the total monthly REC of the dewatering system, where the results are displayed in Table 42.

Table 42: Calculated REC of the dewatering system by scaling for gold produced in 2017

Calculated REC of dewatering system for 2017 production data [MWh/month]					
Pump station	**May**	**June**	**July**	**Aug**	**4-month average**
115L	2 414	2 134	1 901	1 758	**2 051**
100L	4 598	4 064	3 620	3 348	**3 907**
75L	2 982	2 635	2 348	2 171	**2 534**
52L	3 276	2 895	2 579	2 385	**2 784**
29L	3 140	2 775	2 472	2 286	**2 668**
Total	**16 409**	**14 503**	**12 919**	**11 948**	**13 945**

The scaled volume flow rate for the reference WRS was also used in simulations to predict the REC of the dewatering system for 2017 production data.

Table 43 displays the results for the average simulated power consumption for the four months evaluated.

Table 43: Simulated power consumption of the dewatering system for the reference WRS

Simulated power consumption of dewatering system for reference WRS [kW]					
Pump station	**May**	**June**	**July**	**Aug**	**4-month average**
115L	3 104	2 839	2 450	2 262	**2 664**
100L	6 705	6 248	5 364	4 961	**5 820**
75L	4 011	3 771	3 229	2 996	**3 502**
52L	4 013	3 774	3 232	3 009	**3 507**
29L	4 053	3 814	3 262	3 041	**3 543**
Total	**21 886**	**20 446**	**17 537**	**16 269**	**19 035**

Table 44 includes the results for the simulated total monthly REC of the dewatering system by scaling according to gold production.

Table 44: Simulated REC of the dewatering system by scaling for gold produced in 2017

Simulated REC of dewatering system for reference WRS [MWh/month]					
Pump station	**May**	**June**	**July**	**Aug**	**4-month average**
115L	2 309	2 044	1 823	1 683	**1 965**
100L	4 989	4 499	3 991	3 691	**4 292**
75L	2 984	2 715	2 402	2 229	**2 583**
52L	2 986	2 717	2 405	2 239	**2 587**
29L	3 015	2 746	2 427	2 263	**2 613**
Total	**16 283**	**14 721**	**13 048**	**12 104**	**14 039**

Note that the calculation and simulation prediction methods were verified with actual analysed power consumption results for the original WRS in Section 4.2.5. This ensured these methods were accurate in predicting the REC for 2017 production data. The results are used in later sections to accurately calculate energy and cost savings of the dewatering system for the reconfigured WRS. The percentage difference between the calculated and simulated 4-month average REC can be calculated by using Equation 41.

$$Difference_{\ Calc.\ vs.\ Sim._{REC.}} = \left(1 - \frac{REC_{Avg\ Calc.}}{REC_{Avg\ Si}}\right) \times 100 \quad [\%]$$

Thus: $$Difference_{\ Calc.\ vs.\ Sim._{REC.}} = \left(1 - \frac{13\,945\ MWh}{14\,039\ MW}\right) \times 100 = 0.7\%$$

Equation 41: Difference for average calculated- and simulated REC results

It can be observed that the percentage difference is significantly lower that 5%, which confirms the verification for these methods obtained in Section 4.4.

After all steps discussed in this section were completed, the next process was applied to the WRS investigated.

4.5 Process 4 results: Predicted EC of dewatering system for reconfigured WRS

This process applies the reduction in cold-water demand for CWCs removed from the WRS. As mentioned, there were 42 CWCs removed from the original WRS after the CBACs were tested for several weeks. The total reduction in the volume flow rate for the total number of CWCs removed can be calculated by using Equation 24 on page 72. The result for removing the 42 CWCs, with an average flow rate of 3 ℓ/s per CWC, is a total reduction in flow rate of 126 ℓ/s, or 0.126 m^3/s when converted to volume flow rate.

Equation 25 on page 72 was used to calculate the predicted volume flow rate for the reconfigured WRS after the CWCs were removed, where Table 45 displays the results.

Table 45: Calculated reduction in volume flow rate from the removed CWCs in 2017

Predicted volume flow rate for reconfigured WRS in 2017				
Month	**May**	**Jun**	**Jul**	**Aug**
Q $[m^3/s]$	0.294	0.258	0.205	0.180

The results in Table 45 were then used to calculate the predicted average power consumption of the dewatering for the reconfigured WRS by using Equation 26 on page 72, where Table 46 includes the results.

Table 46: Predicted calculated power consumption of the dewatering system in 2017

Calculated predicted power consumption of dewatering system in 2017 [kW]					
Pump station	**May**	**June**	**July**	**Aug**	**4-month average**
115L	2 472	2 125	1 712	1 500	**1 952**
100L	4 702	4 042	3 256	2 853	**3 713**
75L	3 049	2 621	2 111	1 850	**2 408**
52L	3 024	2 600	2 094	1 835	**2 388**
29L	3 032	2 607	2 100	1 840	**2 395**
Total	**16 279**	**13 995**	**11 272**	**9 879**	**12 856**

Table 47 includes the results for the calculated predicted monthly EC of the dewatering system for the reconfigured WRS.

Table 47: Predicted calculated EC of the dewatering system in 2017

Calculated predicted EC of dewatering system in 2017 [MWh/month]					
Pump station	**May**	**June**	**July**	**Aug**	**4-month average**
115L	1 839	1 530	1 273	1 116	**1 440**
100L	3 498	2 910	2 422	2 123	**2 738**
75L	2 269	1 887	1 571	1 377	**1 776**
52L	2 250	1 872	1 558	1 365	**1 761**
29L	2 256	1 877	1 562	1 369	**1 766**
Total	**12 112**	**10 076**	**8 387**	**7 350**	**9 481**

The simulation method was also used to predict the actual EC of the dewatering system for the reconfigured WRS. Table 48 displays the results for the simulated predicted average power consumption of the dewatering for the reconfigured WRS.

Table 48: Predicted simulated power consumption of the dewatering system in 2017

Simulated predicted power consumption of dewatering system in 2017 [kW]					
Pump station	**May**	**June**	**July**	**Aug**	**4-month average**
115L	2 253	1 934	1 579	1 490	**1 814**
100L	4 952	4 282	3 443	3 264	**3 985**
75L	3 002	2 597	2 360	2 281	**2 560**
52L	2 995	2 600	2 361	2 282	**2 560**
29L	3 024	2 626	2 274	2 314	**2 560**
Total	**16 227**	**14 039**	**12 017**	**11 631**	**13 478**

Table 49 includes the results for the simulated predicted monthly EC of the dewatering system for the reconfigured WRS.

Table 49: Predicted simulated EC of the dewatering system in 2017

Simulated predicted EC of dewatering system in 2017 [MWh/month]					
Pump station	**May**	**June**	**July**	**Aug**	**4-month average**
115L	1 677	1 393	1 175	1 108	**1 338**
100L	3 685	3 083	2 561	2 429	**2 939**
75L	2 233	1 870	1 756	1 697	**1 889**
52L	2 229	1 872	1 756	1 698	**1 889**
29L	2 250	1 891	1 692	1 722	**1 889**
Total	**12 073**	**10 108**	**8 940**	**8 653**	**9 944**

After the EC of the dewatering system for the reconfigured WRS was predicted by using the calculation and simulation methods, the next process in the developed methodology could begin.

4.6 Process 5 results: Analysed actual EC of dewatering system for reconfigured WRS

This process entails analysis of the actual EC of the dewatering system for the reconfigured WRS. The results are then compared to the prediction results obtained from the calculation and simulation methods.

Raw data from REMS-P was analysed to obtain the average power consumption of the dewatering system for the reconfigured WRS. Table 50 includes the results for the analysed average power consumption of the dewatering system in 2017, which were obtained from Table 70 on page 142.

Table 50: Actual analysed power consumption of the dewatering system in 2017

Actual analysed power consumption of dewatering system in 2017 [kW]					
Pump station	**May**	**June**	**July**	**Aug**	**4-month average**
115L	2 438	2 205	2 041	2 000	**2 171**
100L	3 445	3 132	2 948	3 595	**3 280**
75L	2 567	2 321	2 149	2 678	**2 429**
52L	2 924	2 765	2 367	2 700	**2 689**
29L	2 798	2 557	2 317	2 991	**2 666**
Total	**14 172**	**12 980**	**11 822**	**13 964**	**13 234**

Table 51 includes the results for the actual analysed total monthly EC of the dewatering system for the reconfigured WRS in 2017, which were obtained by using Equation 29.

Table 51: Actual analysed EC of the dewatering system in 2017

Actual analysed EC of dewatering system in 2017 [MWh/month]					
Pump station	**May**	**June**	**July**	**Aug**	**4-month average**
115L	1 814	1 588	1 519	1 488	**1 602**
100L	2 563	2 255	2 193	2 675	**2 421**
75L	1 910	1 671	1 599	1 992	**1 793**
52L	2 175	1 991	1 761	2 009	**1 984**
29L	2 082	1 841	1 724	2 225	**1 968**
Total	**10 544**	**9 346**	**8 795**	**10 389**	**9 769**

After results for EC of the dewatering system for the reconfigured WRS are analysed and predicted through the calculation and simulation methods, the percentage error for these methods can be calculated.

Equation 30 and Equation 31 was used to obtain the results presented in Table 52.

Table 52: Percentage error of calculated- and simulated EC of dewatering system in 2017

Percentage error of calculated- and simulated predicted EC results in 2017					
Pump station	**4-month average analysed**	**4-month average calculated**	**4-month average simulated**	**% error calculated**	**% error simulated**
115L	1 602	1440	1 338	-11.25	-19.73
100L	2 421	2 738	2 939	11.58	17.63
75L	1 793	1 776	1 889	-0.96	5.08
52L	1 984	1 761	1 889	12.66	-5.03
29L	1 968	1 766	1 889	-11.44	4.18
Total	**9 769**	**9 481**	**9 944**	**3.04**	**1.76**

It can be observed that the percentage error for both prediction methods were smaller than 5%; however, the simulations predicted the EC of the dewatering system for the reconfigured WRS more accurately. The EC results from this method are used to calculate the predicted annual cost saving of the dewatering system for the reconfigured WRS. Results for energy and cost savings are included in the following section.

4.7 Results for energy and cost savings

Figure 69 shows a bar chart of the results obtained in the processes discussed in Sections 4.3–4.6.

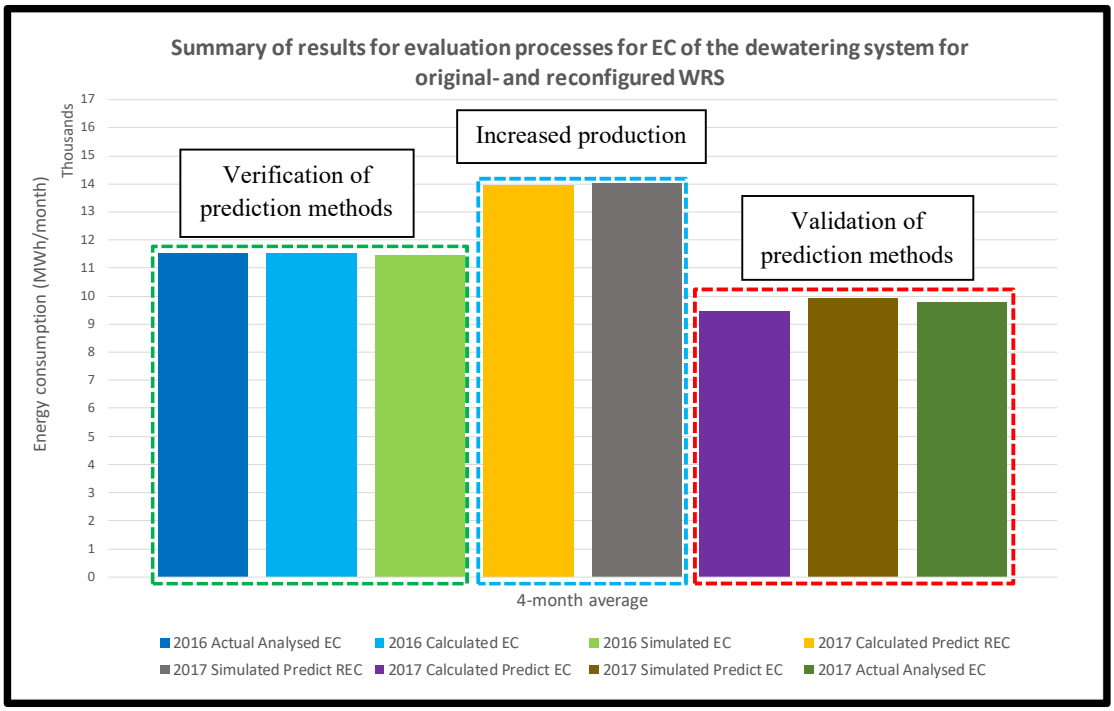

Figure 69: Bar chart of results for processes applied on the specified reconfigured WRS

As mentioned, the results from Process 3 and Process 4 need to be used for quantification of energy and cost savings. From Table 52 on the previous page, it can be observed that the simulation method predicted the EC of the dewatering system for the reconfigured WRS more accurately. Equation 33 was used to obtain the average monthly EE saving of the dewatering system for the investigated reconfigured WRS.

The results for the average monthly EE saving is displayed in Equation 42.

$$\frac{EE_{Saving_{Avg}}}{month} = 14\,039\frac{MWh}{month_{Ref.}} - 9\,944\frac{MWh}{month_{Reconf.}} = \mathbf{4\,095\ \frac{MWh}{month}}$$

Equation 42: Average monthly EE saving according to simulated results

The predicted EE saving per year if the performance of the reconfigured WRS can be sustained can be calculated by using Equation 43.

$$\frac{EE_{Saving_{Avg}}}{year} = \frac{EE_{Saving_{Avg}}}{month}\left[\frac{MWh}{month}\right] \times \frac{12\ months}{year} = \mathbf{49\,140\ \frac{MWh}{year}}$$

Equation 43: Predicted annual EE saving according to simulated results

To calculate the total monthly and yearly cost savings for the EE saving, the average energy tariff for the year in which savings were calculated should be obtained. The 2017/2018 Eskom Megaflex tariffs in Appendix B were analysed and converted to obtain the average energy tariff per kWh. Table 53 displays the winter and summer TOU periods with the respective tariffs.

Table 53: Summary of Eskom Megaflex tariffs and TOU hours per day

Eskom Megaflex 2017/2018 – (Transmission < 300 km) – (Voltage > 500 V & < 66 kV)				
TOU Period	**2017/2018 Tariff [c/kWh]**	**Hours per weekday**	**Hours per Saturday**	**Hours per Sunday**
Off-peak summer	39.2	8	17	24
Standard summer	61.8	11	7	0
Peak summer	89.8	5	0	0
Off-peak summer	45.3	8	17	24
Standard summer	83.4	11	7	0
Peak summer	275.3	5	0	0

The average tariff per weekday, Saturday and Sunday was obtained by averaging the TOU periods by their hours per day and summing them together. The average daily tariff results are displayed in Table 54.

Table 54: Average calculated daily energy tariffs

Average daily tariff calculated		
Daily	**Average tariff [c/kWh]**	**Days per week**
Weekday summer	60.10	5
Saturday summer	45.79	1
Sunday summer	39.20	1
Weekday winter	110.68	5
Saturday winter	56.41	1
Sunday winter	45.30	1

The average seasonal tariffs were obtained by averaging the daily tariffs by their number of days per week and summing them. The average seasonal tariff results are displayed in Table 55.

Table 55: Average calculated seasonal energy tariffs

Average seasonal tariff calculated		
Seasonal	**Average daily tariff [c/kWh]**	**Days per year**
Summer	55.07	273
Winter	93.59	92

The average yearly tariff for 2017/2018 can be calculated by averaging the seasonal daily tariffs by their number of days per year and summing them, which results in an average yearly energy tariff of **64.78c per kWh**.

The monthly predicted cost saving was calculated and is displayed in Equation 44.

$$\frac{Cost_{Saving}}{month} = 4\,095\,000\,\frac{kWh}{month} \times 0.6478\left[\frac{R}{kWh}\right] = \boldsymbol{\frac{R\ 2.653\ million}{month}}$$

Equation 44: Predicted monthly cost saving for reconfigured WRS

The predicted yearly cost saving can thus be calculated by multiplying by the number of months per year, where the result is shown in Equation 45.

$$\frac{Cost_{Saving}}{year} = \frac{R\ 2.653\ million}{month} \times \frac{12\ months}{year} = \boldsymbol{\frac{R\ 31.83\ million}{year}}$$

Equation 45: Predicted yearly cost saving for reconfigured WRS

The next section will discuss the results for validation of the methodology.

4.8 Validation of methodology

Refer to Figure 69 for the paragraphs that follow. It can be observed that the processes applied in the green border resulted in the verification of prediction methods developed in the methodology. This step was crucial in obtaining accurate savings results. If the percentage error of the calculated and simulated methods was greater than 5%, the prediction methods would not have provided valid results.

The blue border shows the EC results for the original WRS; however, production data is used from the reconfigured WRS for scaling purposes. It was important to investigate if there was a change in production to enable scaling to be applied. It can be observed that the average production increased after the WRS was reconfigured. This can only be achieved if the number of miners increased or if their productivity increased.

It was found that there was no major increase in the workforce for underground mining activities, which means the productivity of the miners increased. Figure 7 on page 6 displays an example of a study that entails the productivity of miners versus underground WB temperatures. The results have shown that miners work more efficiently at cooler air temperatures. This confirms that air temperatures at working areas should be cooler than what they were before the WRS was reconfigured.

From Table 35 and Table 38, the average amount of gold produced for the four evaluated months increased by approximately 16%. Figure 70 below displays the reduction in underground WB temperatures from the increase in miner productivity. This means that no energy and cost savings are achieved from FPs; however, service delivery is improved by approximately 1–3°C with a 16% increase in production.

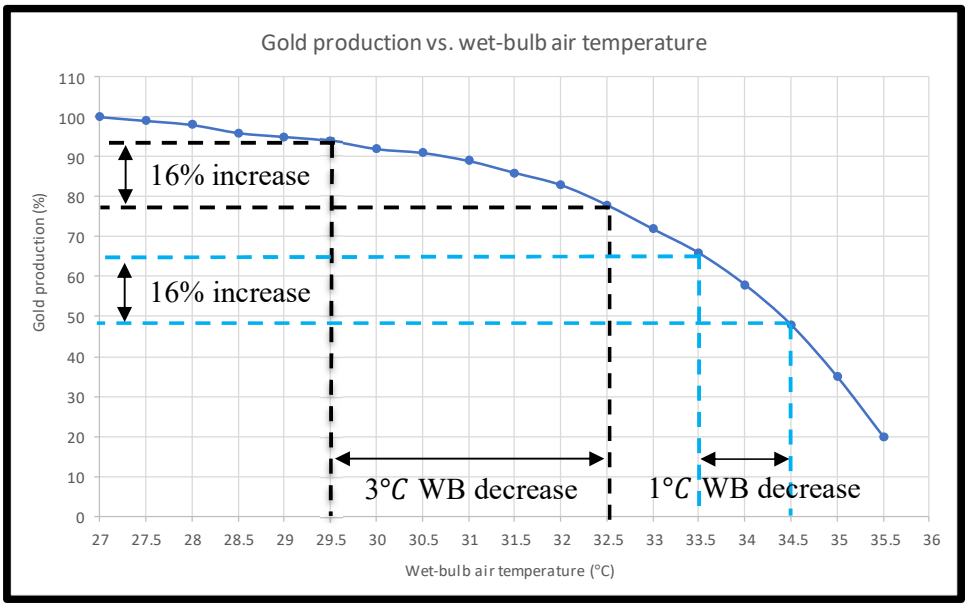

Figure 70: Gold production for 2016 and 2017 versus underground WB air temperatures

Note that if scaling is not applied, the EE savings is calculated as the original EC minus the reconfigured EC. Mining employees will observe the unscaled saving, which includes an energy saving of 1.76 GWh per month, a 1–3°C decrease in underground WB temperature and an average production increase of 16%. However, for the calculations and results of this dissertation, scaling according to production was applied. This resulted in an average energy saving of 4.1 GWh per month.

Because data accuracy was verified in Section 4.3, it could also be used as inputs in simulations and calculations to validate the developed methodology. Process 4 and 5, which was applied in the red border, was used for validation of the methodology. To attest the validity of the developed methodology, it is required that the predicted EC is less than 5% of the actual EC of the reconfigured WRS.

From Table 52 it can be observed that the percentage error for the calculation method is 3.04% and the simulation method is 1.76%. Both methods predict the EC of the reconfigured WRS within 5% of the actual EC of the reconfigured WRS, however the simulation method is more accurate. This confirms that the methodology was correctly formulated to achieve valid prediction models for WRSs such as described in this dissertation.

4.9 Conclusion

The five methodology processes developed in Chapter 3 were applied on the specified gold mine. Calculation and simulation methods were investigated to accurately predict energy and cost savings of the dewatering system for a reconfigured WRS.

The results obtained from both methods achieved a percentage error lower than 5% from the actual analysed EC of the dewatering system for the reconfigured WRS. This means that these methods predicted the EC with an accuracy greater than 95% and the developed methodology is proven valid. It should be noted that this methodology only applies if there are no three-way valves installed on underground CWCs. If these valves are installed, another approach should be followed; however, this falls beyond the scope of this study.

The predicted EE saving for the specified reconfigured WRS is **49.1 GWh** per annum. By using 2017/2018 Eskom Megaflex tariffs, the predicted cost saving was calculated as **R31.8 million** per annum.

CHAPTER 5 CONCLUSION AND RECOMMENDATIONS

[19]

"I have not failed. I have just found 10 000 ways that will not work."

- Thomas Edison

[19] Courtesy of Abram Maditane Ditshego, Hernic Ferrochrome.

5.1 Potential of reconfiguring a mine water reticulation system

Rising electricity costs in SA force companies, including gold mines, to minimise their EC. More than 30% of the total energy demand for deep-level mines is consumed by the WRS. Energy intensive centrifugal pumps are housed in the dewatering system of the WRS. Significant energy and cost savings can be achieved by decreasing the amount of water transferred through the dewatering system.

WSO is a typical DSM initiative that reduces EC of the dewatering system. This initiative only reduces the cold-water supply to underground within blasting shifts, which is 6–8 hours per day. LS is a DSM initiative that optimises the TOU operating schedule on dewatering pumps. Decreasing the water supply will increase LS performance; however, investigation of this initiative was not included in the scope of this research.

Previous studies investigated WSO techniques and TOU optimisation on mining WRSs. These studies reduced energy and cost savings for only short periods within a day. Reconfiguration of the WRS achieved a reduction in cold-water demand for the entire day. This resulted in increased energy and cost savings potential.

The reconfigured WRS investigated in this dissertation entailed the removal of CWCs and replacement with CBACs at the entrance of each active mining level's east/west sides. There were no three-way valves installed on the CWCs, which simplified calculations for water reduction. The total water reduction can be obtained by multiplying the number of CWCs removed by their specified flow rate. This reduction was then subtracted from the scaled water consumption of the original WRS, by scaling with gold production data.

A methodology was developed to accurately evaluate energy and cost savings of the dewatering system for a reconfigured WRS. Actual data obtained from the SCADA system on the mine was verified through calculations and simulations. This data was then used as inputs to evaluate EC of the dewatering system for the original and reconfigured WRS. The developed methodology can be applied on any reconfigured WRS like the one specified in this dissertation. Energy and cost savings are valid if the percentage error of the prediction methods is lower than 5%.

The methodology was applied on a gold mine near Carletonville in SA, where its WRS was reconfigured and commissioned at the end of 2016. The results showed that a predicted EE saving of **49.14 GWh** per annum is achievable. This results in a predicted annual cost saving of **R31.83 million**, by using the average electricity price per kWh for the 2017/2018 Eskom Megaflex tariff.

It can be concluded that energy and cost savings can be evaluated accurately by applying the developed methodology processes on a reconfigured WRS, which in turn concludes the objective of this study.

5.2 Recommendations for further research

There are several limitations to the application of the developed methodology. As mentioned, this methodology can only be applied on mines that do not have three-way valves installed on CWCs. If these valves were installed, a different approach would need to be taken to obtain the reduction in water demand. Investigation into this was not included in the scope of this research and could be included in further studies.

Due to limited time and data availability at the time of writing this dissertation, evaluation of energy and cost savings are only predicted from four months' data. Savings calculations can be done more accurately by evaluating data for more months. Using average electricity tariffs for winter and summer months will also increase the validity of cost savings.

Scaling according to production was the only method that had a good correlation to water consumption of the WRS. Note that at least 20–30 data points are needed to increase the accuracy of scaling. Additional scaling methods could be investigated, which includes scaling according to the number of mining teams working underground. An even higher correlation may be achieved by scaling according to production and the number of mining teams.

Reconfiguring a mine WRS has several benefits, which includes the following:

- Reduction in EC of the dewatering system.
- Increased potential for LS.
- Decreased underground air temperatures.
- Increased service delivery from FPs.

Note that energy and cost savings of the FPs were not evaluated in this dissertation. Future studies may investigate the effects of the reconfiguration on FPs. An increase in service delivery will be observed if the flow rate through FPs decreases. This will result in decreased underground water temperatures, which in turn will improve ventilation air WB temperatures and gold production.

Energy and cost savings will not be realised until there exists a significant improvement in service delivery. This means that guide vanes in FPs will need to be throttled to ensure water temperature inside the HX does not decrease below a pre-defined allowable value.

It is concluded that reconfiguring a mine WRS achieves significant energy and cost savings on the dewatering system, with the added benefit of increased service delivery and gold production.

REFERENCES

[1] Eskom, "Eskom - Company information overview," Eskom, 30 April 2017. [Online]. Available: http://www.eskom.co.za/OurCompany/CompanyInformation/Pages/Company_Information.aspx.

[2] energypedia, "South Afica Energy Situation," energypedia, 09 December 2015. [Online]. Available: https://energypedia.info/wiki/South_Africa_Energy_Situation. [Accessed 26 September 2017].

[3] Eskom, "Securing continuity of supply: Load shedding - demand exceeds supply," Eskom, 2008.

[4] Powertime, "Who use electricity in South Africa?," Powertime, 15 May 2015. [Online]. Available: http://powertime.co.za/online/use-electricity-south-africa/. [Accessed 28 April 2017].

[5] M. Howells, "The targeting of industrial audits for DSM planning," *Journal of Energy in Southern Africa,* vol. 17, no. 1, pp. 58-65, 2006.

[6] Eskom, "Eskom - 2017/18 Tariffs and charges," Eskom, 1 January 2017. [Online]. Available: http://www.eskom.co.za/CustomerCare/TariffsAndCharges/Pages/Tariffs_And_Charges.aspx. [Accessed 1 April 2017].

[7] SAPA, "Eskom: electricity used should switch off during peak times," MyBroadband, 23 April 2013. [Online]. Available: https://mybroadband.co.za/news/general/76282-eskom-electricity-users-should-switch-off-during-peak-times.html. [Accessed 30 April 2017].

[8] S. Govender, "Energy saving mechanisms in the mining industry: a case study of switching off non-essential power," University of Stellenbosch, Stellenbosch, 2008.

[9] P. Neingo and T. Tholana, "Trends in productivity in the SA gold mining industry," *The Journal of Southern African Institute of Mining and Metallurgy,* vol. 116, pp. 283-290, 2016.

[10] Chamber of Mines of SA, "Mine SA 2016 - Facts and Figures Pocketbook," Chamber of Mines of SA, Johannesburg, 2016.

[11] Eskom, "Tariff history - Historical average price increase," 21 October 2017. [Online]. Available: http://www.eskom.co.za/CustomerCare/TariffsAndCharges/Pages/Tariff_History.aspx. [Accessed 21 October 2017].

[12] Chamber of Mines of SA, "Facts and Figures 2016," Chamber of Mines of SA, Johannesburg, 2017.

[13] W. le Roux, "Mine ventilation notes for beginners," *Mine ventilation society of South Africa,* vol. 4, 1990.

[14] G. du Plessis, "A variable water flow strategy for energy savings in large cooling systems," NWU, Potchefstroom, 2013.

[15] D. Stephenson, "Distribution of water in deep gold mines in South Africa," *International Journal of Mine Water,* vol. 2, no. 2, pp. 21-30, 1983.

[16] C. Cilliers, "Cost savings on mine dewatering pumps by reducing preparation- and comeback loads," NWU, Potchefstroom, 2014.

[17] P. Oberholzer, "Best practices for automation and control of mine dewatering systems," NWU, Potchefstroom, 2014.

[18] L. Mackay, S. Bluhm and J. van Rensburg, "Refrigeration and cooling concepts for ultra-deep platinum mining," *The South African Institute of Mining and Metallurgy,* pp. 285-292, 2010.

[19] REEEP, "Demand-side management," in *Developing energy regulation and policymaking for Africa*, UNIDO, pp. 14.1-14.95.

[20] R. T. Lidbetter and L. Liebenberg, "Load-shifting opportunities for typical cement plants," *Journal of Energy in Southern Africa,* vol. 24, no. 1, 2013.

[21] R. Corson, R. Regan and S. Carlson, "Implementing energy storage for peak load shifting," 12 December 2012. [Online]. Available: http://www.csemag.com/single-article/implementing-energy-storage-for-peak-load-shifting/95b3d2a5db6725428142c5a605ac6d89.html. [Accessed 08 May 2017].

[22] Mining-technology.com, "The top ten deepest mines in the world," mining-technology.com, 11 September 2013. [Online]. Available: http://www.mining-technology.com/features/feature-top-ten-deepest-mines-world-south-africa/. [Accessed 28 October 2017].

[23] M. J. McPherson, "Refrigeration plant and mine air conditioning systems," in *Subsurface Ventilation and Environmental Engineering*, Netherlands, Springer Netherlands, 1993, pp. 651-738.

[24] A. van Niekerk, "Implementing DSM interventions on water reticulation systems of marginal deep-level mines," NWU, Potchefstroom, 2014.

[25] J. C. Vosloo, "A new minimum cost model for water reticulation systems on deep mines," NWU, Potchefstroom, 2008.

[26] M. Hooman, "A decision analysis guideline for underground bulk air heat exchanger design specifications," University of Pretoria, Pretoria, 2013.

[27] J. du Plessis, D. Scott and H. Moorcroft, "Modern cooling strategies for ultra-deep hydropower mines," *Journal of the Mine Ventilation Society of South Africa,* vol. July/September, no. 1, pp. 94-99, 2006.

[28] W. Schoeman, "The integrated effect of DSM on mine chilled water systems," NWU, Potchefstroom, 2014.

[29] J. Vosloo, L. Liebenberg and D. Velleman, "Case study: Energy savings for a deep mine water reticulation system," *Applied Energy,* vol. 92, no. 1, pp. 328-335, 2012.

[30] Z. Satterfield, "Fundamentals of Hydraulics: Pressure," *NESC Tech Brief,* vol. 9, no. 4, pp. 1-4, 2010.

[31] A. Botha, "Optimising the demand of a mine water reticulation system to reduce electricity consumption," NWU, Potchefstroom, 2010.

[32] ChemTreat, "Flocculants & Coagulants," ChemTreat, 09 November 2017. [Online]. Available: http://www.chemtreat.com/solutions/coagulants-flocculants/. [Accessed 09 November 2017].

[33] McNally Institute, "Series and parallel operation of centrifugal pumps," 09 November 2017. [Online]. Available: http://www.mcnallyinstitute.com/18-html/18-1.htm. [Accessed 09 November 2017].

[34] Sulzer, "HPH and HPL High-Lift Centrifugal Pumps," Sulzer, 18 June 2017. [Online]. Available: https://www.sulzer.com/hu/Products-and-Services/Pumps-and-Systems/Dewatering-Pumps/High-Lift-Centrifugal-Pumps. [Accessed 18 June 2017].

[35] Grundfos, The centrifugal pump, Bjerringbro, Denmark: Grundfos, 2010.

[36] B. Munson, D. Young, T. Okiishi and W. Heubsch, Fundamentals of fluid mechanics, 6th ed., Hoboken: Wiley & Sons, 2006.

[37] USGS, "The USGS water science school," U.S. Department of the Interior, 23 March 2017. [Online]. Available: URL: http://water.usgs.gov/edu/density.html. [Accessed 09 November 2017].

[38] R. Astall, "Understanding pump curves #3: centrifugal pumps in parallel," United Pumps Australia, 24 April 2013. [Online]. Available: https://www.pumpindustry.com.au/understanding-pump-curves-3-centrifugal-pumps-in-parallel/. [Accessed 20 June 2017].

[39] W. Schoeman, J. van Rensburg and G. Bolt, "Cost-effective methods for automisation of a mine pumping system to realise energy cost savings," in *The 8th conference on the Industrial and Commercial Use of Energy (ICUE)*, Cape Town, 2011.

[40] J. Stols, "Quantifying the effects of system constraints on the electricity cost of dewatering pumps," NWU, Potchefstroom, 2016.

[41] P. Maré, J. Marais and C. Kriel, "Reducing energy consumption of mine cooling systems by controlling chilled water demand of mobile cooling units," CRCED Pretoria, Pretoria, 2014.

APPENDICES

Appendix A Eskom Megaflex time-of-use schedules

Table 56 displays the Eskom Megaflex time schedule for summer months.

Table 56: Megaflex summer season time schedule

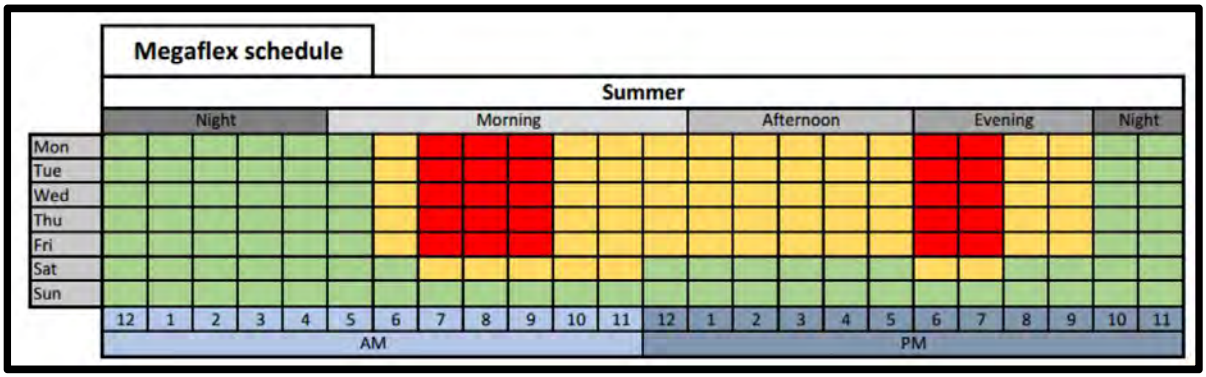

Table 57 displays the Eskom Megaflex time schedule for winter months.

Table 57: Megaflex winter season time schedule

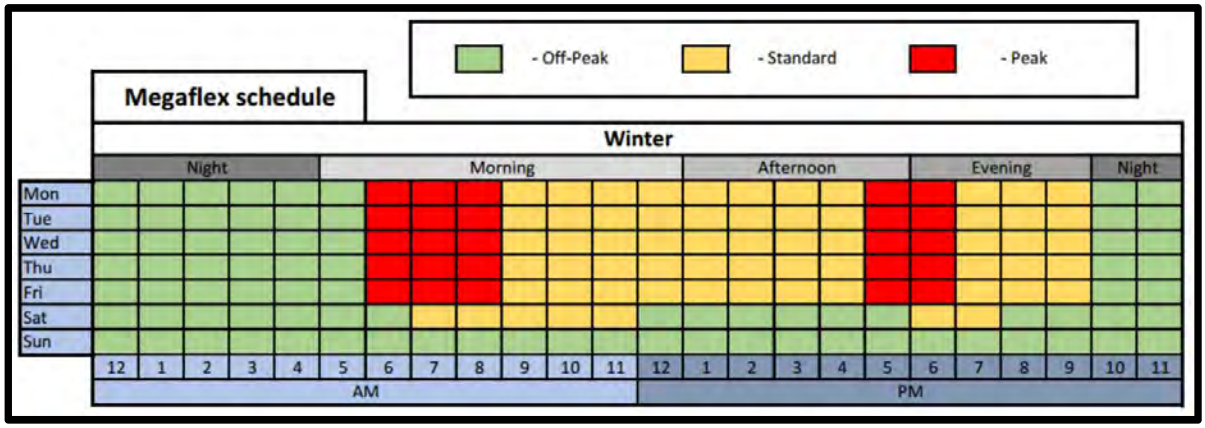

Appendix B Eskom Megaflex time-of-use tariffs 2017/2018

Table 58 displays the 2017/2018 Eskom Megaflex TOU tariffs for summer months.

Table 58: 2017/2018 Megaflex summer tariffs [6]

Megaflex tariff		Local Authority			
		Energy charge [c/kWh]			Transmission network charges [R/kVA/m]
		Summer			
Transmission zone	Voltage	Peak	Standard	Off Peak	
≤ 300km	< 500V	91.6	63.2	40.3	R 7.79
	≥ 500V & < 66kV	89.8	61.8	39.2	R 7.11
	≥ 66kV & ≤ 132kV	87.0	59.9	38.0	R 6.92
	> 132kV*	82.0	56.4	35.8	R 8.76
> 300km and ≤ 600km	< 500V	92.0	63.3	40.2	R 7.83
	≥ 500V & < 66kV	90.7	62.4	39.6	R 7.18
	≥ 66kV & ≤ 132kV	87.8	60.4	38.3	R 6.97
	> 132kV*	82.8	57.0	36.1	R 8.84
> 600km and ≤ 900km	< 500V	92.9	64.0	40.6	R 7.93
	≥ 500V & < 66kV	91.6	63.0	40.0	R 7.24
	≥ 66kV & ≤ 132kV	88.7	61.0	38.7	R 7.03
	> 132kV*	83.6	57.6	36.5	R 8.96
> 900km	< 500V	93.8	64.6	41.0	R 7.97
	≥ 500V & < 66kV	92.5	63.7	40.4	R 7.31
	≥ 66kV & ≤ 132kV	89.6	61.7	39.1	R 7.08
	> 132kV*	84.5	58.2	36.9	R 9.03

* 132 kV or Transmission connected

Table 59 displays the 2017/2018 Eskom Megaflex TOU tariffs for winter months.

Table 59: 2017/2018 Megaflex winter tariffs [6]

Megaflex tariff		Local Authority			
		Energy charge [c/kWh]			Transmission network charges [R/kVA/m]
		Winter			
Transmission zone	Voltage	Peak	Standard	Off Peak	
≤ 300km	< 500V	279.7	85.1	46.4	R 7.79
	≥ 500V & < 66kV	275.3	83.4	45.3	R 7.11
	≥ 66kV & ≤ 132kV	266.6	80.8	43.9	R 6.92
	> 132kV*	251.3	76.1	41.3	R 8.76
> 300km and ≤ 600km	< 50	2.0	85.4	46.4	R 7.83
	≥ 500V & < 66kV	278.1	84.2	45.7	R 7.18
	≥ 66kV & ≤ 132kV	269.2	81.6	44.3	R 6.97
	> 132kV*	253.8	76.9	41.7	R 8.84
> 600km and ≤ 900km	< 500V	284.8	86.3	46.8	R 7.93
	≥ 500V & < 66kV	280.9	85.1	46.2	R 7.24
	≥ 66kV & ≤ 132kV	272.0	82.4	44.7	R 7.03
	> 132kV*	256.3	77.7	42.2	R 8.96
> 900km	< 500V	287.7	87.2	47.3	R 7.97
	≥ 500V & < 66kV	283.7	85.9	46.7	R 7.31
	≥ 66kV & ≤ 132kV	274.7	83.2	45.2	R 7.08
	> 132kV*	258.8	78.5	42.6	R 9.03

* 132 kV or Transmission connected

Appendix C Sulzer/Donnlee centrifugal pump information

Table 60 include pump information for the dewatering pumps installed on the investigated gold mine.

Table 60: Sulzer/Donnlee centrifugal pump sizing specifications

Donnlee Pump Tech - Products

Sulzer Equivalent Mining Pumps

PUMP TYPES | POWER: 50Hz
HPH 24-12½-22½°f
HPH 28-15-25°f
HPH 32-17½-19°f
HPH 48-20-27°f
HPH 50-20-"o"
HPH 50-20-"w"
HPH 54-25-27°
HPH 58-25-27°
PUMP TYPES | POWER: 60Hz
HPH 24-12½-22½°f
HPH 28-15-25°f
HPH 32-17½-19°f
HPH 48-20-27°f
HPH 50-20-"o"
HPH 50-20-"w"
HPH 54-25-27°
HPH 58-25-27°

HPH 50-20-"w"

Suction Branch: 225mm
Delivery Branch: 200mm
Best Efficiency Point: 80%
Kw-Input per stage: 150kw
Static Head Per Stage (Meter): 92.5m
Litre Per Second: 135L/Sec
Cubes Per Hour: 487m³/Hour
NPSH: 9.5m
RPM: 1480rpm
Pole Motor: 4 Pole

Donnlee Pump Tech - Products

Sulzer Equivalent Mining Pumps

PUMP TYPES | POWER: 50Hz
HPH 24-12½-22½°f
HPH 28-15-25°f
HPH 32-17½-19°f
HPH 48-20-27°f
HPH 50-20-"o"
HPH 50-20-"w"
HPH 54-25-27°
HPH 58-25-27°
PUMP TYPES | POWER: 60Hz
HPH 24-12½-22½°f
HPH 28-15-25°f
HPH 32-17½-19°f
HPH 48-20-27°f
HPH 50-20-"o"
HPH 50-20-"w"
HPH 54-25-27°
HPH 58-25-27°

HPH 54-25-27°

Suction Branch: 300mm
Delivery Branch: 250mm
Best Efficiency Point: 83%
Kw-Input per stage: 225kw
Static Head Per Stage (Meter): 100m
Litre Per Second: 174L/Sec
Cubes Per Hour: 625m³/Hour
NPSH: 6m
RPM: 1490rpm
Pole Motor: 4 Pole

Donnlee Pump Tech - Products

Sulzer Equivalent Mining Pumps

PUMP TYPES | POWER: 50Hz
HPH 24-12½-22½°f
HPH 28-15-25°f
HPH 32-17½-19°f
HPH 48-20-27°f
HPH 50-20-"o"
HPH 50-20-"w"
HPH 54-25-27°
HPH 58-25-27°
PUMP TYPES | POWER: 60Hz
HPH 24-12½-22½°f
HPH 28-15-25°f
HPH 32-17½-19°f
HPH 48-20-27°f
HPH 50-20-"o"
HPH 50-20-"w"
HPH 54-25-27°
HPH 58-25-27°

HPH 58-25-27°

Suction Branch: 300mm
Delivery Branch: 250mm
Best Efficiency Point: 83%
Kw-Input per stage: 325kw
Static Head Per Stage (Meter): 115m
Litre Per Second: 228L/Sec
Cubes Per Hour: 820m³/Hour
NPSH: 6.25m
RPM: 1490rpm
Pole Motor: 4 Pole

Appendix D Pump data logged in REMS-P

Table 61: Example of actual 2-minute data logged in REMS-P

#	Time on 16/04/16	52L Col A Flow rate [ℓ/s]	52L Col B Flow rate [ℓ/s]	52L_P1 Status	52L_P2 Status	52L_P3 Status	52L_P4 Status	52L_P1 Power [kW]	52L_P2 Power [kW]	52L_P3 Power [kW]	52L_P4 Power [kW]
1	13:50	0	0	0	0	0	0	0	0	0	0
2	13:52	0	0	0	0	0	0	0	0	0	0
3	13:54	0	0	0	0	0	0	0	0	0	0
4	13:56	0	0	0	0	0	0	0	0	0	0
5	13:58	0	0	0	0	0	0	0	0	0	0
6	14:00	0	0	0	0	0	0	0	0	0	0
7	14:02	0	0	0	0	0	0	0	0	0	0
8	14:04	0	132.99	0	0	1	0	0	0	1332.65	0
9	14:06	0	127.6	0	0	1	0	0	0	1296.07	0
10	14:08	0	129.34	0	0	1	0	0	0	1304.39	0
11	14:10	0	124.83	0	0	1	0	0	0	1288.8	0
12	14:12	0	125.69	0	0	1	0	0	0	1300.1	0
13	14:14	0	125	0	0	1	0	0	0	1289.66	0
14	14:16	0	123.09	0	0	1	0	0	0	1264.19	0
15	14:18	0	122.74	0	0	1	0	0	0	1268.39	0
16	14:20	127.43	125.35	0	1	1	0	0	1264.57	1292.5	0
17	14:22	126.91	123.61	0	1	1	0	0	1260.43	1279.1	0
18	14:24	128.47	124.83	0	1	1	0	0	1270.96	1286.43	0
19	14:26	127.95	125.87	0	1	1	0	0	1287.38	1303.95	0
20	14:28	132.12	129.69	0	1	1	0	0	1309.38	1320.17	0
21	14:30	130.21	126.91	0	1	1	0	0	1293.24	1316.25	0
22	14:32	123.09	125.69	0	1	1	0	0	1255.81	1298.3	0
23	14:34	123.44	124.83	0	1	1	0	0	1250.67	1300.63	0
24	14:36	118.4	236.28	1	1	1	0	1263.89	1224.12	1212.45	0
25	14:38	121.88	236.98	1	1	1	0	1272.85	1244.45	1225.02	0
26	14:40	123.96	239.93	1	1	1	0	1279.88	1256.12	1237.3	0
27	14:42	126.04	241.15	1	1	1	0	1285.44	1267.92	1247.08	0
28	14:44	126.22	242.19	1	1	1	0	1282.13	1264.85	1243.19	0
29	14:46	129.51	241.32	1	1	1	0	1289.88	1283	1255.16	0
30	14:48	127.08	240.45	1	1	1	0	1285.72	1280.71	1249.09	0
31	14:50	122.4	241.49	1	1	1	0	1269.22	1246.53	1232.31	0
32	14:52	116.49	236.46	1	1	1	0	1247.75	1197.52	1207.04	0
33	14:54	115.8	237.15	1	1	1	0	1244.63	1191.24	1202.59	0
34	14:56	114.76	235.59	1	1	1	0	1239.04	1183.86	1198.54	0
35	14:58	111.98	234.38	1	1	1	0	1233.26	1161.66	1189.54	0
36	15:00	111.81	232.47	1	1	1	0	1228	1159.3	1181.78	0
37	15:02	112.67	233.68	1	1	1	0	1232.52	1165.49	1185.62	0
38	15:04	111.46	231.77	1	1	1	0	1227.57	1158.37	1180.24	0

Appendix E REMS-P simulation platform component descriptions

Figure 71 shows a water storage dam icon on the REMS-P platform. It displays the dam level and water temperature. Figure 72 shows the dam editor window. This is where dam characteristics are specified, which includes volume capacity, *SCADA tags* and simulation values. The in- and out-flows should be included, where certain pumps are transferring water into and out of the dam.

There may also be additional in-flows, such as fissure water entering the WRS at some levels or municipal water added to the system. This which can also be included in the dam editor. Simulation of temperature changes falls beyond the scope of this dissertation. Only dam levels, volume capacity, water flow rate and pump power consumption will be used in simulations.

Figure 71: Dam icon

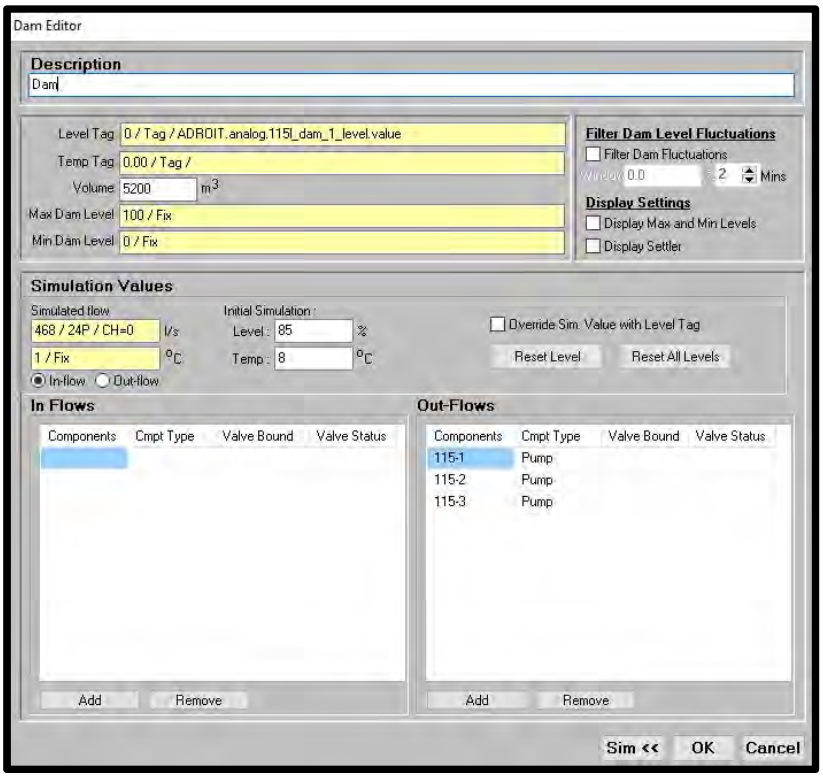

Figure 72: Dam editor window

Figure 73 shows a centrifugal pump icon on the REMS-P platform. The pump may be in three positions, which are standby, locked-out or running. Figure 74 shows the pump editor window. This is where pump characteristics are specified, which includes power consumption, flow rate, *SCADA tags* and control characteristics.

Pump power and flow rate may be a fixed value, or it may be obtained from tag. This may either be an existing SCADA tag or the user can write a programmable tag. In the case of 100L pumps in Figure 63, pumps sometimes deposit water into 75L dams and other times into the 71L dam. Due to a difference in head the pumps need to overcome, the flow rate and power consumption differ. This can be observed in Table 21 and Table 22. Programmable tags were created to vary the flow rate and power consumption of the 100L pumps when the 73L valve position changes.

Figure 73: Pump icon

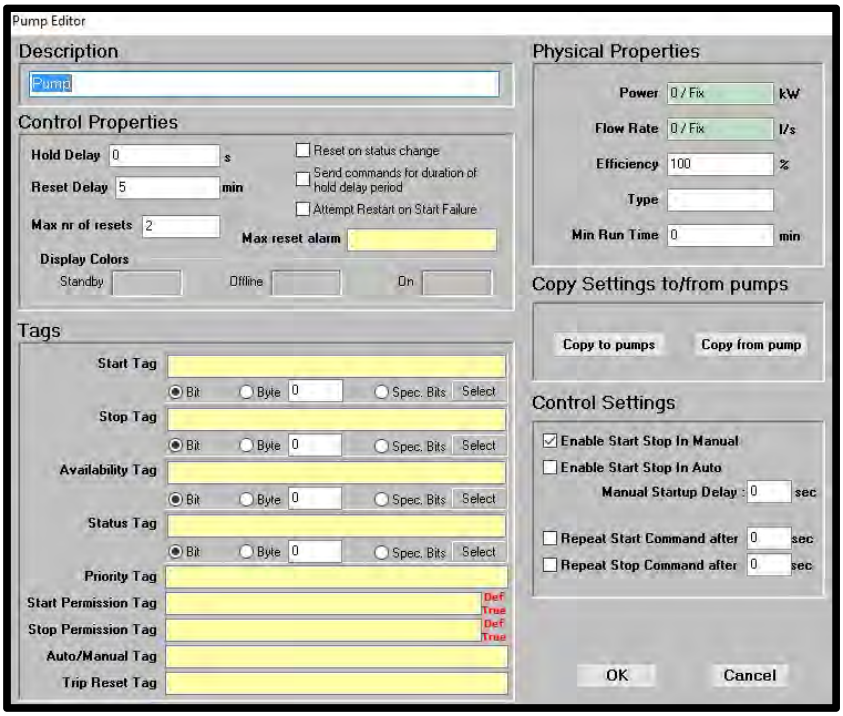

Figure 74: Pump editor window

Figure 75 shows a pump controller icon on the REMS-P platform. The function of this component is to control all pumps assigned to a pump station. Each level of pumps needs its own pump controller, because it controls pumps according to a specific control dam level. Each level has its own control dam, with volume capacity the sum of all dams on that level.

The pump controller icon displays the scheduled number of pumps and the status, which is the number of pumps running. The mode in which the controller is in, is displayed at the bottom. Automatic mode needs to be enabled for simulations to run. Figure 76 shows the pump controller editor window. This is where characteristics such as control dams, number of pumps and control settings are specified. The maximum number of pumps running simultaneously can be included, because transformers should not be overloaded. Pump priorities can also be included in the editor window if multiple columns are utilised.

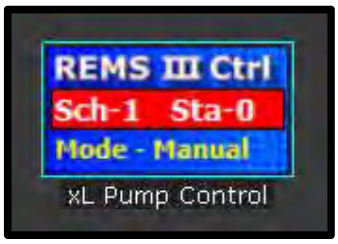

Figure 75: Pump controller icon

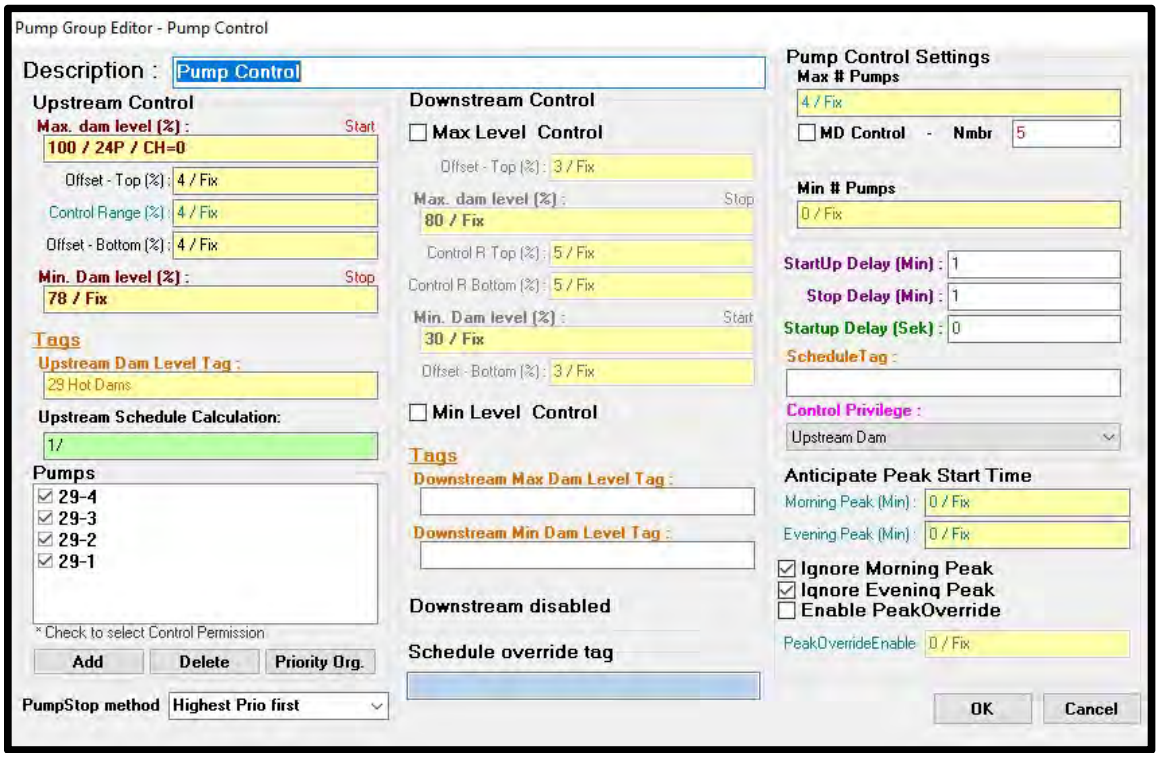

Figure 76: Pump controller editor window

Appendix F REMS-P simulation layout of dewatering system

Figure 77 shows the layout of the dewatering system designed in REMS-P. It is designed from Figure 63 on page 88, which shows the layout of the investigated dewatering system's components. The reconfiguration of the WRS did not entail changes to the layout of the dewatering system. This enables the simulation layout to remain the same throughout the entire dissertation.

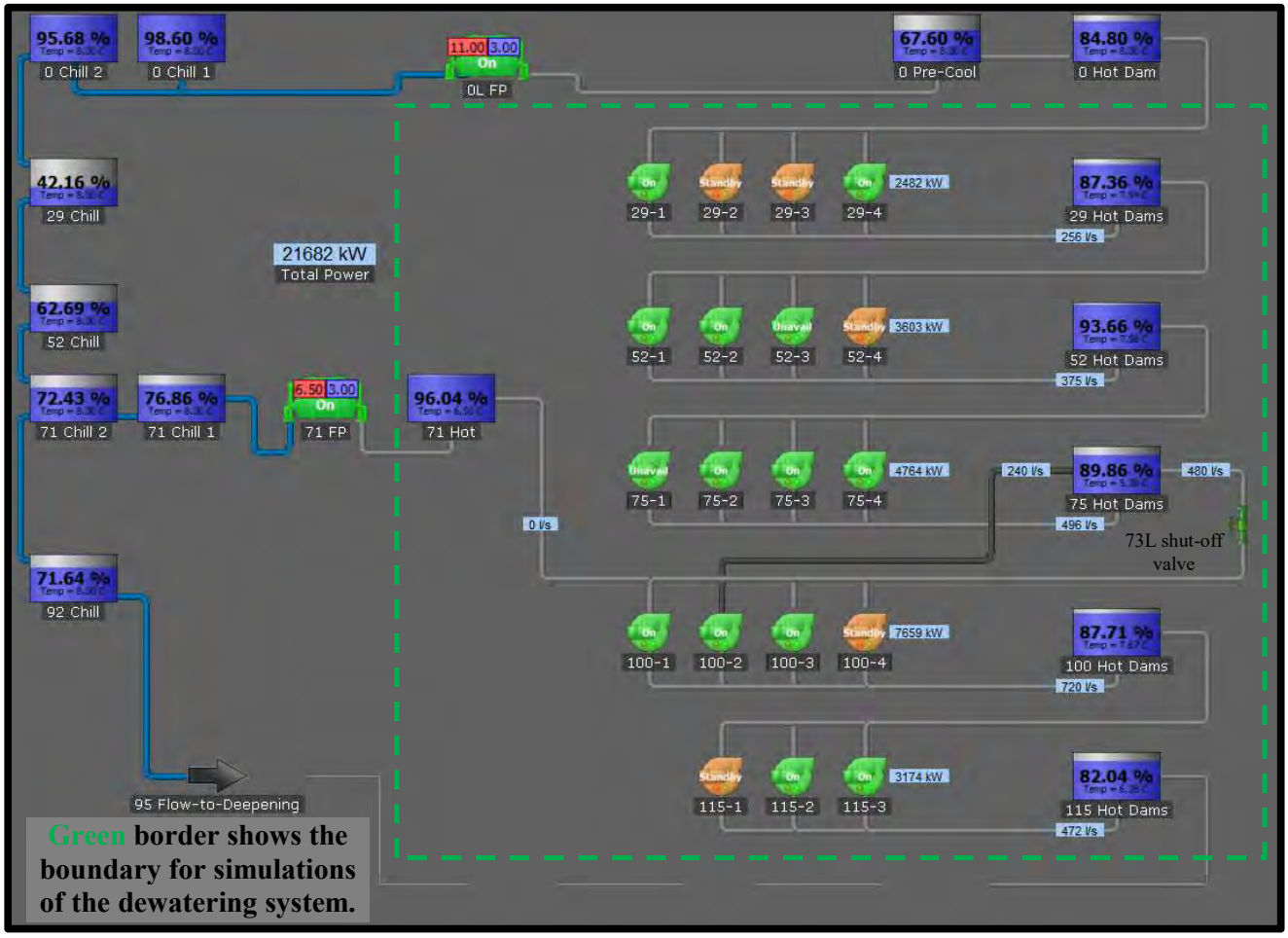

Figure 77: REMS-P simulation layout of investigated dewatering system

Appendix G REMS-P simulation inputs and specifications

The following paragraphs include the required inputs and specifications for the dewatering system components. Characteristics for pump controllers are also included to ensure automatic control of pumps are done correctly.

The following pump specifications were inserted within REMS-P pump editors:

- Analysed individual power consumption.
- Analysed individual flow rate.

Evaluation of individual flow rate of each pump was completed, and the results are displayed in Table 15–Table 20. It can be observed, there are minor differences in flow rates on each pumping level. This is due to small variations in efficiencies of the pumps.

To simplify inputs to the simulation components, averages of the flow rates were calculated (see Table 21). These values were used as inputs for each pump on its respective level. Using one average value for each pump in its station results in sufficient accuracy for simulations.

The same method was used to evaluate the average individual pump power consumption per station. The results of the average flow rates and power consumptions are displayed in Table 62.

Table 62: Physical pump specifications used in pump editors

Physical pump characteristics	115L-100L	100L-71L	100L-75L	75L-29L	52L-29L	29L-0L
Pump power [kW]	1587	1411	2553	1191	1201	1241
Flow rate [l/s]	236	125	240	124	125	128

It should be noted, for 100L pumps there are two values for power consumption and flow rate. This is because the 100L pumps transfer water to 71L and 75L hot dams. This variation is due to the difference in head from 71L to 75L (see Figure 59 and Figure 63).

The following pump control characteristics were inserted within REMS-P pump controller editors:

- Minimum and maximum dam levels.
- Control range, bottom- and top offsets.
- Control dam level tags.
- Upstream dam control privilege selection.
- Maximum and minimum number of pumps.
- Pump priorities.

Volumes of all hot dams on a level were added into one upstream control dam. This was done to simplify the layout of the simulation. Each pump controller has its own set of operating instructions, because it schedules and controls according to a specific control dam. Table 63 includes characteristics for each pump controller.

Table 63: Pump control characteristics used in pump controller editors

Pump control characteristics	115L	100L	75L	52L	29L
Minimum dam level [%]	80	87	83	81	78
Maximum dam level [%]	98	99	98	98	99
Control range [%]	8	5	4	4	4
Top offset [%]	7	4	3	4	4
Bottom offset [%]	5	3	4	4	4
Control dam tag	115 Hot Dams	100 Hot Dams	75 Hot Dams	52 Hot Dams	29 Hot Dams
Maximum # pumps	2	3	4	4	4
Minimum # pumps	0	0	0	0	0
Pump priorities	1,2,3	3,2,1,4	1,3,2,4	2,3,1,4	3,2,4,1

Refer to Figure 77, it can be observed that water can be pumped from 100L to 71L and 75L. When the 73L shut-off valve is closed, water is transferred to 71L hot dam. If the valve opens, water is transferred to 75L hot dams.

Pump number two on 100L (100-2) can only transfer water to 75L hot dams; thus, it is running on its own column. The other 100L pumps can transfer to 75L or 71L hot dams, depending on the 73L valve position.

The 73L valve is controlled manually by the operators in the control room. The valve is closed when 71L hot dam reaches 96% and is opened when it is at 100%. A high dam level needs to be maintained for the 71L hot dam. This ensures ample water is available for the 71L FPs to utilise. For the simulation, the 73L valve was automated to open or close at the specified levels.

The pumps on 115L share a single column, where a maximum of two pumps may run simultaneously. This is because the transformer feeding the pumps have a limited capacity. If it is attempted to run tree pumps together, the transformer may be overloaded, which can cause it to trip. Also, the flow rate and discharge pressure of three pumps in one column may cause it to burst.

On 75L, 52L and 29L, two pumps are connected per column. All pumps on these levels exert the same characteristics. This means they are identical in design and achieve approximately equal flow rates at a constant head. Their power consumptions will also be equal if they have the same efficiencies. If multiple pumps must be running simultaneously, it is recommended to operate them according to their priorities in Table 63.

Other inputs inserted in the simulations are as follows:

- Analysed flow rate of fissure water entering 100L hot dams.
- Analysed 71L FPs flow rate.
- Analysed flow rate into 115L hot dams.
- Volume capacity of hot dams.

Appendix H CBAC measured inlet water pressures

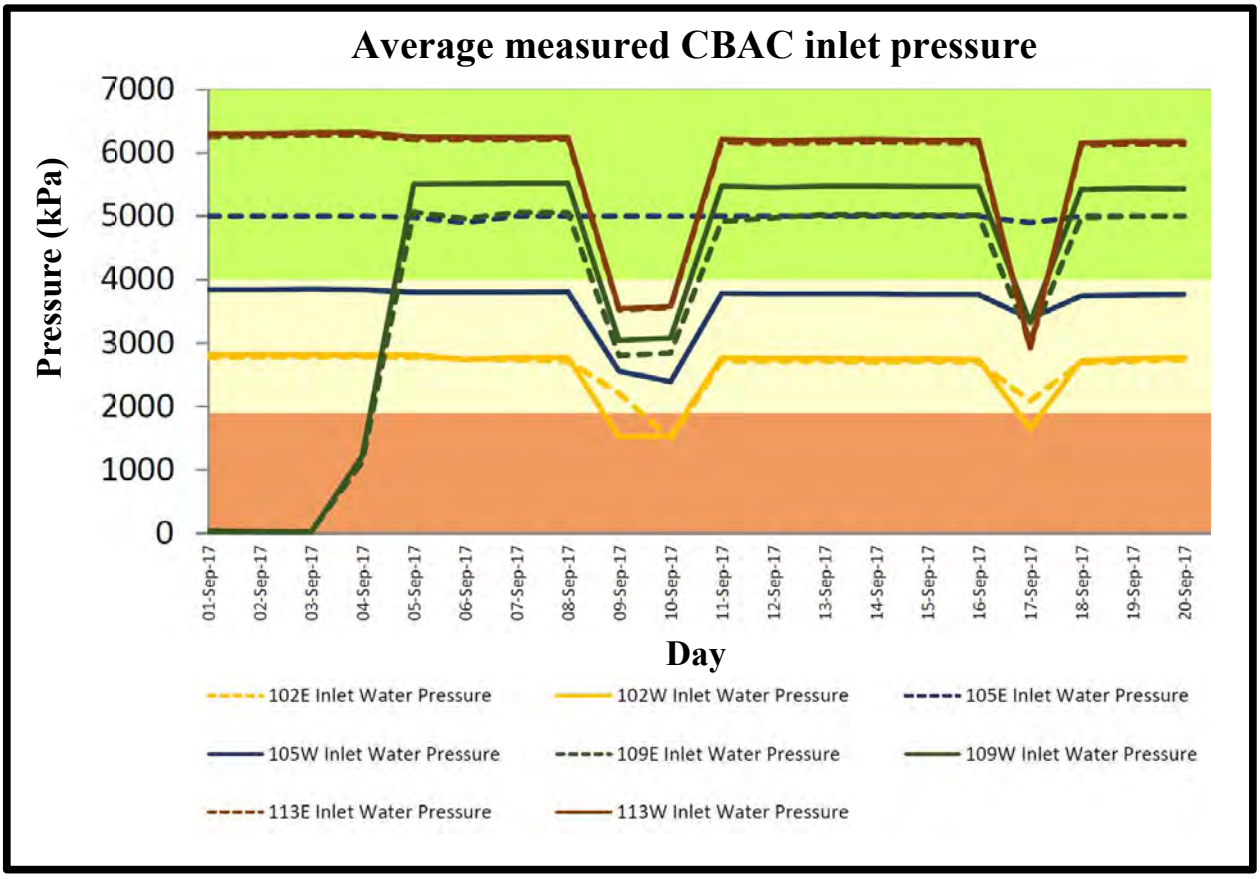

Figure 78: Average daily water pressures measured on inlet of CBACs

Appendix I Pump identification and information sheet example

Table 64: Pump identification sheet example

Pump Identification				Pump Utilisation			Pump Average		
Level	Supplier	Pump Model	Installed	Total Hours	Months Hours	Months Util, %	Eff [%]	Load, kW	kW.hrs / ML
29L_P1	Donnlee	HPH 50-20 9	2014/03/14	11 065	506	68.0	68.0	1 148	2 554
29L_P2	Sulzer	HPH 50-20 9	2015/08/01	2 616	611	82.0	75.3	1 248	2 679
29L_P3	Cemo	HPH 50-20 9	2014/05/01	10 275	569	76.0	69.0	1 214	2 941
29L_P4	Cemo	HPH 50-20 9	2014/06/12	7 723	353	47.0	75.7	1 172	2 742
Total/ Average -->				31 680	2 040	68.3	71.8	1 201	2 732
52L_P1	Donnlee	HPH 50-20 9	2015/04/01	4 144	581	78.0	55.0	1 061	3 742
52L_P2	Aklin Cardide	HPH 50-20 9	2015/06/01	3 714	630	84.0	73.7	1 225	2 755
52L_P3	Sulzer	HPH 50-20 9	2015/11/01	1 521	551	74.0	79.0	1 294	3 136
52L_P4	Donlee	HPH 50-20 9	2015/04/01	4 893	389	52.0	72.1	1 145	2 822
Total/ Average -->				14 272	2 151	72.0	69.7	1 184	3 131
75L_P1	Cemo	HPH 50-20 9	2014/03/01	11 859	545	73.0	71.0	1 043	3 048
75L_P2	Alkin Carbide	HPH 50-20 9	2014/12/01	6 330	433	58.0	78.9	1 241	2 562
75L_P3	Aklin Carbide	HPH 50-20 9	2015/04/01	4 442	572	76.0	80.0	1 142	2 440
75L_P4	Alkin Carbide	HPH 50-20 9	2014/10/01	5 266	498	66.0	79.0	1 166	2 621
Total/ Average -->				27 897	2 048	68.3	77.1	1 142	2 672
100L_P1	Aklin Carbide	HPH 58-25 8	2014/07/14	8 463	383	51.0	76.1	2 962	3 179
100L_P2	Cemo	HPH 58-25 8	2015/05/01	2 395	247	33.0	71.5	2 769	3 258
100L_P3	Cemo	HPH 58-25 8	2015/10/01	1 729	600	80.0	75.0	2 694	3 041
100L_P4	Cemo	HPH 58-25 8	2014/03/01	6 393	0				
Total/ Average -->				18 981	1 231	54.7	74.7	2 793	3 127
115L_P1	Donlee	HPH 54-25 7	2015/12/01	441	132	17.0	72.1	2 054	2 090
115L_P2	Sulzer	HPH 54-25 7	2015/11/01	554	412	55.0	79.0	1 912	2 132
115L_P3	Alkine Carbide	HPH 54-25 7	2014/07/01	4 253	368	49.0	72.0	1 874	2 107
Total/ Average -->				5 247	914	30.3	75.1	1 919	2 117

Appendix J Evaluated dewatering system power consumption

The results in Table 65-Table 68 were obtained by analysing and simulating the EC of the dewatering system for six random days in 2016 and 2017. It is used for verification of individual pump flow rate and power consumption. The process for verification of individual pump characteristics is included in Section 3.3.

Table 65: Analysed power consumption of dewatering system for the original WRS in 2016

***Analysed* individual pump characteristics in 2016 [kW]**							
Time of day	**2016/09/02**	**2016/09/05**	**2016/09/06**	**2016/09/19**	**2016/09/20**	**2016/09/26**	**6-day average**
1:00	11 824	12 554	14 309	18 862	17 260	19 495	**15 717**
2:00	13 570	18 831	14 978	19 371	18 300	21 591	**17 774**
3:00	17 367	17 494	15 290	19 052	19 362	21 852	**18 403**
4:00	21 523	17 281	20 128	18 374	20 370	20 314	**19 665**
5:00	21 646	17 976	17 047	15 452	20 049	21 680	**18 975**
6:00	19 633	17 839	17 307	13 623	17 782	20 775	**17 826**
7:00	20 719	19 245	20 028	12 598	13 819	21 409	**17 970**
8:00	18 969	21 275	17 436	10 595	13 665	21 210	**17 192**
9:00	20 050	20 913	16 158	12 728	11 642	19 777	**16 878**
10:00	20 498	21 209	12 773	13 110	9 117	17 154	**15 644**
11:00	20 136	19 468	15 770	20 671	13 493	14 914	**17 409**
12:00	19 801	20 677	14 288	20 305	16 028	15 118	**17 703**
13:00	21 335	20 295	11 259	18 818	16 489	8 831	**16 171**
14:00	18 869	17 489	12 480	20 017	16 754	9 429	**15 840**
15:00	19 839	15 668	15 673	18 962	19 962	12 145	**17 041**
16:00	19 894	17 385	16 572	18 414	20 809	13 662	**17 789**
17:00	19 877	18 876	22 765	18 436	20 205	18 077	**19 706**
18:00	15 519	16 214	19 946	18 670	20 602	20 414	**18 561**
19:00	12 698	15 501	18 030	19 190	20 093	20 951	**17 744**
20:00	12 717	12 258	15 506	18 164	21 291	20 718	**16 776**
21:00	17 979	17 572	17 333	19 389	21 667	20 794	**19 122**
22:00	21 389	17 385	11 062	17 660	20 291	22 008	**18 299**
23:00	19 731	8 382	3 013	16 816	19 668	21 110	**14 787**
0:00	13 946	13 583	4 811	14 866	20 373	18 027	**14 268**
Average	**18 314**	**17 307**	**15 165**	**17 256**	**17 879**	**18 394**	**17 386**

Table 66: Simulated power consumption of dewatering system for the original WRS in 2016

Simulated individual pump characteristics in 2016 [kW]							
Time of day	**2016/09/02**	**2016/09/05**	**2016/09/06**	**2016/09/19**	**2016/09/20**	**2016/09/26**	**6-day average**
1:00	12 333	12 898	13 330	14 323	14 519	16 746	**14 025**
2:00	17 958	20 338	13 551	22 282	15 955	19 014	**18 183**
3:00	23 474	24 247	11 897	23 431	20 226	19 381	**20 443**
4:00	24 006	22 899	14 566	22 867	20 307	18 742	**20 564**
5:00	24 066	20 529	22 572	20 646	16 255	18 429	**20 416**
6:00	22 944	19 967	22 754	18 936	15 379	18 379	**19 726**
7:00	16 547	21 261	17 767	19 018	14 490	19 026	**18 018**
8:00	18 034	17 135	14 334	20 087	14 417	17 780	**16 965**
9:00	23 571	20 701	16 949	21 566	14 827	17 473	**19 181**
10:00	23 417	21 152	20 722	22 747	16 845	18 018	**20 483**
11:00	23 739	17 495	18 639	21 832	21 754	19 108	**20 428**
12:00	23 179	21 643	19 693	21 671	18 211	18 274	**20 445**
13:00	19 259	20 930	16 956	18 183	15 315	18 617	**18 210**
14:00	15 505	16 439	13 488	19 498	14 647	18 431	**16 335**
15:00	20 650	18 540	14 488	19 502	16 715	17 495	**17 898**
16:00	24 085	15 956	14 854	17 930	16 992	17 516	**17 889**
17:00	21 316	13 020	13 220	18 332	14 578	17 774	**16 373**
18:00	14 834	12 944	9 028	13 476	15 142	17 487	**13 819**
19:00	16 625	11 986	3 961	14 447	15 608	16 839	**13 244**
20:00	18 285	11 576	6 488	13 359	15 723	16 838	**13 712**
21:00	12 920	7 886	12 218	12 498	15 010	17 550	**13 014**
22:00	12 817	7 509	12 450	12 527	17 265	17 424	**13 332**
23:00	12 734	12 280	8 031	10 535	17 443	16 748	**12 962**
0:00	12 372	12 962	6 972	12 057	14 993	17 398	**12 792**
Average	**18 945**	**16 762**	**14 122**	**17 990**	**16 359**	**17 937**	**17 019**

Table 67: Analysed power consumption of dewatering system for the original WRS in 2017

Analysed individual pump characteristics in 2017 [kW]							
Time of day	**2017/04/24**	**2017/05/02**	**2017/05/03**	**2017/05/04**	**2017/05/17**	**2017/05/18**	**6-day average**
1:00	18 351	17 334	17 823	20 324	11 331	15 047	**16 702**
2:00	13 960	13 472	18 806	20 226	18 655	15 149	**16 711**
3:00	9 574	14 592	16 411	20 487	17 889	18 306	**16 210**
4:00	11 868	18 689	16 845	18 540	14 549	17 754	**16 374**
5:00	16 469	18 786	15 838	18 887	18 717	19 269	**17 994**
6:00	17 290	19 201	16 307	19 431	19 832	17 203	**18 211**
7:00	14 439	20 778	15 135	14 105	21 676	15 877	**17 001**
8:00	11 623	20 960	15 792	15 483	18 865	16 475	**16 533**
9:00	12 184	19 088	15 723	17 001	20 505	11 361	**15 977**
10:00	14 789	20 964	17 588	18 084	16 225	14 564	**17 035**
11:00	14 002	20 783	19 585	20 720	17 034	19 971	**18 682**
12:00	12 921	16 822	16 302	22 505	15 944	19 903	**17 400**
13:00	11 075	16 128	20 356	19 163	19 693	15 419	**16 972**
14:00	15 780	17 827	22 671	18 305	20 840	19 610	**19 172**
15:00	16 597	13 408	22 034	20 888	17 938	19 437	**18 384**
16:00	15 540	14 243	16 333	17 328	20 680	20 663	**17 464**
17:00	14 998	15 324	15 747	16 148	19 136	20 846	**17 033**
18:00	16 696	16 778	17 905	9 061	19 285	17 450	**16 196**
19:00	16 464	13 577	17 895	9 474	17 769	16 248	**15 238**
20:00	17 113	13 698	16 801	8 082	19 570	8 396	**13 943**
21:00	16 768	6 723	7 808	7 897	17 175	6 815	**10 531**
22:00	15 583	6 659	3 371	5 361	18 883	8 887	**9 791**
23:00	15 613	11 462	2 897	8 261	17 502	11 880	**11 269**
0:00	16 801	14 876	16 079	9 594	19 170	14 075	**15 099**
Average	**14 854**	**15 924**	**15 919**	**15 640**	**18 286**	**15 858**	**16 080**

Table 68: Simulated power consumption of dewatering system for the original WRS in 2017

Simulated individual pump characteristics in 2017 [kW]							
Time of day	**2017/04/24**	**2017/05/02**	**2017/05/03**	**2017/05/04**	**2017/05/17**	**2017/05/18**	**6-day average**
1:00	16 529	13 089	16 908	12 090	11 655	6 942	**12 869**
2:00	23 602	14 467	13 002	17 260	17 996	17 900	**17 371**
3:00	22 949	18 570	12 335	14 599	23 866	23 317	**19 273**
4:00	21 789	24 172	12 875	16 047	23 789	22 170	**20 140**
5:00	22 451	23 423	16 446	21 818	23 921	18 335	**21 066**
6:00	17 712	22 474	19 455	21 112	24 451	16 520	**20 287**
7:00	14 056	22 894	16 013	15 109	21 440	18 333	**17 974**
8:00	13 499	15 015	18 479	15 432	19 819	19 434	**16 946**
9:00	16 662	15 236	21 503	21 636	18 090	16 217	**18 224**
10:00	21 820	20 021	15 333	22 022	23 782	18 500	**20 246**
11:00	22 722	24 147	16 814	21 513	22 162	19 208	**21 094**
12:00	16 020	22 233	22 314	20 685	17 580	19 036	**19 645**
13:00	14 401	15 541	22 006	20 862	20 164	18 916	**18 648**
14:00	18 316	15 798	16 060	21 556	23 196	13 501	**18 071**
15:00	19 887	20 770	16 422	17 775	19 636	15 098	**18 265**
16:00	13 600	17 051	19 414	12 282	14 010	13 901	**15 043**
17:00	12 817	16 718	13 148	13 022	14 089	13 818	**13 935**
18:00	12 741	13 595	12 817	16 080	15 464	5 784	**12 747**
19:00	12 362	12 665	12 762	13 179	15 090	10 493	**12 759**
20:00	11 241	12 789	12 369	11 740	12 557	16 681	**12 896**
21:00	8 849	11 545	10 754	11 715	6 718	9 012	**9 765**
22:00	5 020	11 711	6 146	11 292	7 131	6 200	**7 917**
23:00	5 306	10 633	7 058	11 226	15 750	15 332	**10 884**
0:00	9 654	12 136	16 104	8 784	15 140	13 875	**12 616**
Daily total	**15 584**	**16 946**	**15 272**	**16 202**	**17 812**	**15 355**	**16 195**

Appendix K Actual analysed power consumption of the dewatering system for the original WRS in 2016

Table 69: Actual analysed power consumption of dewatering system for 2016

Analysed average power consumption of dewatering system for 2016				
Time of day	**May power consumption [kW]**	**June power consumption [kW]**	**July power consumption [kW]**	**August power consumption [kW]**
01:00	14 093	16 368	14 840	14 997
02:00	15 119	17 943	14 697	15 065
03:00	15 694	18 717	14 708	15 559
04:00	15 894	18 868	14 414	15 909
05:00	16 351	18 423	14 286	16 308
06:00	14 573	17 502	14 290	16 263
07:00	14 196	18 067	13 888	15 565
08:00	15 229	17 148	14 202	14 607
09:00	15 080	18 092	15 135	15 916
10:00	15 997	17 361	15 255	14 668
11:00	16 261	17 373	14 790	15 934
12:00	16 846	17 607	15 199	15 743
13:00	16 308	17 381	15 622	15 937
14:00	15 868	17 677	15 570	16 362
15:00	16 190	17 720	15 926	15 861
16:00	15 213	17 255	16 586	16 096
17:00	15 074	16 860	14 628	15 252
18:00	13 304	16 526	13 712	15 262
19:00	10 996	16 830	14 581	15 630
20:00	12 443	16 691	15 698	15 477
21:00	14 566	15 387	15 703	14 366
22:00	13 907	15 561	16 516	13 990
23:00	13 563	15 535	16 785	13 839
00:00	14 066	16 053	14 891	14 514
Daily Average	**14 868**	**17 206**	**15 080**	**15 380**

Appendix L Actual analysed power consumption of the dewatering system for the reconfigured WRS in 2017

Table 70: Actual analysed power consumption of dewatering system for 2017

Analysed average power consumption of dewatering system for 2017				
Time of day	**May power consumption [kW]**	**June power consumption [kW]**	**July power consumption [kW]**	**August power consumption [kW]**
01:00	15 711	12 132	12 892	13 770
02:00	16 197	14 117	12 420	12 750
03:00	15 528	13 989	11 817	13 461
04:00	15 630	13 830	12 894	14 624
05:00	15 992	14 134	12 840	13 679
06:00	15 703	13 240	12 905	12 958
07:00	14 784	11 635	11 978	12 814
08:00	14 068	9 387	11 290	12 377
09:00	14 033	11 307	10 596	11 862
10:00	15 461	12 955	11 918	14 841
11:00	15 494	13 575	12 768	15 014
12:00	15 368	13 750	13 429	14 357
13:00	16 581	15 188	13 017	14 289
14:00	15 408	13 390	12 694	14 025
15:00	15 241	14 180	12 257	14 674
16:00	14 024	14 992	12 047	15 363
17:00	13 249	9 232	9 064	14 029
18:00	11 692	9 470	8 698	14 329
19:00	10 152	12 945	9 752	13 714
20:00	9 573	15 167	10 307	13 830
21:00	9 727	13 696	11 239	14 952
22:00	11 597	13 734	11 959	14 940
23:00	13 629	13 564	12 221	15 180
00:00	15 282	11 909	12 729	13 304
Daily Average	**14 172**	**12 980**	**11 822**	**13 964**

Appendix M Average analysed flow rate of each pump station

Table 71: Average analysed flow rate of all pump stations for the original WRS in 2016

Average flow rate of pump stations in 2016 [ℓ/s]					
Month	**115L Station**	**100L Station**	**75L Station**	**52L Station**	**29L Station**
May	294	423	258	268	262
Jun	333	460	310	301	310
Jul	307	426	283	281	285
Aug	320	371	283	283	288
Average	**314**	**420**	**283**	**283**	**286**

Table 72: Average analysed flow rate of all pump stations for the reconfigured WRS in 2017

Average flow rate of pump stations in 2017 [ℓ/s]					
Month	**115L Station**	**100L Station**	**75L Station**	**52L Station**	**29L Station**
May	307	326	261	259	264
Jun	284	292	231	250	236
Jul	275	274	260	274	268
Aug	292	286	304	286	302
Average	**290**	**295**	**264**	**267**	**267**

Appendix N Total water transferred through each pump station

Table 73: Total water transferred through each pump station for the original WRS in 2016

Total water transfer through pump stations in 2016 [Mℓ/month]					
Month	**115L Station**	**100L Station**	**75L Station**	**52L Station**	**29L Station**
May	772	1 110	677	703	689
Jun	875	1 207	813	790	813
Jul	806	1 118	743	738	748
Aug	841	975	744	744	756
Average	**824**	**1 103**	**744**	**744**	**752**

Table 74: Total water transferred through each pump station for the reconfigured WRS in 2017

Total water transfer through pump stations in 2017 [Mℓ/month]					
Month	**115L Station**	**100L Station**	**75L Station**	**52L Station**	**29L Station**
May	806	857	686	680	693
Jun	747	768	606	657	619
Jul	721	719	682	719	704
Aug	768	751	798	750	792
Average	**761**	**774**	**693**	**702**	**702**